SPECTRUM SENSING IN TIME AND FREQUENCY DOMAINS

BY

HUMAYUN KHALID Y. KATHURIA

A Thesis Presented to the

DEANSHIP OF GRADUATE STUDIES

KING FAHD UNIVERSITY OF PETROLEUM & MINERALS

DHAHRAN, SAUDI ARABIA

In Partial Fulfillment of the
Requirements for the Degree of

MASTER OF SCIENCE

In

TELECOMMUNICATION ENGINEERING

DECEMBER 2012

KING FAHD UNIVERSITY OF PETROLEUM & MINERALS

DHAHRAN- 31261, SAUDI ARABIA

DEANSHIP OF GRADUATE STUDIES

This thesis, written by **HUMAYUN KHALID Y. KATHURIA** under the direction of his thesis advisor and approved by his thesis committee, has been presented and accepted by the Dean of Graduate Studies, in partial fulfillment of the requirements for the degree of **MASTER OF SCIENCE IN TELECOMMUNICATION ENGINEERING.**

Dr. Mohamed A. Deriche
(Advisor)

Dr. Ali Ahmad Al-Shaikhi
Department Chairman

Dr. Wessam Mesbah
(Co-Advisor)

Dr. Salam A. Zummo
Dean of Graduate Studies

Dr. Adil S. Balghonaim
(Member)

9/2/13
Date

Dr. Ali Ahmad Al-Shaikhi
(Member)

Dr. Samir Al-Ghadhban
(Member)

Dedicated to my parents and siblings for their sincere love and support through every walk of my life

ACKNOWLEDGMENTS

I would like to thank Allah for all the support without which this work would not have been completed.

Also, I would like to thank my advisor, Dr. Mohamed A. Deriche, who always encouraged me towards achieving my objectives in research and has helped me in every way possible for achieving those objectives.

Furthermore, I would like to thank my co-advisor, Dr. Wessam Mesbah, for his extremely valuable inputs and the time that he has dedicated during our regular meetings.

Moreover, I would like to appreciate the helpful comments provided by Dr. Adil S. Balghonaim, Dr. Ali Ahmad Al-Shaikhi, and Dr. Samir Al-Ghadhban for the improvement of my thesis work. Also, I would like to pay high regards to my graduate advisor, Dr. Maan Kousa, whom I hold in high esteem. He has always provided me very useful advises both for my academics and professional career.

In addition, I am exceedingly grateful to my parents whose love, prayers, and support has always been with me. I would like to thank my sister, Halah, for all those cheerful moments that we have spent together. My brother, Wajeeh ur Rahman, has always supported and encouraged me in my educational endeavors, for which I have great respect for him in my heart. I would like express my affection for my cute little nephew, Hamoud, who is really a blessing upon us from Allah. Also, I would like to thank my fiancé, Amnah, for all the confidence that she has built in me.

Finally, I would like to thank my colleague, Raza Umar, for his continuous support throughout the course of my degree program. Also I would like to thank Syed Asim Hussain, Shoieb Arshad, Hussain Ali, Muhammad Haris Khan, and Mohammed Fahham for their humorous attitude which was a great source of keeping me unstressed during the research.

TABLE OF CONTENTS

LIST OF FIGURES

LIST OF ABBREVIATIONS

AWGN	:	Additive White Gaussian Noise
BPF	:	Band-Pass Filter
CWT	:	Continuous Wavelet Transform
C-ROC	:	Complementary Receiver Operating Characteristics
CR	:	Cognitive Radio
CROWN	:	Cognitive Radio Oriented Wireless Networks
CSS	:	Cooperative Spectrum Sensing
DWT	:	Discrete Wavelet Transform
ED	:	Energy Detector
EGC	:	Equal Gain Combining
FT	:	Fourier Transform
FC	:	Fusion Center
HDCR	:	Hard-Decision CR
IDWT	:	Inverse Discrete Wavelet Transform
I.I.D	:	Independent and Identically Distributed
MRC	:	Maximal Ratio Combining

PDF	:	Probability Density Function
PU	:	Primary User
PSD	:	Power Spectral Density
ROC	:	Receiver Operating Characteristics
SS	:	Spectrum Sensing
SNR	:	Signal-to-Noise-Ratio
SDCR	:	Soft-Decision CR
WT	:	Wavelet Transform
WRAN	:	Wireless Regional Area Network

ABSTRACT

Full Name : Humayun Khalid Yusuf Kathuria

Thesis Title : SPECTRUM SENSING IN TIME AND FREQUENCY DOMAINS

Major Field : Signal Processing and Communications

Date of Degree : December 2012

With the advent of commercial wireless devices, we are witnessing a continuous demand for larger bandwidths from different multimedia services. So much so, that the current situation of commercial spectrum does not allow for new wireless systems. On the other hand, the spectrum bands already assigned to certain services are not constantly utilized by the primary (licensed) users. It is this situation which attracted the attention of researchers from around the world towards Cognitive Radio and Spectrum Sensing.

Cognitive Radio is seen as an excellent solution to the problem of spectrum scarcity by efficient utilization of the radio spectrum. In order to achieve that, the Cognitive Radio approach makes nodes aware of their environment, and parameters are modified in real-time, based on the predicted situation of the targeted frequency bands. In this way, *the foremost operation of a Cognitive Radio is to sense the targeted spectrum, and then make a decision on the availability of spectrum so that secondary users can benefit from it*. Note that the spectrum sensing operation is a very challenging task and needs to be accurate and efficient in order to enable the Cognitive Radio system to work effectively.

In this thesis, we make two contributions towards efficient Spectrum Sensing using Energy Detection.

First, a recent Wavelet-based approach effectively introduced for spectrum sensing is discussed. In particular, we show that the Wavelet Transform (WT) can effectively be used to identify holes in the spectrum. We enhanced previous work based on the WT and showed that it works even when spectrum measurements are very noisy. Compared to previous work, we show that the proposed approach is robust, computationally efficient, and provides accurate bandwidth detection results in spectrum sensing.

Second, we investigate Energy Detectors that operate on time-domain samples of the sensed signal. Single-threshold and Bi-threshold Energy Detectors are discussed with their pros and cons.

Finally, we propose a new hybrid approach to Spectrum Sensing using a Bi-threshold energy detector combining decision- and data-fusion techniques. We derive all the mathematical models relevant to the detector and validate our model using numerous simulation results.

ملخص الرسالة

الاسم الكامل: هومايون خالد يوسف كتهوري

عنوان الرسالة: استشعار الترددات في نطاقي الزمن و التردد

التخصص: معالجة الإشارات و الاتصالات

تاريخ الدرجة العلمية: ديسمبر 2012

مع التقدم في الأجهزة اللاسلكية التجارية، نشهد طلبا مستمرا على زيادة سعة الترددات المتاحة لخدمات الوسائط المتعددة المختلفة. لدرجة أن الوضع الحالي للطيف التجاري لا يسمح بتطوير المزيد من الأنظمة اللاسلكية. من ناحية أخرى، فإن حزم الترددات المحجوزة مسبقا لخدمات محددة ليست مستخدمة باستمرار من قبل المستخدمين الأساسيين (المرخص لهم). هذا الوضع جذب انتباه الباحثين من جميع أنحاء العالم اتجاه الراديو الذكي و استشعار الطيف.

يعتبر الراديو الذكي حلاً ممتازاً لمشكلة نقص الترددات المتاحة عن طريق الاستخدام الفعال لترددات الراديو. من أجل تحقيق ذلك، طريقة الراديو الذكي تجعل نقاط الاتصال مدركة للبيئة المحيطة بها، و يتم تغيير الخصائص (Parameters) في الزمن الحقيقي اعتمادا على الحالة المتوقعة لحزم التردد المستهدفة. بهذه الطريقة، فإن العملية الرئيسية للراديو الذكي هي استشعار التردد المستهدف، و بعد ذلك اتخاذ القرار حول ما إذا كان بإمكان المستخدمين الثانويين (غير المرخص لهم) الاستفادة من هذا التردد. إنه لمن الجدير بالذكر هنا أن عملية استشعار التردد عملية صعبة للغاية و تحتاج لأن تكون دقيقة و فعالة بحيث تمكن الراديو الذكي من العمل على نحو فعال.

في هذه الأطروحة، نحن نقدم حلين للاستشعار الفعال للترددات باستخدام كشف الطاقة (Energy Detection).

في البداية، سوف تتم مناقشة طريقة حديثة مصممة بفعالية لاستشعار التردد بالاعتماد على المويجات. على وجه الخصوص، سوف نثبت أن التحويل المويجي (Wavelet Transform) يمكن أن يستخدم بفعالية لتمييز الترددات غير المستخدمة. لقد قمنا بتحسين العمل السابق المعتمد على التحويل المويجي و أثبتنا أنه يعمل حتى عندما تكون قراءات التردد مشوشة للغاية. و نثبت في هذا البحث أن الطريقة المقترحة متينة، فعالة حسابيا، و تقدم نتائج دقيقة لاستشعار السعة الترددية (Bandwidth).

ثانياً، ندرس مستشعرات الطاقة التي تعمل على عينات الإشارة المستشعرة في النطاق الزمني (Time Domain).

أخيراً، نحن نقترح طريقة هجينة لاستشعار الترددات باستخدام مستشعر للطاقة ذا حدين (Bi-Threshold Energy Detector) يعتمد على دمج البيانات و القرارات من الأجهزة المختلفة، و نشتق كل النماذج الرياضية ذات العلاقة بالمستشعر المقترح و نتحقق من صحة نموذجنا باستخدام نتائج محاكاة متعددة.

CHAPTER 1

INTRODUCTION

1.1 Motivation

Traditional wireless systems operate under the policy of *static* spectrum allocation. Once a wireless service provider gets a license for using a certain band from the commercially available spectrum for a particular geographic location, he and only himself has the right to operate in that frequency band no matter whether he wants to use it 100% of the time or only 10% of the time. Any unlicensed user is prohibited to benefit from the licensed frequency band. As the trend of wireless services is shifting from voice-only to multimedia services, e.g., mobile TV, the service providers are demanding higher and higher bandwidths. Realizing the fact that the spectrum band is a limited resource, we are at the verge of spectrum unavailability for new wireless systems. In addition to this problem, a more disappointing note published in a FCC survey report pointed out that the spectrum utilization in the 0-6 GHz band varies from 15% to 85%, meaning that the actual licensed spectrum is mostly underutilized in vast temporal and geographical dimensions [1]. Hence, this inefficient utilization of licensed spectrum can be thought of as the outcome of wasteful *static* spectrum allocation. In order to solve the problems of spectrum scarcity and inefficient utilization, both researchers and policy makers got attracted to the recently introduced concept of *Cognitive Radio*, which was originally

presented by Mitola and Maguire in [2]. Recently, the IEEE 802.22 cognitive radio wireless regional area network (WRAN) standard was introduced as the first effort towards the practical use of cognitive radio [3]. Simon Haykin, in [4], defined the term *Cognitive Radio* as:

"*Cognitive radio is an intelligent wireless communication system that is aware of its surrounding environment (i.e., outside world), and uses the methodology of understanding-by-building to learn from the environment and adapt its internal states to statistical variations in the incoming RF stimuli by making corresponding changes in certain operating parameters (e.g., transmit-power, carrier-frequency, and modulation strategy) in real-time, with two primary objectives in mind:*

- *Highly reliable communications whenever and wherever needed;*
- *Efficient utilization of the radio spectrum.*"

1.2 Problem Statement

In order to sense the surrounding environment reliably, the *spectrum sensing* ability of a cognitive radio must be accurate and robust. However, spectrum sensing becomes a very challenging task when the cognitive user has no prior information about the signal characteristics of the primary (licensed) user that might be active in a particular frequency band of interest. Besides the inability of the cognitive user to know about the primary user's signal characteristics beforehand, the situation becomes more complicated under the so-called fading effect due to environmental obstacles.

1.3 Objectives of the thesis

In this thesis, we make two major contributions to the area of spectrum sensing. More specifically, the main objectives of the thesis are:

- Development of a Frequency-domain spectrum sensing approach using the Wavelet transform.
- Development of a Time-domain spectrum sensing approach using a double-threshold energy detector and cooperation among multiple single-antenna cognitive users.

1.4 Main Contributions of the Thesis

We list in what follows the main contributions achieved in this thesis:

- Application of median filtering to the received signals' PSD to reduce the effects of noise in wavelet-based spectrum sensing.
- Improving the overall wavelet edge detection results by combining wavelet coefficients from different scales. The detected edges are used to find the spectral holes.
- Comprehensive analysis of different mother wavelets and their performance in spectrum sensing.

- Development of a new hybrid two-threshold energy detector based spectrum sensing algorithm to reduce the cost over the reporting channels under cooperative spectrum sensing scenario.
- Derivation of the closed form expressions for the probability of detection & false-alarm, and the total average number of reporting bits for the proposed algorithm.

1.5 Thesis outline

The rest of the thesis is organized as follows. Chapter 2 presents the background of the problem and a thorough literature survey of different spectrum sensing techniques. It also outlines the fundamentals of the two approaches used in this work. In Chapter 3, the wavelet based approach to spectrum sensing is detailed and is accompanied with several simulation results. The second approach, energy detector based sensing, is discussed in Chapter 4 along with all the mathematical derivations and numerous simulation results. Finally, Chapter 5 summarizes the work presented in this thesis and potential future research directions.

CHAPTER 2

BACKGROUND & LITERATURE REVIEW

The concept of a cognitive radio (CR) network has been efficiently explained by Haykin and Akyildiz in [4] and [5]. This intelligent radio has the cognitive capability to sense its surrounding environment, and to determine appropriate operating parameters for it in order to adapt to the dynamic radio environment, all in real-time. The fundamental role of a CR is to acquire the best available spectrum for its users, based on its cognitive capability and re-configurability. As mentioned before, since most of the commercially available spectrum is already allocated, the real challenge is to share seamlessly the unused spectrum of the primary user. Consider an example model of spectrum usage across time and frequency displayed in Figure 2.1.

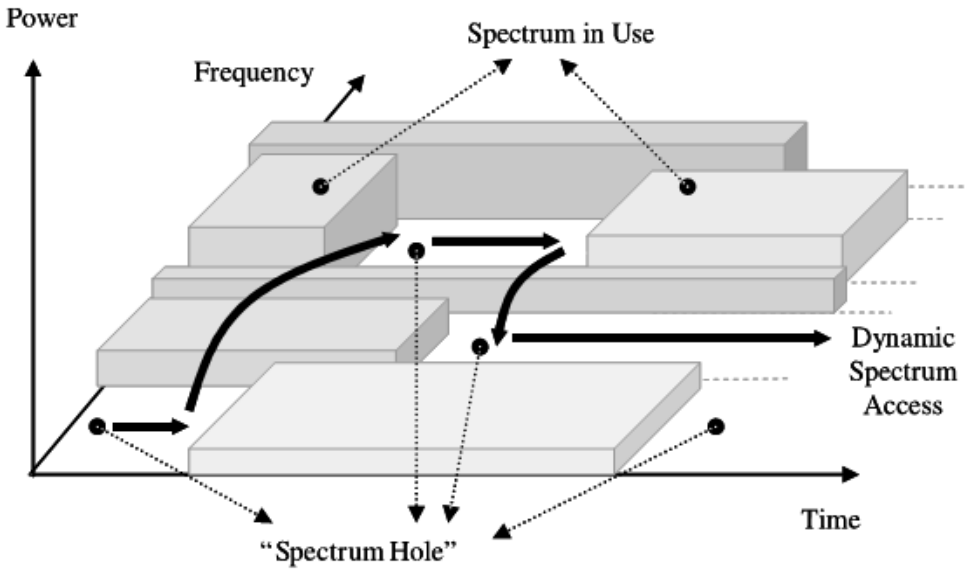

Figure 2.1: The concept of spectrum hole

The primary users are only active within certain time intervals. The no-activity gaps between active intervals are referred to as *spectrum holes* or *white spaces* [4]. If such spectrum white-spaces can be detected efficiently, then these can be used by secondary users resulting in better spectrum utilization. During the opportunistic (dynamic) spectrum access, if the primary user becomes active, the cognitive radio system has either to move to another spectrum hole or continue using the same band with a change in its operating parameters, e.g., modulation scheme, in order to avoid interference with the primary transmission [5].

In effect, the whole operation of a cognitive radio can be represented graphically as a cycle, the so called *cognitive cycle*, as show in Figure 2.2.

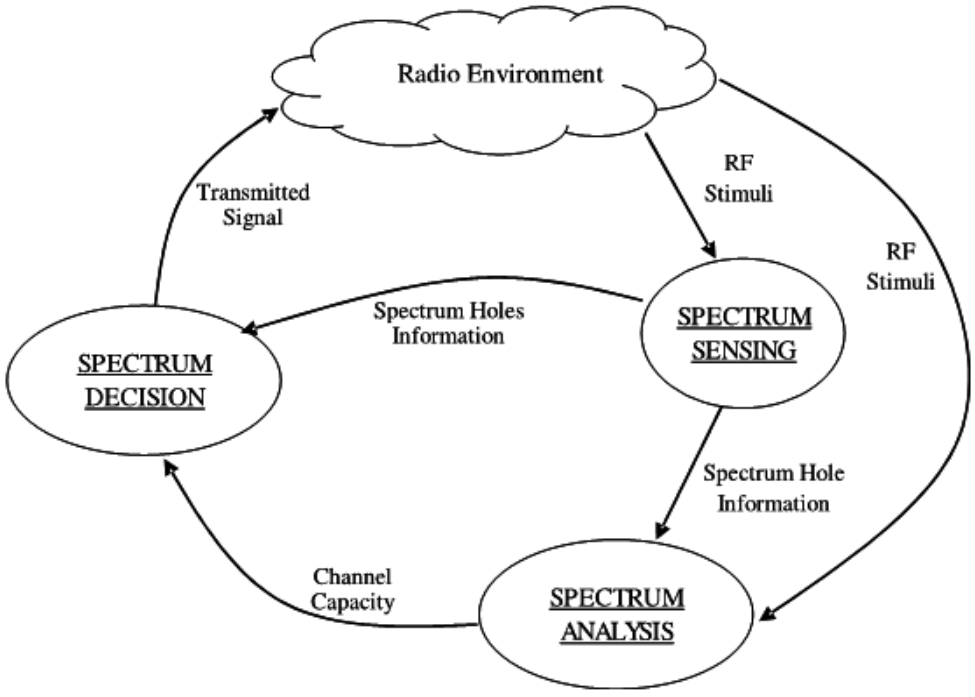

Figure 2.2: A simple representation of a cognitive radio cycle [5]**.**

The Cognitive Cycle steps shown in Figure 2.2 can be interpreted as follows:

1. *Spectrum Sensing*: A CR examines the targeted frequency band(s), extracts relevant information, and identifies possible spectrum holes.
2. *Spectrum Analysis*: The detected spectrum holes are characterized and channel conditions are estimated within each hole.
3. *Spectrum Decision*: Based on the cognitive user requirements, e.g., data rate and required bandwidth, the cognitive radio determines the best available spectrum hole for the secondary user transmission.

However, while the cognitive user is transmitting over a licensed frequency band, it is important to keep track of the changes in the radio environment. For example, when the current channel conditions become worse or when the licensed user reappears, the operation of *spectrum mobility* comes into play, as shown in Figure 2.1. During this operation, the cognitive radio switches from the current channel to some other spectrum hole, a phenomenon referred to as *spectrum handoff* [5].

From the previous discussion, it is clear that a necessary task prior to dynamic spectrum access is *Spectrum Sensing*. It is the first phase in the cognitive cycle. In this phase, efficient spectrum sensing techniques are used to track the radio environment which may change in time and space. Several spectrum sensing methods have been discussed in the literature with their merits and demerits [6], [7]. Spectrum sensing techniques can be classified into two main categories, namely, *transmitter detection*, and *interference-based detection* [5].

The interference-based detection method calculates the maximum amount of interference that the primary receiver could tolerate [5]. As long as the cumulative RF energy from multiple sources, including the secondary users, is below under a certain limit, the secondary users are allowed to transmit in a specific spectrum band. One model to measure the interference at the receiver was introduced by FCC in [8], referred to as *interference temperature model*. Using this model, a radio receiver can be designed to operate over a range at which the received interference level is below the interference temperature limit. The limitations of this model are that it needs information about the unlicensed user's signal modulation, activity patterns of the primary and secondary users, in addition to having control over the power levels of the SU [9]. Also the cognitive user may not be aware of the exact location of the primary receivers, which makes it impossible to measure the influence of the cognitive user's transmission on all the potential primary receivers. Because of the inherent complexities in the receiver's interference detection method, the method has gained less attention as compared to the transmitter detection methods for cognitive radios.

Transmitter detection techniques have attracted most attention because of their simplicity. When this technique is used, the cognitive radio focuses on the local observation of the signal from a primary user (transmitter). Transmitter detection can be performed either with one cognitive radio or by a group of cognitive radios cooperatively sensing a targeted spectrum band. The latter case is sometimes referred to as *collaborative (cooperative) detection* [10]. These (transmitter detection) techniques can be further divided into *Blind/Semi-Blind Spectrum Sensing* and *Non-Blind Spectrum Sensing* [6]. The key difference among these schemes lies in the amount of *a priori* knowledge about

the Primary User (PU) signal that is required by the cognitive radio to perform spectrum sensing. The former approach (*Blind/Semi-Blind SS*) is usually used when the CR have no prior information about the characteristics of the primary user signal, channel, and the noise power. The best possible knowledge the CR can have is the estimate of noise variance, hence the term Semi-Blind SS. *Energy detection* [11], [12] and *statistical-analysis-based detection* [13], [14], [15], [16] falls under the category of Blind/Semi-Blind SS. When prior information is not available or cannot be extracted by the CR, Energy Detector is the best and simplest option to perform sensing. Energy detection is the least demanding approach as it makes the receiver implementation task relatively simple. Under the category of Non-Blind Spectrum Sensing, we have the following techniques: 1) *Matched Filter detection*, and 2) *Cyclostationary feature detection* [17]. Matched filter detection and Cyclostationary feature detection techniques require a priori knowledge about the PU signal.

When the characteristics of the PU's signal is known by the secondary user, the optimum detection technique was found to be matched filtering, since the matched filtering technique maximizes the signal-to-noise ratio of the received signal [18]. The output of the matched filter is obtained by correlating the unknown received signal with a known signal, or template, in order to find out the presence of the known signal in the unknown received signal. Matched filtering is a coherent detection approach, as a consequence of which, it requires less time to achieve high detection accuracy as compared to other techniques discussed earlier [19]. The downside of the matched filtering technique is the amount of a priori information that is needed to demodulate the received signals, such as the pulse shape, bandwidth, modulation type, etc. Unless the a priori information is not

perfect, the matched filter performs poorly. Furthermore, the implementation of the matched filter based sensing unit becomes impractically large since it would require dedicated receivers for each type of primary user signals [20].

An alternative non-blind spectrum sensing method is the cyclostationay feature detection [21], [22]. This detection method exploits the embedded periodicity in the modulated signal. The periodic mean and autocorrelation of a modulated signal characterizes the signal as a cyclostationary process. The feature detection based sensing unit analyzes a spectral correlation function in order to detect the built-in periodicity of a modulated signal. Since a noise is a wide-sense stationary process without correlation, while modulated signals have spectral correlation due to the periodicity, the feature detection based technique has the capability to distinguish between the noise energy and the modulated signal energy. Consequently, a cyclostationary feature detector is robust to noise power uncertainty [23]. The feature detector can also differentiate between a PU signal and other CR users' signal provided that all the signals exhibit different cyclic features, which is usually the case. However, the complexity of the cyclic feature detector comes from the facts that it requires the knowledge of different signal's modulation formats, as well as requires long observation times. These complexities make the feature detector implementation less favorable as compared to energy detector [5], [24].

Wavelet based sensing, which is studied in this work, is shown to fall under the category of Energy Detection. A summary of these approaches is displayed in Figure 2.3.

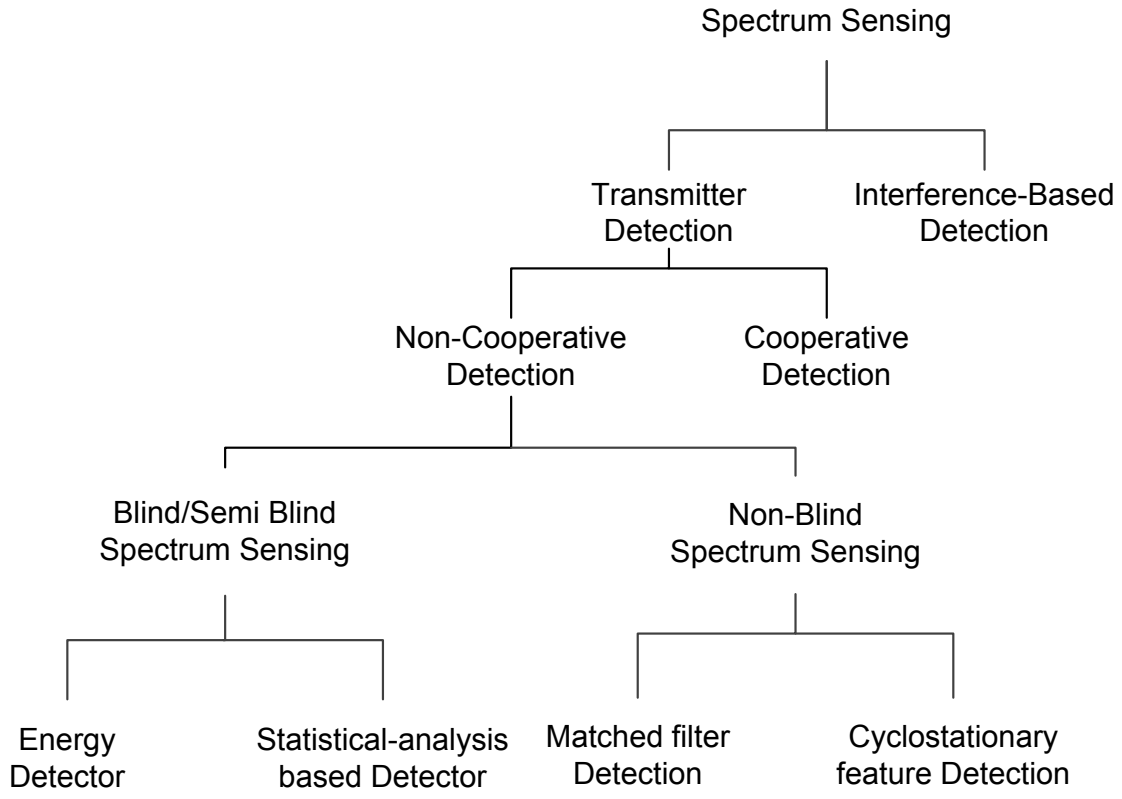

Figure 2.3: Classification of spectrum sensing techniques

2.1 Energy Detection using Frequency Domain Analysis: Wavelet-based Sensing

When the targeted frequency band is narrowband, the radio system front end can be implemented using tunable narrowband Band-Pass Filters (BPF). However, when the spectrum utilization is high, one needs to sense a wideband spectrum in order to detect efficiently spectrum whitespaces. Under this scenario, it is inefficient to install multiple narrowband BPFs at the radio front-end to perform the sensing task. Alternatively, if only

one narrowband BPF is used to scan the entire wideband (frequency range) in blocks, this becomes time consuming hence reducing the overall performance of the cognitive radio.

Observing the fact that a wideband spectrum can be thought of as a sequence of consecutive subbands, where the Power Spectral Density (PSD) within each subband is almost flat and some discontinuities exist at the boundaries of subbands. These discontinuities in the wideband PSD carry key information about the location of boundaries and the potential spectrum holes. A powerful mathematical tool for analyzing signal's local singularities is the *Wavelet Transform*, which can be used to extract information about edges in the signal spectrum [25]. In our case, edges in the wideband PSD refer to the boundaries of two consecutive subbands of different power levels within the wideband of interest. After the identification of subbands, energy is estimated for each of these, which carries important information on spectrum holes available for opportunistic sharing. This idea of using Wavelet Transform on the received wideband signal's PSD was first proposed by Tian and Giannakis [26]. In the following section, we briefly introduce the theory of Wavelet Transform and its application to spectrum sensing for cognitive radios. We highlight the shortcomings of the original Wavelet approach to spectrum sensing [26], and later, in chapter 3, this idea is further investigated with several enhancements.

2.1.1 Wavelets: A Robust Tool for Processing Non-stationary Signals

Wavelets are simply a set of basis functions. A wavelet is effectively a limited-duration waveform that has an average value of zero. The Wavelet Transform (WT) is a mathematical tool used for projecting signals, similar to other tools that are used for signal analysis, e.g., Fourier Transform (FT). Fourier analysis is perhaps the most well-known transformation to date, which transforms a time-domain signal into the frequency-amplitude representation of the signal. The FT provides the global information on frequencies presented in the signal regardless of the exact time they appear in the signal. When looking at a Fourier transform of a signal, it is impossible to tell when a particular event has happened. This property, on one hand, does not negatively affect the suitability of FT to *stationary signals*, but, on the other hand, makes the FT unsuitable when the signal being analyzed is *non-stationary*. For analyzing non-stationary signals, a transformation technique that can provide time-frequency information is necessary. Instead of the traditional FT transformation, we focus here on the Wavelet Transform. While the FT provides information only about the frequency components contained in a signal, the Wavelet Transform provides both time and frequency or time and scale representation of a signal under analysis.

The bases of the Fourier Transform are time-unlimited sinusoidal waves; they extend from $-\infty$ to $+\infty$. Also sine waves are predictable and smooth, as compared to wavelet functions which tend to be rough and anti-symmetric. (Figure 2.4)

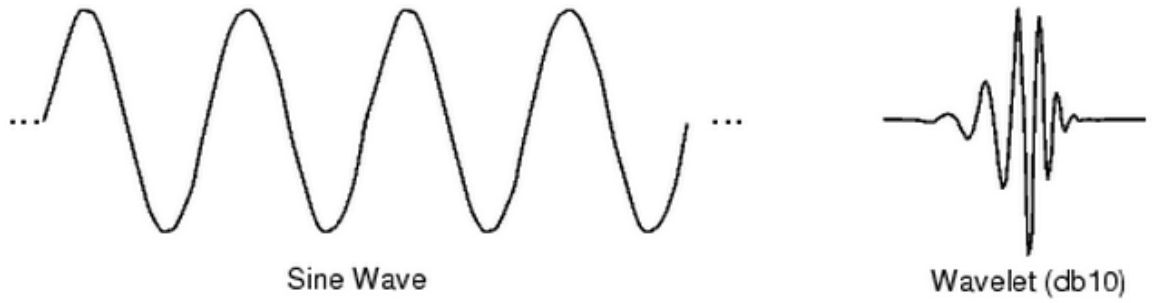

Figure 2.4: Comparison of Fourier transform and Wavelet transform basis functions

While the FT is a process of decomposing a signal into sine waves of different frequencies, the Wavelet Transform decomposes the signal into shifted and scaled versions of the original (or mother) wavelet. Since a wavelet is an irregular (or anti-symmetric) wave, it is better suited for analyzing signals with local singularities (or sharp edges) than the more regular sinusoids.

2.1.2 The Continuous Wavelet Transform

The Continuous Wavelet Transform (CWT) of a signal, *s(t)*, is defined as the sum over all times of the signal multiplied by scaled and shifted versions of a mother wavelet function $\psi(t)$. Mathematically, the CWT of a finite energy signal, *s(t)*, is defined as [27]:

$$C(a,b) = \int_R s(t)\frac{1}{\sqrt{a}}\psi\left(\frac{t-b}{a}\right)dt, \quad a \in R^+, b \in R, s \in L^2(R) \qquad (2.1)$$

where $C(a,b)$ are the continuous wavelet transform coefficients and a is a positive scaling parameter, and b denotes the amount of time-shift. The result of this transformation is a scale-position or scale-time representation $C(scale, time)$. The inverse CWT can be used to recover the original signal $s(t)$.

To recover the original signal from its CWT coefficients, the Inverse Continuous Wavelet Transform is used, and is defined by:

$$s(t) = \frac{1}{K_\psi} \int_{R+} \int_{R} C(a,b) \frac{1}{\sqrt{a}} \psi\left(\frac{t-b}{a}\right) \frac{da \quad db}{a^2}, \tag{2.2}$$

where K_ψ is a constant depending on ψ.

It is important to understand the difference between the CWT and its discrete counter-part, the Discrete Wavelet Transform (DWT).

The CWT can operate at any arbitrary scale. We can control the range of scales at which we would like to compute wavelet coefficients. The scales can range from one up to some maximum value determined depending on the level of details needed and the application of interest.

2.1.3 The Discrete Wavelet Transform

In contrast with the CWT, the Discrete Wavelet Transform (DWT) calculates wavelet coefficients at specific set of scales. When the scales and positions are expressed as powers of two, we call these *dyadic scales* and *dyadic positions*. In this way, DWT is less

computationally expensive than the CWT, yet as accurate. Mathematically, it can be defined after discretizing Equation (2.1) by limiting a and b to a discrete lattice ($a = 2^j, b = k2^j, (j,k) \in Z^2$):

$$C(j,k) = \int_R s(t)\psi_{j,k}(t)dt, \qquad (j,k) \in Z^2, s \in L^2(R) \tag{2.3}$$

where $C(j,k)$ are the discrete wavelet transform coefficients. $\psi_{j,k}(t)$ are the wavelet basis functions or wavelet expansion functions, which are related to the original mother wavelet function $\psi(t)$ as follows:

$$\psi_{j,k}(t) = 2^{-j/2}\psi(2^{-j}t - k) \tag{2.4}$$

where j and k are the dilation and translation parameters, respectively.

To reconstruct the original signal, the Inverse Discrete Wavelet Transform (IDWT) is given by:

$$s(t) = \sum_{j \in Z}\sum_{k \in Z} C(j,k)\psi_{j,k}(t) \tag{2.5}$$

2.1.4 Implementation of the Wavelet Transform

An efficient scheme for implementing the wavelet transform using filters was introduced by Mallat in [28] and is classically known as a *two-channel subband coder* [29]. This method provides a fast implementation of the wavelet transform.

2.1.4.1 The Dyadic Wavelet Decomposition

The wavelet decomposition is composed of low-pass and high-pass filters. The signal of interest is fed into both of these filters. The output of the filters is followed by dyadic decimation. Finally, the resulting coefficients are called *approximations* and *details*, respectively. The approximation coefficients (that correspond to the low-pass filter) are the high-scale, low-frequency components of the input signal, whereas the detail coefficients (that correspond to the high-pass filter) are the low-scale high-frequency components of the input signal. The wavelet decomposition at the first step is illustrated in Figure 2.5.

In Figure 2.5, the input signal *s* is fed into the two complementary filters and the outputs are the approximation coefficients, cA_1, and the detail coefficients, cA_2. The wavelet decomposition can be continued iteratively where at each level of decomposition; the approximations are decomposed into the next level's approximation and detail coefficients. This process leads to the analysis of the signal by decomposing it into several low resolution components and can be represented as the *wavelet decomposition tree*. (Figure 2.6)

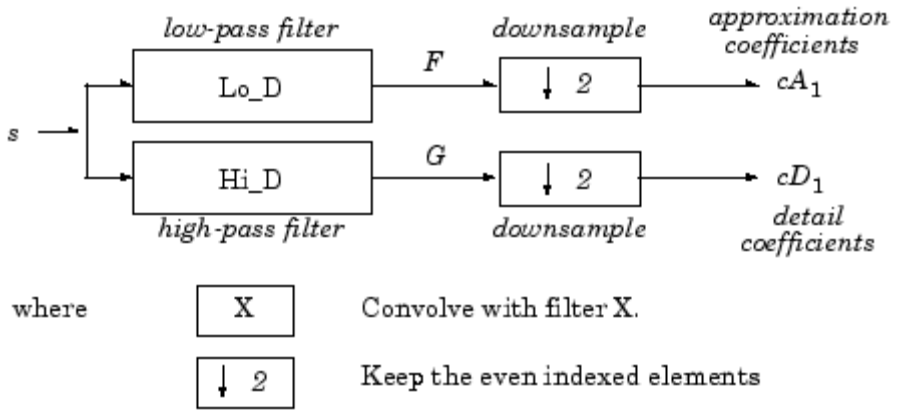

Figure 2.5: First step of wavelet decomposition.

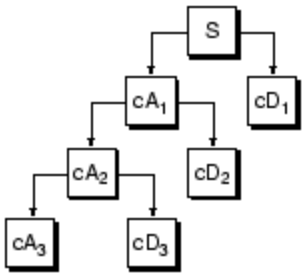

Figure 2.6: Multiple-Level wavelet decomposition.

As mentioned before, non-stationary signals can be best dealt with the wavelet transform. In addition to that, an attractive property of the WT is its ability to perform local analysis of a larger signal, and to detect singularities (discontinuities) in the signal. This property of WT can be used in edge detection [30] and is the focus of the next section.

2.1.5 Edge Detection using Wavelets

In a certain wideband spectrum, wireless signals from the licensed users shall exist together in their assigned non-overlapping frequency bands with possibly non-similar Powers, which give rise to edges in the received wideband signal's PSD. It was this observation that motivated Tian and Giannakis [26] to reformulate the problem of spectrum sensing as an edge detection problem. Note that this view of spectrum sensing deals with the problem in frequency domain. Although, the traditional applications of Wavelets are in time domain and spatial domain (image processing), in this problem, the Wavelet is applied in the frequency domain (PSD). As a consequence, the noise component in this problem has different behavior from that in conventional wavelet applications.

In this section, the original edge detection method [26] is described in brief, then we move to our contribution.

Suppose that the radio signal received at the CR has N frequency bands; the range being sensed by the CR is supposed to have a total of B Hz in the interval $[f_0, f_N]$. The CR is only aware of the wideband boundaries, i.e., f_0, and f_N. The intermediate frequency boundaries and PSD levels are to be identified and detected, which are located at $f_0 < f_1 < \ldots < f_N$. The n^{th} subband is thus defined by $B_n = [f_{n-1}, f_n]$. To simplify the model, the PSD in each frequency band is assumed to be flat. (See Figure 2.7)

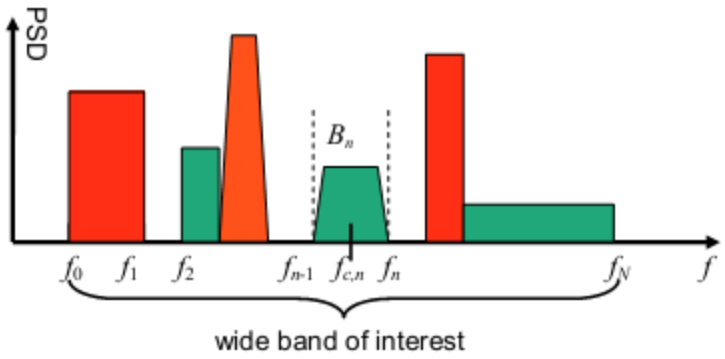

Figure 2.7: Wideband of interest containing subbands with flat PSDs

At a certain time burst, the wideband received signal *r(t)* corrupted with white Gaussian noise (WGN) at the CR front-end will have a certain PSD, which can be mathematically represented as:

$$S_r(f) = \sum_{n=1}^{N} \alpha_n^2 S_n(f) + S_w(f), \quad f \in [f_0, f_N] \tag{2.6}$$

Where α_n^2 represents the PSD of the n^{th} band B_n, $S_n(f)$ denotes the normalized PSD, and $S_w(f) = N_0/2$ is the two-sided noise PSD. Based on these assumptions, the observed wideband signal PSD will exhibit discontinuities, as shown in Figure 2.7. These discontinuities correspond to the frequency boundaries $\{f_n\}_{n=1}^{N-1}$, which are to be detected. It will be shown later in this section that the identification of these boundaries can be performed using the *wavelet transform*.

After identifying $\{f_n\}_{n=1}^{N-1}$, the PSD level within each subband is averaged using:

$$\beta_n = \frac{1}{f_n - f_{n-1}} \int_{f_{n-1}}^{f_n} S_r(f) df \tag{2.7}$$

As in [26], we will assume that there will always be an empty band present in our targeted wideband spectrum such that we can calculate the noise PSD from it. This noise floor is denoted by $\beta_{n'} = N_0/2$. For all other identified subbands, the PSD α_n^2 will be given as:

$$\hat{\alpha}_n^2 = \beta_n - \min_{n'} \beta_{n'}, \qquad n = 1, \dots, N \tag{2.8}$$

Now let's start by discussing the work of Tian and Giannakis [26] in using wavelets to identify the different frequency boundaries $\{f_n\}_{n=1}^{N-1}$.

Define $\varphi(f)$ to be a wavelet smoothing function. The dilation of the wavelet smoothing function $\varphi(f)$ by a scale factor *s* is given by:

$$\varphi_s(f) = \frac{1}{s}\,\varphi\left(\frac{f}{s}\right) \tag{2.9}$$

The CWT of $S_r(f)$ is defined as the convolution of the observed signal PSD with the wavelet function:

$$W_s S_r(f) = S_r * \varphi_s(f) \tag{2.10}$$

Assuming that $\varphi(f)$ is a function with compact support, the result of the convolution in (2.10) depends mainly upon the values of $S_r(f)$ in association with the specific scale used. Hence, $W_s S_r(f)$ will provide information on the local structure of $S_r(f)$. It is well understood that irregularities of a function can be well represented by its derivatives, therefore, the derivative of $S_r(f)$ smoothed by the scaled wavelet $\varphi_s(f)$ will provide the required information, and is expressed as:

$$W_s' S_r(f) = s \frac{d}{df} (S_r * \varphi_s)(f) \tag{2.11}$$

So, the local modulus maxima $W_s' S_r(f)$ (i.e., canny edge detection) represent the edges in the PSD $S_r(f)$. More formally, the identification of frequency boundaries $\{f_n\}_{n=1}^{N-1}$ can be expressed as:

$$\widehat{f_n} = maxima_f \{|W_s' S_r(f)|\}, \quad f \in [f_0, f_N] \tag{2.12}$$

For the scale factor *s*, dyadic scales have been used in [26], i.e., $s = 2^j, j = 1, 2, \dots, J$.

An improvement of the above method has also been discussed in [26] by observing the fact that at different dyadic scales, the information on edges of a signal is distinct. With small scales, even the finer edges will appear in result which might represent edges due to noise, while with the large scale, only the significant edges remains. Hence, with the goal of suppressing the noise-induced spurious local maxima (which are random at each scale), multiscale product was proposed. It is defined as:

$$U_J S_r(f) = \prod_{j=1}^{J} W'_{s=2^j} S_r(f) \tag{2.13}$$

The method provides the estimation of frequency edges $\{f_n\}$ of interest, by picking the maxima of the multiscale product in (2.13). The noise-induced spurious local maxima of $|W_s' S_r(f)|$ are random at every scale and tend not to propagate though all *J* scales; hence, they do not show up as the local maxima of $|U_J S_r(f)|$ and peaks are enhanced due to edges while noise is suppressed:

$$\widehat{f_n} = maxima_f \{|U_J S_r(f)|\}, \quad f \in [f_0, f_N] \tag{2.14}$$

2.1.6 Simulation Results: Wavelet Detection

In this section, we discuss the performance of the spectrum sensing algorithm developed in Section 2.1.5.

Figure 2.8 shows the simulated received signal's PSD $S_r(f)$ at a certain time burst. Here the wideband of interest is in the range of [0, 250] MHz.

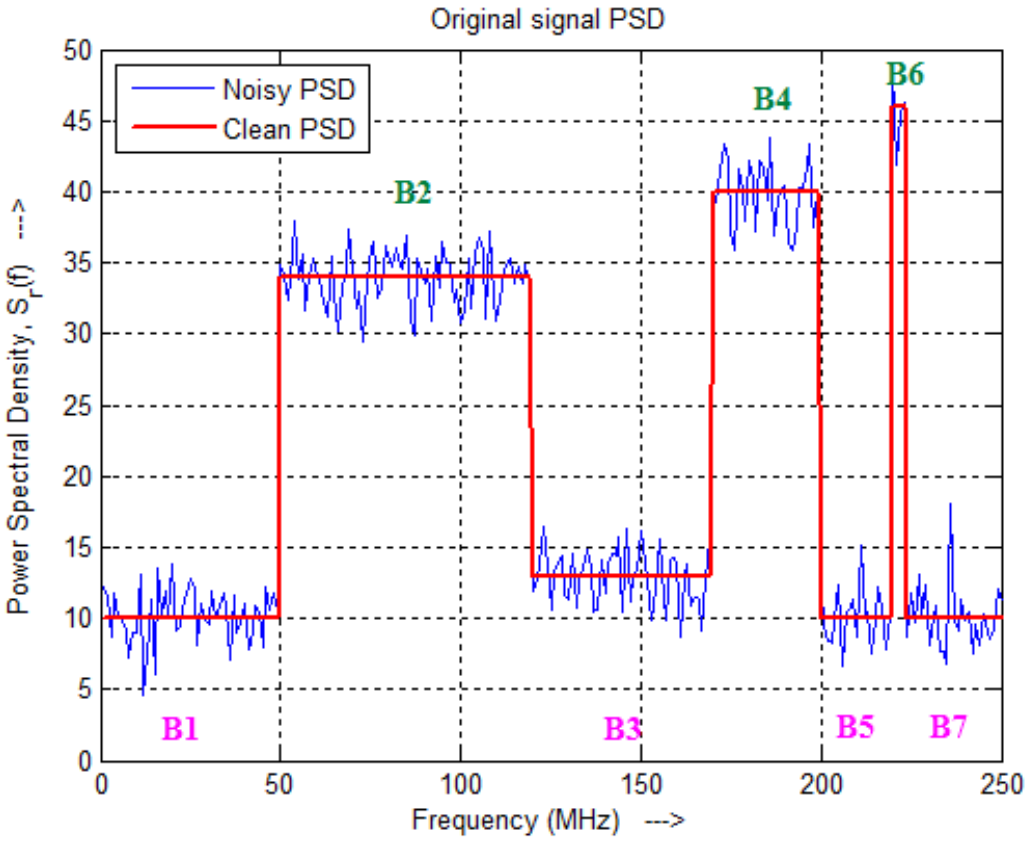

Figure 2.8: Observed signal's PSD

In this experiment, we assumed the PSD of the noise floor to be $S_w(f) = 10$. The CR is only aware of the extreme-end boundaries of the wideband spectrum, i.e., $f_0 = 0$ and $f_N = 250$. The number of subbands N and their locations within the wideband is unknown to the CR. At the observed time burst, it can be seen that there are a total of $N = 7$ bands $\{B_n\}$, with frequency boundaries located at $\{f_n\}_{n=1}^{N-1=6} = [50, 120, 170, 200, 220, 224]$. Within these bands B_2, B_4, and B_6 have relatively high signal PSD at levels 24, 30, and 36, respectively, while B_3 has a very low level of 3, all with reference to $S_w(f) = 10$. The rest three bands, B_1, B_5, and B_7, are empty bands and can be thought of as spectrum holes.

An important issue not fully discussed in [26] is that of PSD-disturbance due to noise is neglected at the receiver. In Figure 2.8, there are two types of signal PSDs shown: Clean PSD and Noisy PSD. The Clean PSD represents the ideal PSD which, based on our initial assumption, should have flat behavior within each band. However, it's a well-accepted fact that we can't avoid certain types of noise that arises due to electronic components of the communication system, thermal, or Johnson noise for example. This random noise is characterized by a Gaussian distribution [31]. Some famous manufacturers of spectrum analyzers have reported in their data sheet that the Absolute Amplitude Accuracy of their devices is within $\pm$ 0.4 dB $= (1.1)_{\text{linear}}$ [32], [33]. To be more conservative, in our simulations, we have kept a standard deviation of this Gaussian disturbance at $\sigma = 2$.

In order to detect edges in the PSD of Figure 2.8, the Gaussian wavelet (Figure 2.9) along with four dyadic scales $s = 2^j, j = 1, 2, 3, 4$, was used [26]. Figure 2.10 illustrates the results of wavelet modulus as computed from (2.11). The four graphs in Figure 2.10 correspond to the WT coefficients at four different scales mentioned above.

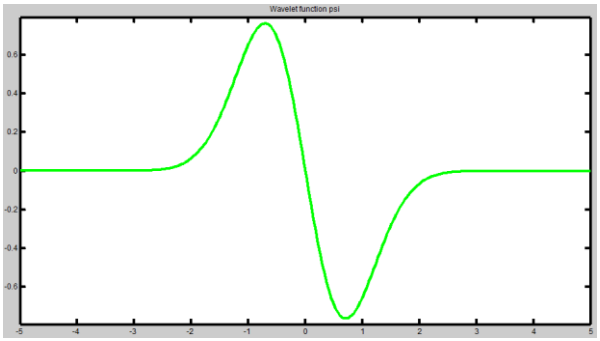

Figure 2.9: Gaussian wavelet

The values of the wavelet coefficients are much higher at locations where there was frequency edges in the received signal's PSD $S_r(f)$. The information about the edges in PSD $S_r(f)$ have been captured by the wavelet transform in all curves, except the last one where the relatively narrowband B_6 was not detected at scale $s = 2^4 = 16$. This is because; the wavelet at higher scales corresponds to the most "stretched" wavelets. The more stretched the wavelet, the longer the portion of the signal with which it is being compared, and thus the coarser the signal features being measured by the wavelet coefficients. This can be clearly observed in Figure 2.10, as the scale 2^j increases the wavelet transform becomes smoother, ignoring the rapid fluctuations due to noise disturbance.

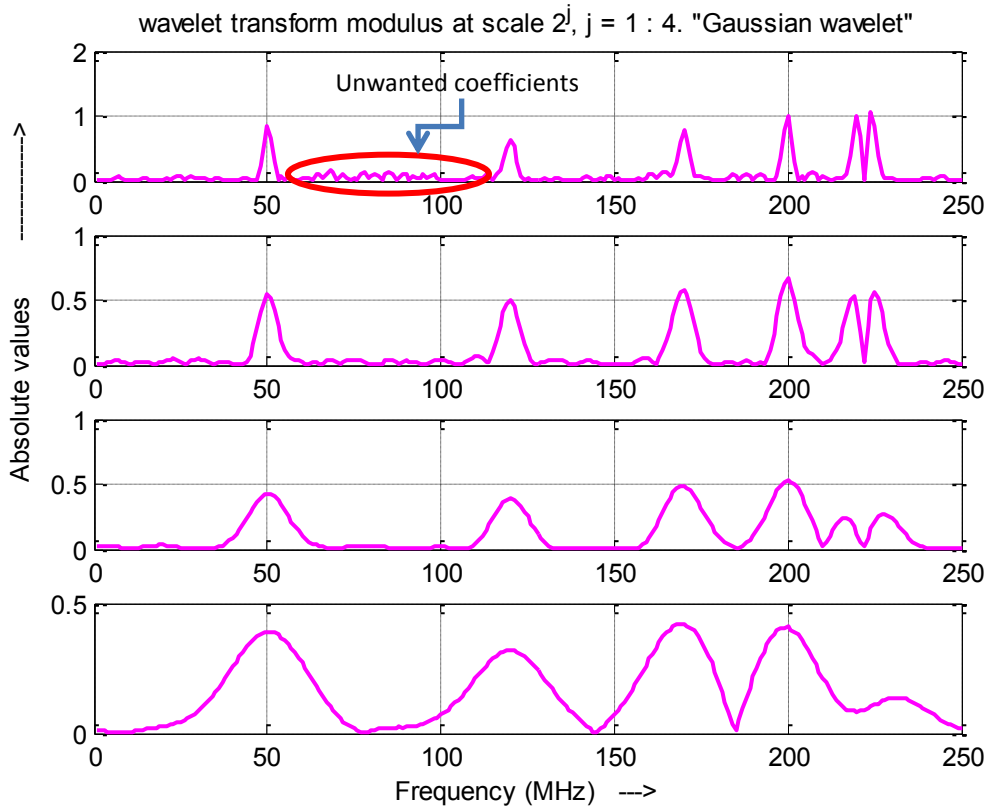

Figure 2.10: Wavelet transforms modulus at scales *s = 2^j, j = 1, 2, 3, and 4*. (Top-bottom)

As mentioned in Section 2.1.5, an improvement would be observed when integrating *multi-scales* of wavelet transforms, defined as in Equation (2.13). Let us now consider Figure 2.11. The first curve shows the wavelet transform at scale $s = 2^1$, while the other three depict the multi-scale products of wavelet transforms at different scales. P12 represents a curve that is a result of the wavelet transform coefficients' product at scales $s = 2^1$ and $s = 2^2$. Similarly, P123 and P1234 are the products of the respective scales.

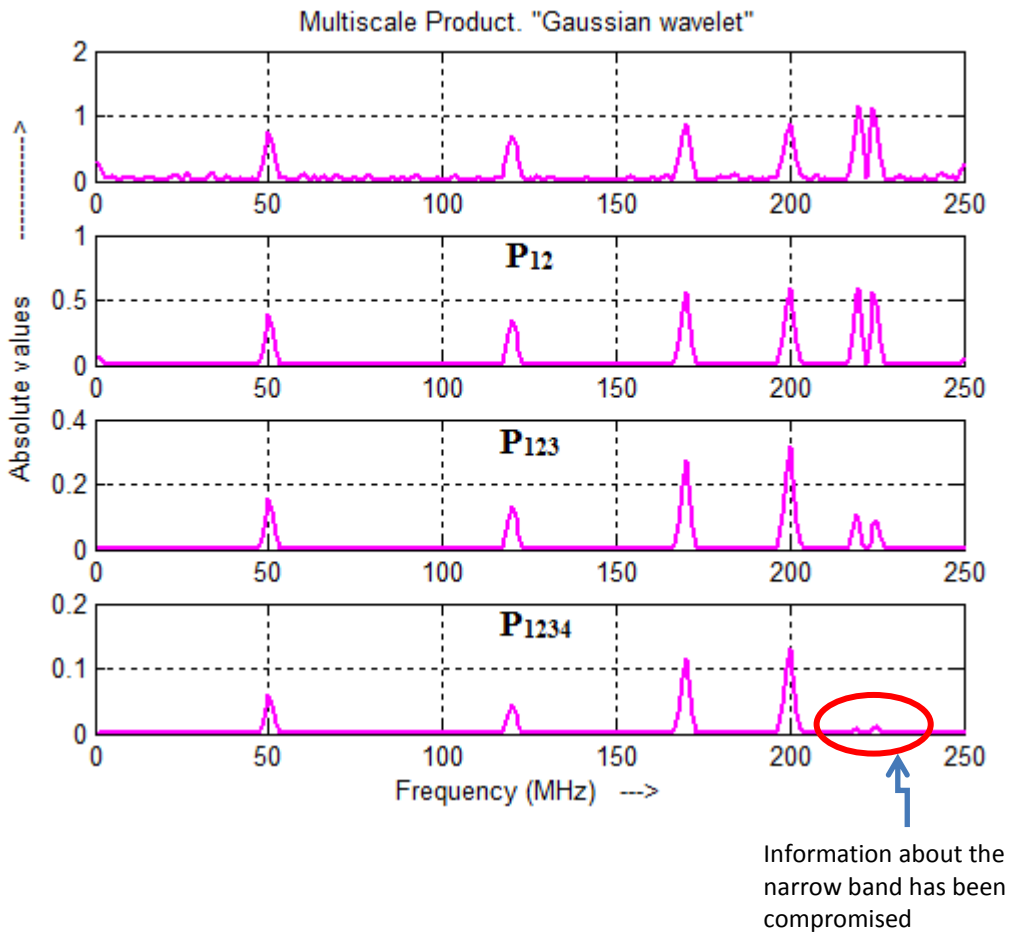

Figure 2.11: Multi-scale products using the wavelet transform coefficients, at scales $s = 2^j$, $j = 1, 2, 3,$ and 4 (Top-bottom), of Figure 2.10.

The figures show that, the multi-scale product method effectively suppresses the spurious local extrema caused by noise. Consequently, there will be an improvement in detecting the edges in the PSD of Figure 2.8. However, the graph P1234 shows that, as a result of multi-scale product, the information about the narrow band (B_6) has also been compromised.

In order to calculate the PSD within each frequency band B_n, α_n^2, equation (2.8) was discussed in [26]. However, we would need the exact location of frequency boundaries to

be able to use (2.8) and (2.7). The wavelet transform coefficients' curves shown above do not only contain peaks due to frequency edges $\{f_n\}$, but also other peaks due to noise disturbance in the received signal's PSD $S_r(f)$. Even with the multiscale product operation, the noise coefficients do not reduce to zero. The issue of how to distinguish between the true peaks, due to frequency edges $\{f_n\}$, and the noise-induced spurious local maxima has not been discussed in [26]. We will introduce a method to deal with this issue in chapter 3. For the sake of completion, we will also discuss in the next section Energy Detection which is of fundamental importance in deriving our own algorithm (chapter 3 and 4)

2.2 Energy Detection using a Time Domain approach

Instead of transform-domain analysis, let us discuss in more details the problem of spectrum sensing in time domain. One of the most common techniques used in time domain is Energy Detection. As mentioned before, when a cognitive radio receiver does not have any prior knowledge on the primary user's signal and the only thing that is known is the power of the random Gaussian noise, then the optimal solution in terms of implementation is an Energy Detector (ED) [11]. The idea of determining the presence of unknown deterministic signals using Energy Detector was first reported by Urkowitz in his work [12]. Figure 2.12 depicts a simple block diagram of an energy detector.

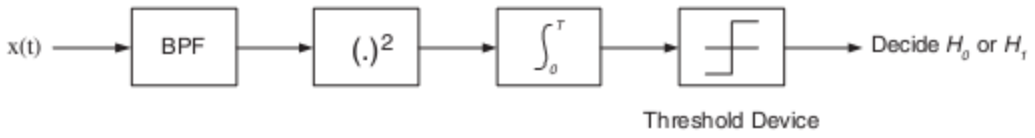

Figure 2.12: Example of energy detector

The observed signal *x(t)* is fed to a band-pass filter which limits the bandwidth to *W* and selects some center frequency f_c. Following the BPF, squaring device and an integrator of a certain observation interval, *T*, are used. Finally, the measured energy from the integrator is compared to a pre-threshold, λ, and a decision about the presence or the absence of the primary user is made. The value of the threshold λ depends mainly upon the noise variance [34].

The input signal *x(t)* can have several possible forms based on whether the primary user is present or absent, which we denote by hypotheses H_1, and H_0, respectively:

$$x(t) = \begin{cases} n(t), & H_0 \\ h \times s(t) + n(t), & H_1 \end{cases} \tag{2.15}$$

where *s(t)* represents the primary user's signal, *h* is the channel gain, and *n(t)* is modeled as AWGN.

In Figure 2.12, the output of the integrator is effectively the decision statistic, which we will represent by *Y*. In order to analyze the performance of the above mentioned energy detector, the statistical distribution of *Y* has to be known under both hypotheses. Following the original work of Urkowitz [12], we understand that the decision statistic *Y* will have the following distributions:

$$Y \sim \begin{cases} \chi^2_{2TW}, & H_0 \\ \chi^2_{2TW}(2\gamma), & H_1 \end{cases} \quad (2.16)$$

where χ^2_{2TW} denotes a central chi-square distribution and $\chi^2_{2TW}(2\gamma)$ denotes a non-central chi-square distribution, both with the same degrees of freedom, i.e., *2TW* (*TW* is the time-bandwidth product). The non-central chi-square distribution has a non-centrality parameter of 2γ, where γ is the receiver SNR (cognitive radio). For simplicity, we denote the time-bandwidth product as $u = TW$, and assume that T and W are chosen such that u has an integer value.

Figure 2.13 depicts the two regions, H_0 and H_1, separated by a single threshold λ. This threshold divides the decision as either present if the observed energy is above the threshold (hypothesis H_1 is true), or otherwise absent (hypothesis H_0 is true).

Figure 2.13: Energy detection with one threshold

The performance of the energy-detector based spectrum sensing is established mainly on two parameters, namely, probability of misdetection P_m and probability of false alarm P_f. If the CR decides an absence while the PU is present; this error is represented with the probability of misdetection P_m, which would cause a substantial interference at the PU. On the other hand, if the CR decides a presence while the PU is absent, the SU would miss a spectrum usage opportunity; a phenomenon represented by the probability of false

alarm P_f. Jointly, the probability of misdetection P_m and the probability of false alarm P_f define what is called *Complementary Receiver Operating Characteristics (C-ROC)*. Sometimes instead of P_m, we use the probability of detection P_d which is related to P_m as 1- P_m. Probability of detection P_d defines the probability with which the CR will detect the presence of PU, given the PU is actually active. These parameters can generally be evaluated as:

$$P_m = Pr(Y < \lambda | H_1) \tag{2.17}$$

$$P_f = Pr(Y > \lambda | H_0) \tag{2.18}$$

$$P_d = 1 - P_m = Pr(Y > \lambda | H_1) \tag{2.19}$$

where, as before, λ is the decision threshold. The plot of P_d vs. P_f is called *Receiver Operating Characteristics (ROC)*.

There is always a trade-off between P_d (or P_m) and P_f. As illustrated in Figure 2.14, we can have two distinct PDFs of a received signal, corresponding to two possible hypotheses, H_0 and H_1. By varying the threshold, we can control the two type errors, namely, P_m and P_f. If the threshold is kept excessively low, P_m decreases at the expense of increased P_f. A high P_f implies spectrum inefficient utilization because of high false alarms. Alternatively, if the threshold is set needlessly high, we can reduce P_f at the cost of increasing P_m. A high P_m implies a high probability of interfering while PU is active. Evidently, we cannot reduce both types of error simultaneously. The optimal approach is to use Neyman-Pearson detector [35], where we constrain P_f to a fixed value, and minimize P_m. In other words, we fix the value of P_f, and try to maximize P_d.

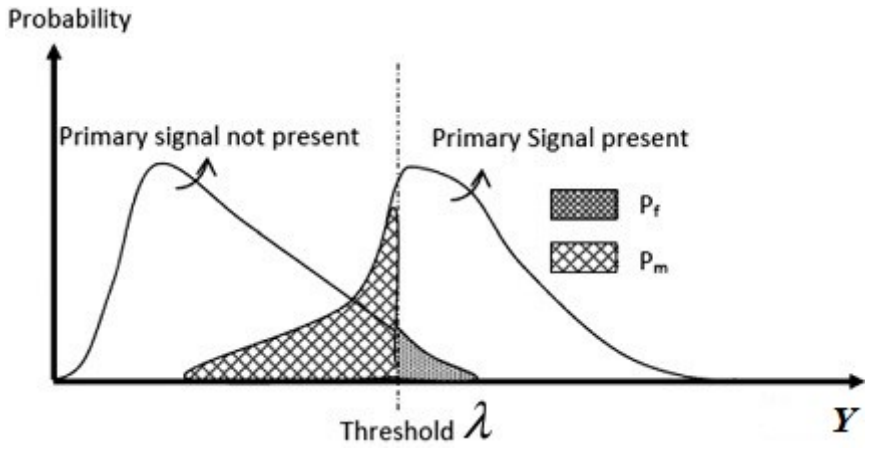

Figure 2.14: Trade-off between P_m and P_f

If we consider no fading, then h will be a constant in equation (2.15). For such AWGN environment, the closed-form expressions for P_d and P_f has been reported in [36] as:

$$P_{d\ AWGN} = Q_u\left(\sqrt{2\gamma}, \sqrt{\lambda}\right) \tag{2.20}$$

where $Q_u(a, b)$ is the generalized Marcum Q-function [37], and

$$P_f = \frac{\Gamma\left(u, \frac{\lambda}{2}\right)}{\Gamma(u)} \tag{2.21}$$

where $\Gamma(.,.)$ and $\Gamma(.)$ are the incomplete and complete gamma function, respectively.

For the case where we assume the channel fading h to be Rayleigh distributed, only the expression for P_d will change. Under Rayleigh fading, the signal-to-noise-ratio (SNR) γ will follow exponential distribution and for this case $P_{d\ Ray}$ is shown to be derived as [36]:

$$P_{d\,Ray} = e^{-\frac{\lambda}{2}} \sum_{n=0}^{u-2} \frac{1}{n!} \left(\frac{\lambda}{2}\right)^n + \left(\frac{1+\bar{\gamma}}{\bar{\gamma}}\right)^{u-1} \left[e^{-\frac{\lambda}{2(1+\bar{\gamma})}} - e^{-\frac{\lambda}{2}} \sum_{n=0}^{u-2} \frac{1}{n!} \frac{\lambda\bar{\gamma}}{2(1+\bar{\gamma})} \right] \quad (2.22)$$

where $\bar{\gamma}$ is the average received SNR. Since P_f is considered when there is no signal present and as such is independent of SNR γ, therefore, its expression remains the same as in (2.21) for the cases of fading and non-fading channels [36].

2.2.1 Cooperative Communications for Cognitive Radio Networks

As with any wireless communication system, the performance degrades in multipath fading channels. One way to overcome the effects of multipath fading is to use multiple antennas to improve performance [38]. Similarly, fading in wireless channels creates uncertainty in the SNR at the CR receiver input, making it difficult for the CR to provide a reliable decision about the absence or presence of the PU, since when the CR is experiencing a deep fading or shadowing due to large obstacles over the primary-to-secondary channel, the amount of energy observed during a fixed time-bandwidth product, *TW*, may not be enough to decide about the presence of a PU. One way to overcome this problem is to increase the amount of local processing which, in the case of energy detector, translates into increasing the time-bandwidth product. The bandwidth *W*

is usually limited to that of the PU's signal, while, the sensing duration T can be controlled at the CR, but it should be kept below a certain value, T_p, to meet the requirements of sensing period set by the regulator [39]. In such a case, the single CR can use a more sophisticated sensing approaches such as feature detection [40], however, feature detection approach requires a priori information about the PU signal characteristics (cyclic frequencies of the PU's signal) which is assumed to be not known in our spectrum sensing model of the problem. From the above discussion, we can see that with only one CR (no diversity), it is almost impossible to achieve simultaneously a very high value for P_d and a very low value for P_f [36]. The fact that the cognitive radio does not have PU's location information just adds to the performance degradation of local sensing. To make the simple energy detection scheme viable, the neighboring secondary users should cooperate [41]. Since the multipath fading statistics fluctuates considerably on the scale of a fraction of wavelength and shadowing fluctuates considerably on the scale of 20-500 m based on the nature of environment, it is highly unlikely that multiple cooperating CRs will experience deep fade and/or large obstacles at the same time [42]. Hence, the cooperation between multiple CRs was proposed by researchers to improve the sensing performance of CROWN [43], [44]. Having neighboring nodes allowed to collaboratively perform the job of spectrum sensing, it was found that collaboration can improve sensing performance [45]-[46], mitigate the stringent sensing requirements [47], and decrease the overall required detection time [48]-[49]. In addition, the use of cooperation can solve hidden primary user problem [50]. The cooperation between multiple CRs can be carried in either a centralized or a distributed fashion (Figure 2.15).

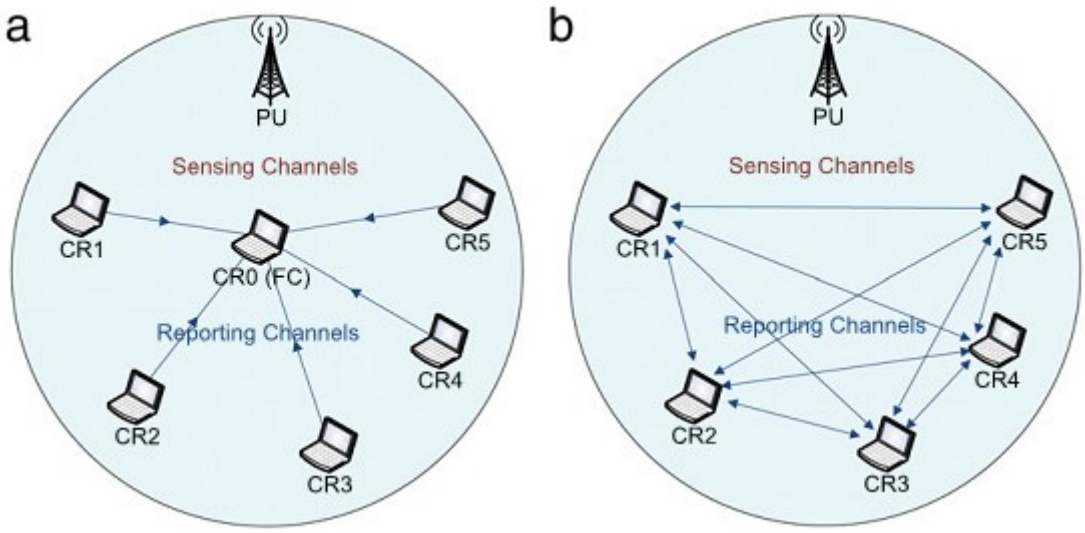

Figure 2.15: Classification of cooperative sensing: (a) centralized, (b) distributed

When a centralized fusion center (CR0 in Figure 2.15 (a)) is used to handle the different cognitive decisions, the cooperative spectrum sensing can be performed in the following manner:

1) All the cooperating cognitive users start by sensing a targeted band independently.
2) Each cooperating node would forward either its local binary decision or it can just send its observation value directly to the fusion center (FC) over the *reporting channel*.
3) Finally, the fusion center fuses all the received data (or decisions) to infer the presence or absence of the PU.

Here, it should be noted that the fusion center [51]-[52] is also recognized in the literature as common receiver [53],[49], master node [54], base station [55], [56], combining node

[57], [58], designated controller [47], etc. As shown in Figure 2.15 (a), CR0 is the FC while CR1-CR5 are the cooperating CR users. When using cooperation among multiple CRs for spectrum sensing, certain protocols need to be defined for the purpose of sharing sensing information over the *reporting channel* (in contrast to the reporting channel, the physical point-to-point connection between the PU and a CR for the purpose of sensing the primary transmitter's signal is called a *sensing channel*). Different architecture for control channels (reporting channels) have been discussed in literature [59]-[60], where the use of ISM band and ultra wide band (UWB) have been proposed. A simple protocol using time division multiple access (TDMA) to share the sensing information with the fusion center is proposed in [61], where the cooperating CRs are divided into clusters based on their geographical location and send their sensing data to the particular cluster head only during the assigned time slots. It is very important to consider that the cooperation mechanism should have as low as possible overhead, and it should be robust to network changes and failures. Also, the amount of delay needs to be minimized for a particular cooperation algorithm. Usually, such type of protocols are defined at Medium Access Layer (MAC) [62].

For simplicity, in the literature, most of the authors assume that the reporting channels are perfect, i.e., the local decisions from the CR users will be reported to the fusion center without any error. Based on whether the CRs are sending their 1-bit binary decision or their observation value to the fusion center, the combination is called either *decision fusion* or *data fusion*, respectively [24]. Instead of using the terms *decision fusion* or *data fusion*, some authors prefer to use *hard combination* and *soft combination*, respectively [42].

2.2.1.1 Cooperative Spectrum Sensing (CSS) Framework

At the physical layer, the framework of the centralized CSS can be represented as shown in Figure 2.16. The framework [44] consists of the PU, cooperating CRs, FC, the RF channels (sensing and reporting channels), and an optional remotely located database.

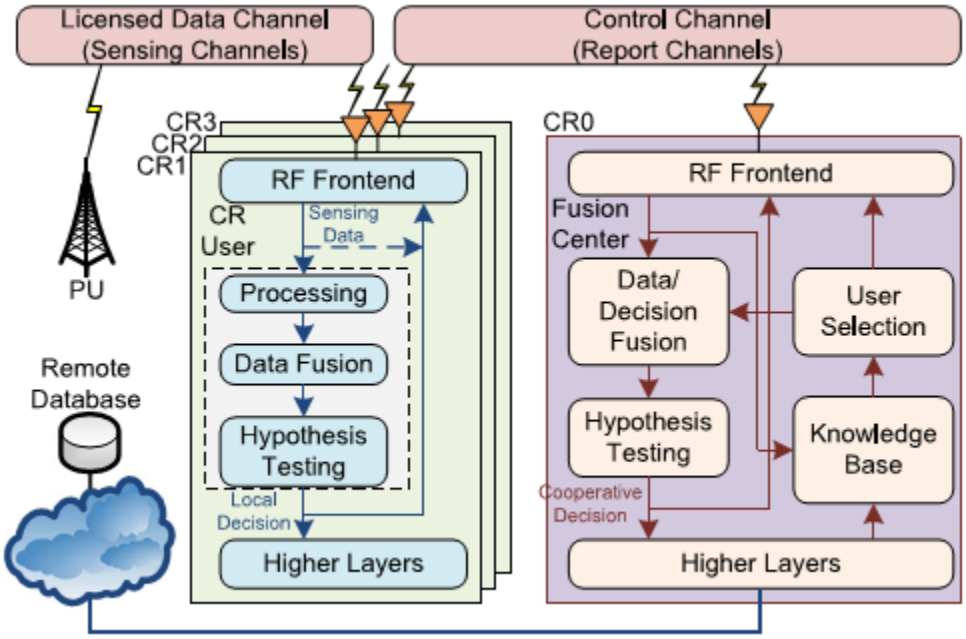

Figure 2.16: Framework of centralized CSS [44].

As shown in the framework, a group of collaborative CRs, presumably independent of each other, perform targeted sensing using their RF frontend. The processing unit of cooperating CRs may include a signal processor, data fusion and hypothesis testing entities, etc. The RF frontend is capable to be configured for data transmission or local sensing. Besides that, analog-to-digital conversion will also be done by the RF frontend. The local observations of the cooperating CRs can directly be transmitted to the FC, or it

can be locally processed to provide a decision to the FC. Usually, certain amount of processing on the local observations is needed to minimize the bandwidth requirement over the reporting channels. The processing may include the evaluation of the energy statistics and thresholds. When the local decision or the observations are ready, a request to a higher layer (e.g., MAC layer) is sent to acquire the access of a control channel. The FC in the centralized CSS framework is a powerful cooperating CR which has all the capabilities as the other CRs. In addition, the FC has other functionalities, such as user selection and knowledge base, to undertake the cooperation tasks successfully. Based on the requirement and the ability of the FC, the FC can be connected to an external (remotely located) database through an ultra-high speed communication medium (e.g., fiber optics). This external database will assist the FC and can provide information regarding the PU activity and white spaces.

2.2.2 Decision-Fusion Criterion

When decision-fusion is used, each CR compares its observed energy value with pre-fixed threshold λ, if the observed value is greater than λ, the reported decision is 1 (H_1), while the reported decision is 0 (H_0) if the value is less than the threshold. After collecting L local 1-bit decisions, the fusion center makes an occupancy-decision based on a certain decision-fusion rule, which can be represented as follows [24]:

$$Z = \sum_{i=1}^{L} D_i \begin{cases} \geq K, & H_1 \\ < K, & H_0 \end{cases} \tag{2.23}$$

If there exists at least *K* out of *L* CRs having their local observation values above the pre-fixed thresholds, then the fusion center will infer presence of the PU, i.e., H_1, otherwise the fusion center will declare that there is no PU signal transmitted, i.e, H_0. Such decision criterion is also called *K-out-of-L* rule [63]. In [39], it was shown that, under the case of distributed individual and independent decisions, the optimum (in terms of detection performance) decision-fusion rule is 1-out-of-*L* rule (i.e., OR rule). Therefore, in the rest of the thesis we shall resort to the OR rule as our final decision-fusion rule. Instead of calculating individual thresholds for each cooperating user, for simplicity, it is assumed that all collaborative cognitive users have the same decision rule (i.e., same threshold λ), according to some fixed cooperative probability of false-alarm, Q_f [10].Then, the overall cooperative probability of detection, probability of false-alarm, and probability of misdetection can be written as [10]:

$$Q_d = 1 - (1 - P_d)^L \tag{2.24}$$

$$Q_f = 1 - (1 - P_f)^L \tag{2.25}$$

$$Q_m = (P_m)^L \tag{2.26}$$

where P_d, P_f, and P_m denotes the individual probabilities of detection and false-alarm, given as (2.19), (2.18), and (2.17), respectively, and *L* is the number of cooperating CR users. It has been shown in [53] that as the number of cooperating users increases, the

cooperative probability of misdetection decreases for a fixed cooperative probability of false-alarm. Sometime the number L is referred to as *sensing diversity order* of cooperative spectrum sensing, since it characterizes the error exponent of Q_m in (2.26).

2.2.3 Data-Fusion Criterion

Alternatively, the fusion center can also exploit the diversity provided by using a data-fusion criterion to determine the occupancy state of the targeted band. In data-fusion, each CR simply reports their original sensing data to the fusion center. Although, data-fusion imposes large amount of communication overhead over the control channel, but it has excellent detection performance [42]. Haykin proposed a data-fusion based cooperative spectrum sensing method in [4], which he called it as *multitaper-method singular-value-decomposition* (MTM-SVD). In the MTM-SVD, the L cooperating CR users cooperatively estimate the interference temperature of the radio environment. Each cooperating CR applies mutitaper method [64] to analyze the spectrum by first computing its k^{th} eigenspectrum for the targeted band as:

$$Y_k^{(l)}(f) = \sum_{n=1}^{N} w_k(n) y_l(n) e^{-i\omega n}, \quad 1 \le k \le K \tag{2.27}$$

where $y_l(n)$ are the observed samples at the l^{th} CR, and $w_k(n)$ represents the k^{th} Slepian sequence [65] that is used for the multitaper spectral analysis. The next step is to for each CR is to send its eigenspectrum vector

$$\boldsymbol{Y}_l(f) = \left(Y_1^{(l)}(f), Y_2^{(l)}(f), \ldots, Y_K^{(l)}(f)\right), \quad 1 \le l \le L \tag{2.28}$$

to the fusion center. Based on such vectors from each of the L cooperating CRs, the fusion center computes an $L \times K$ eigenspectrum matrix as:

$$\boldsymbol{A}(f) = \begin{bmatrix} w_1 Y_1^{(1)}(f) & w_1 Y_2^{(1)}(f) & \ldots & w_1 Y_K^{(1)}(f) \\ w_2 Y_1^{(2)}(f) & w_2 Y_2^{(2)}(f) & \ldots & w_2 Y_K^{(2)}(f) \\ \vdots & \vdots & \ddots & \vdots \\ w_L Y_1^{(L)}(f) & w_L Y_2^{(L)}(f) & & w_M Y_K^{(L)}(f) \end{bmatrix} \tag{2.29}$$

where w_l are the weights of l^{th} CR which is computed after taking into consideration the instantaneous environment information into account. Each row in ***A(f)*** corresponds to the eigenspectrum vector from a particular CR. If the primary user is present, the eigenspectrum vector consists of the PU signal plus noise. The noise is independent for the distributed CRs, while there will be a correlation in the PU signal part. Observing this fact, the MTM-SVD scheme exploits the correlation due to the PU signal by applying SVD to the eigenspectrum matrix (2.29):

$$\boldsymbol{A}(f) = \sum_{k=1}^{K} \sigma_k(f) \boldsymbol{u}_k(f) \boldsymbol{v}_k^H(f) \tag{2.30}$$

where $\sigma_k(f)$ is the k^{th} singular value of $\boldsymbol{A}(f)$, $\boldsymbol{u}_k(f)$ and $\boldsymbol{v}_k(f)$ are the associated left and right singular vectors, respectively. Finally, the fusion center takes the spectrum occupancy decision based on the largest singular value of the matrix $\boldsymbol{A}(f)$. This method (MTM-SVD) provides a means for cooperative spectrum sensing to estimate the presence or absence of the primary user with high accuracy [4], [42].

For the MTM-SVD scheme described above, the complexity of the whole procedure is quite high. Not only sending the K-dimensional vector from each CR to the fusion center would increase lots of communication burden over the reporting channel, but the SVD operation on the matrix $\boldsymbol{A}(f)$ is also computationally very expensive.

Eigenvalue based cooperative spectrum sensing has also been proposed in [66]. In [66], the authors have used the eigenvalue based approach originally proposed in [13]. Observing the fact that the statistical covariance matrix of the observed signal will have different characteristics based on whether the PU is present or not, the authors in [13] have proposed an eigenvalue decomposition based approach. In this approach, the sample covariance matrix is computed from the observed signal's samples. Then the maximum eigenvalue (MEV) of the sample covariance matrix is calculated and the value is compared with a threshold to decide about the spectrum availability. Authors in [66] used the approach of [13] in a cooperative fashion where each cooperating CR user performs the eigenvalue decomposition of the sample covariance matrix, and the MEV is computed. This MEV is compared with prefixed two-thresholds to decide about the reliability of the cooperating CRs. The CRs with reliable decision sends their decision to the fusion center, where the non-reliable ones send directly their MEVs to the fusion center. Finally, the fusion center fuses all the data to decide about the occupancy state of the spectrum. Although, the eigenvalue based spectrum sensing technique provides very good results without any prior knowledge about the channel, noise power, or PU signal, but the whole decomposition process is quite computationally expensive. Also the use of the random matrix theory to set the threshold values makes it difficult to obtain the accurate closed form expression for the thresholds.

In [67], the authors have studied various soft-combination scheme with low-complexity. In these schemes, each CR reports the value of the received energy to the fusion center, and the fusion center takes a decision based on a certain data-fusion (combining) criterion (or diversity combining) rule [68]. In [69], it was shown that, under the case of independent diversity branches, the optimum combining scheme is Maximal Ratio Combining (MRC). However, MRC requires full channel knowledge (amplitude and phase) for all branches. In MRC reception, the received signals $\{x_l(t)\}_{l=1}^{L}$, where L is the number of diversity branches, are first co-phased, weighted proportionately to their channel gain and then summed up to yield a new signal $x_{MRC}(t) = \sum_{l=1}^{L} h_l^* x_l(t)$, where h_l is the channel coefficient of the l^{th} diversity branch. A less complex scheme is the traditional Equal Gain Combining (EGC), which doesn't require channel fading amplitudes estimation, and, under the case of identical and independent diversity branches, provides a comparable detection performance to that of MRC [70], [71]. In EGC reception the received signals $\{x_l(t)\}_{l=1}^{L}$, where L is the number of diversity branches, are co-phased only in each branch and then summed up to yield a new signal $x_{EGC}(t) = \sum_{l=1}^{L} e^{-j\phi_l} x_l(t)$, where ϕ_l is the phase of the l^{th} diversity branch. Since the difference between MRC and EGC is not very large in terms of performance, but in terms of complexity, MRC is more complex than EGC, therefore, in this thesis we shall resort to EGC as our data-fusion rule and assume that a base station has the necessary information to perform EGC of received energy detector outputs. For EGC, the probability of false alarm $P_{f,EGC}$ and probability of detection $P_{d,EGC}$ (in AWGN and Rayleigh fading) is derived as [36], [43]:

$$P_{f,EGC} = \frac{\Gamma\left(Lu, \frac{\lambda}{2}\right)}{\Gamma(Lu)} \tag{2.31}$$

$$P_{d\ AWGN,EGC} = Q_{Lu}\left(\sqrt{2\gamma_t}, \sqrt{\lambda}\right), \tag{2.32}$$

where $u=TW$ (time-bandwidth product) and $\gamma_t = \sum_{l=1}^{L} \gamma_l$.

$$P_{d\ Ray,EGC} = \alpha \left[G_1 + \beta \sum_{n=1}^{Lu-1} \frac{(\lambda/2)^n}{2(n!)} \quad {}_1F_1\left(L; n+1; \frac{\lambda}{2}\frac{L\bar{\gamma}}{L+L\bar{\gamma}}\right) \right], \tag{2.33}$$

where $\alpha = \frac{1}{\Gamma(L)2^{L-1}}\left(\frac{L}{L\bar{\gamma}}\right)^L$, ${}_1F_1(.;.;.)$ is the confluent hypergeometric function, $\beta = \Gamma(L)\left(\frac{2L\bar{\gamma}}{L+L\bar{\gamma}}\right)^L e^{-\lambda/2}$, and

$$G_1 = \frac{2^{L-1}(L-1)!}{\left(\frac{L}{L\bar{\gamma}}\right)^L} \frac{L\bar{\gamma}}{L+L\bar{\gamma}} e^{-\frac{\lambda}{2}\frac{L}{L+L\bar{\gamma}}} \left[\left(1+\frac{L}{L\bar{\gamma}}\right)\left(\frac{L}{L+L\bar{\gamma}}\right)^{L-1} \times L_{L-1}\left(-\frac{\lambda}{2}\frac{L\bar{\gamma}}{L+L\bar{\gamma}}\right) + \sum_{n=0}^{L-2}\left(\frac{L}{L+L\bar{\gamma}}\right)^n L_n\left(-\frac{\lambda}{2}\frac{L\bar{\gamma}}{L+L\bar{\gamma}}\right) \right] \tag{2.34}$$

where $L_n(.)$ is the Laguerre polynomial of degree n.

The expression for the probability of detection for EGC scheme, $P_{d,EGC}$, over Nakagami-m fading channels was also derived in previous work [72] for different number of diversity branches. The results presented in [72] can be used to decide about number of

diversity branches needed to achieve a specified false alarm rate for EGC-based cognitive radio. The work was later extended to derive the $P_{d,EGC}$ over correlated non-identical Nakagami-m fading channels in [73]. It was shown that the performance degrades in the presence of higher correlation between diversity branches. Also, in [74] the authors have derived the expression of $P_{d,EGC}$ for the cases of correlated Rayleigh and Rician fading channels by making the use of the decorrelation transformation proposed in [75]. By applying the decorrelation transformation on the correlated diversity branches, the authors in [75] have transformed the system into an alike system of independent diversity branches, hence not losing any performance. Furthermore, analytical expressions of performance for the case of multi-path channels has been derived in [76]. The performance gain due to multipath diversity have been studied, and it was shown that for the case equal power taps, multipath and antenna diversity behaves in the same way and show similar performance. On the other hand, for the case of exponentially decaying power taps, multipath diversity performs worse as compared to an equivalent number of antennas.

For this work, we will confine our analysis to independent and identically distributed AWGN and Rayleigh fading diversity cases. The extension to other channel models may be studied as a future work.

2.2.4 Simulation Results: Energy Detection

In this section, we discuss the performance of the spectrum sensing for the different cases discussed above.

2.2.4.1 Spectrum Sensing without Cooperation

Let us start with a simple case with a single-antenna CR node under AWGN scenario. Figure 2.17 shows the performance of a conventional single-threshold energy detector as ROC. The performance of ED is based on the received SNR; the higher the SNR, the better the detection performance [77]. SNR, γ, and time-bandwidth product, u, are assumed to be 5 dB and 5, respectively. In literature [71], [43], [78], the authors use $u = 5$ as a benchmark to evaluate the performance of ED. Also, $\gamma = 5$ is considered to be a low SNR when $u = 5$ [77].

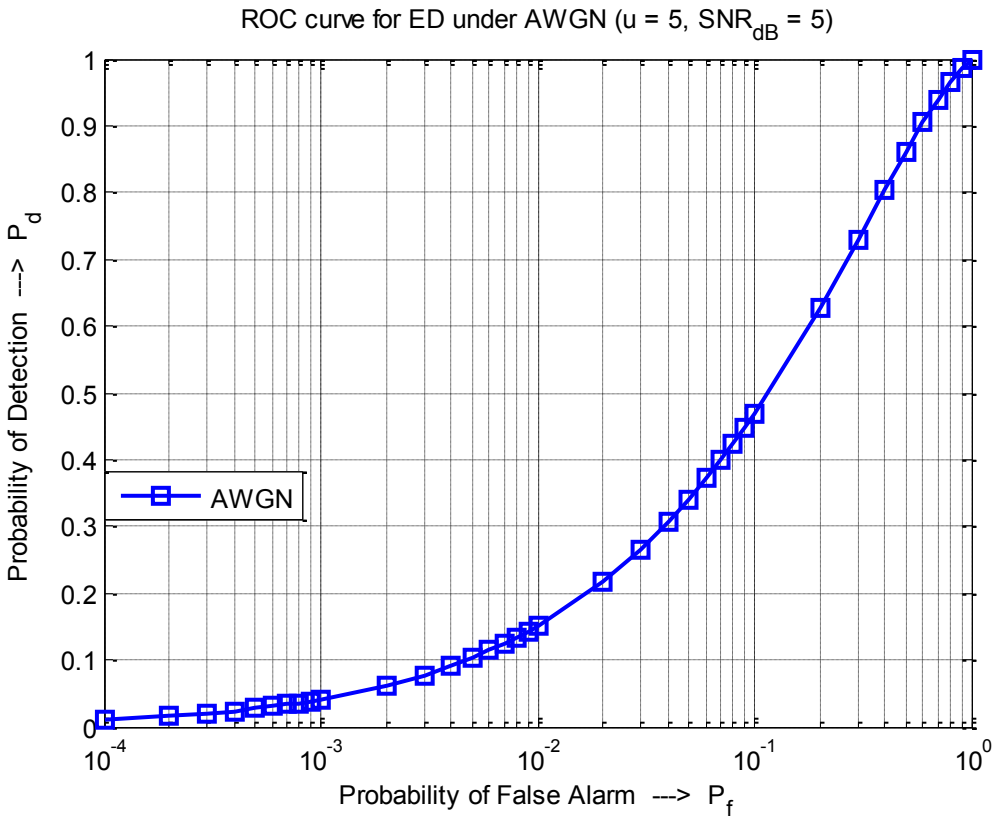

Figure 2.17: ROC for Conventional Single-threshold Energy Detector (AWGN case, SNR = 5 dB)

In IEEE 802.22 cognitive WRAN standard [3], the acceptable values for the probability of false alarm is specified as 0.1, whereas for the probability of detection, the specified value is 0.9 (or 0.1 for probability of misdetection). In Figure 2.17, if we fix probability of false alarm to 0.1, the probability of detection is less than 50%, which is not acceptable. The low performance here can be attributed to the low received SNR.

As mentioned before, the performance can also be viewed as complementary receiver operating characteristics. (See Figure 2.18)

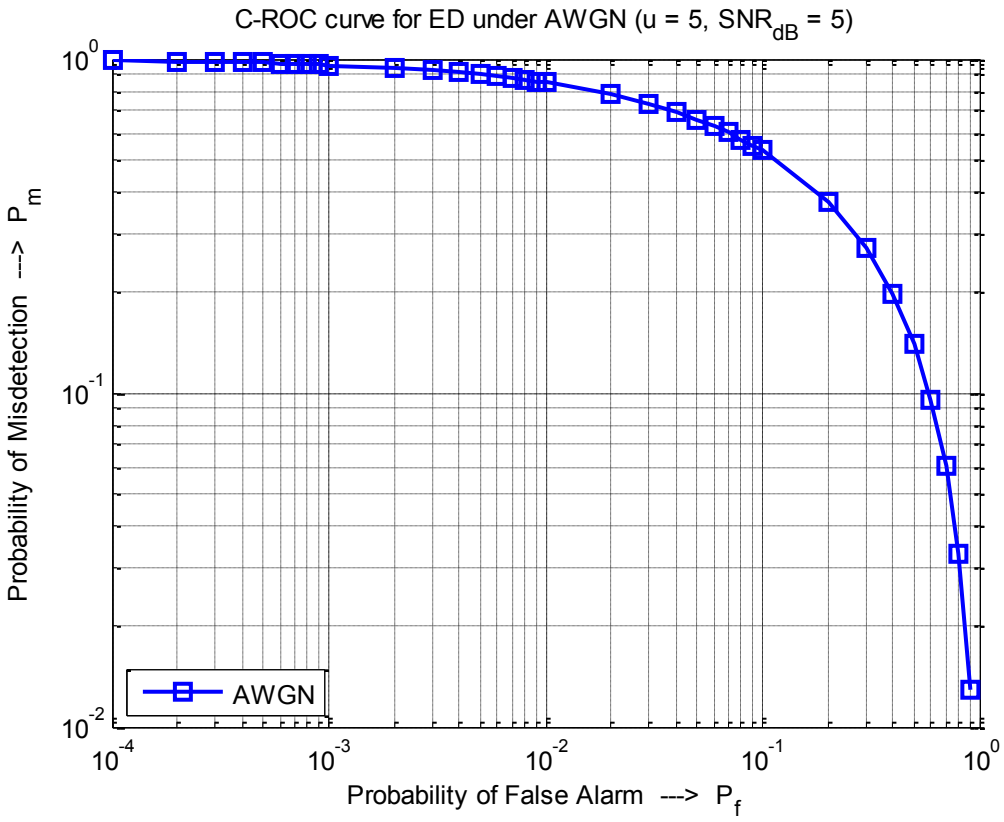

Figure 2.18: C-ROC for Conventional Single-threshold Energy Detector (AWGN case, SNR = 5 dB)

Now, in order to see the effect in terms of detection performance of increased SNR, assume that the received SNR at the single-antenna CR node has been doubled, i.e., SNR = 10 dB, as opposed to the case in Figure 2.17 and Figure 2.18, we observe a definite performance improvement in terms of the probability of detection as shown in Figure 2.19.

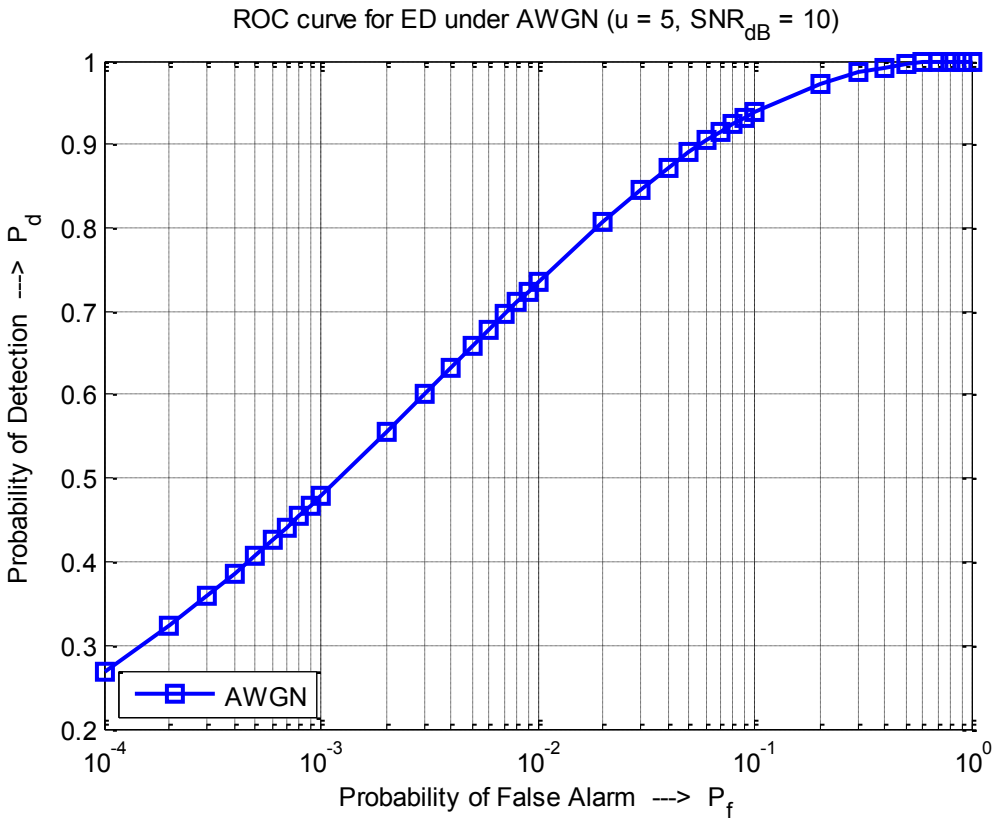

Figure 2.19: ROC for Conventional Single-threshold Energy Detector (AWGN case, SNR = 10 dB)

Again, if we fix the probability of false alarm to 0.1, the probability of detection is above 90%. Alternatively, Figure 2.20 shows a significant reduction in the probability of miss detection at 0.1 probability of false alarm.

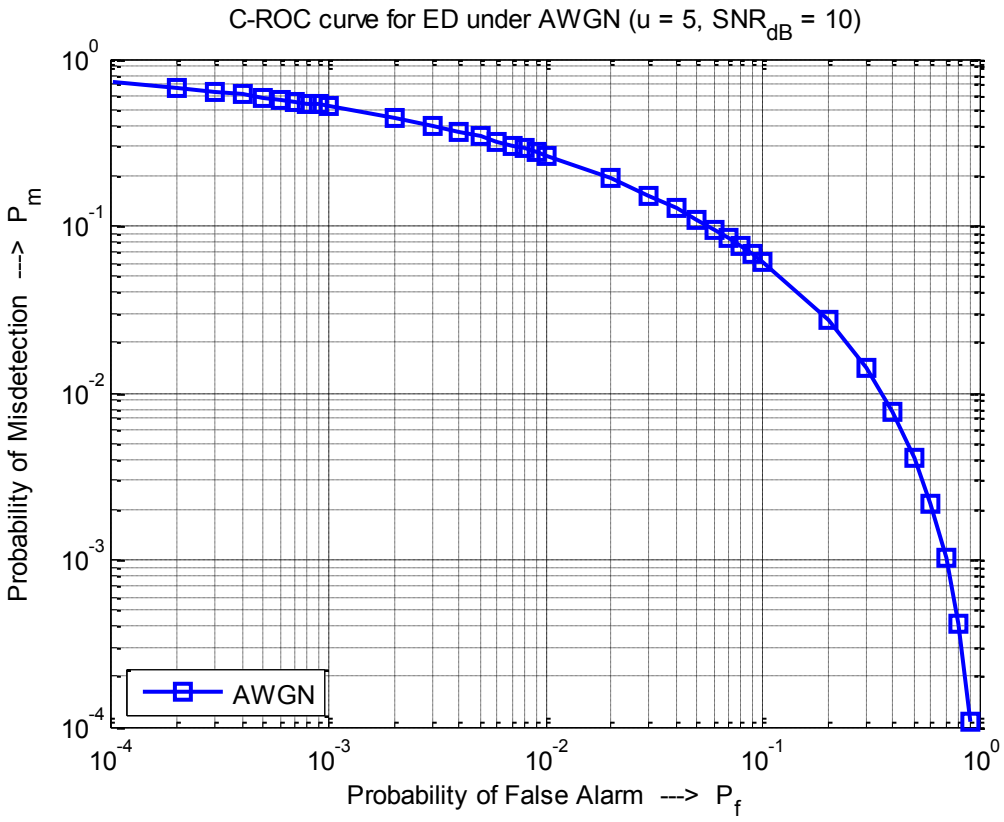

Figure 2.20: C-ROC for Conventional Single-threshold Energy Detector (AWGN case, SNR = 10 dB)

The wireless channels are more realistically modeled as Rayleigh fading channels in order to account for the small-scale fading that occurs in urban environments. The channel randomness brought by fading environments creates uncertainty in the received SNR, and degrades performance of ED. In fading environment, even as high as 10 dB SNR, the detection performance remains below the acceptable level of 0.9. let us now consider the case where the single-antenna CR node is experiencing Rayleigh fading and average SNR = 5 dB, we observed that the spectrum sensing performance of a single CR decreases considerably (Figure 2.21).

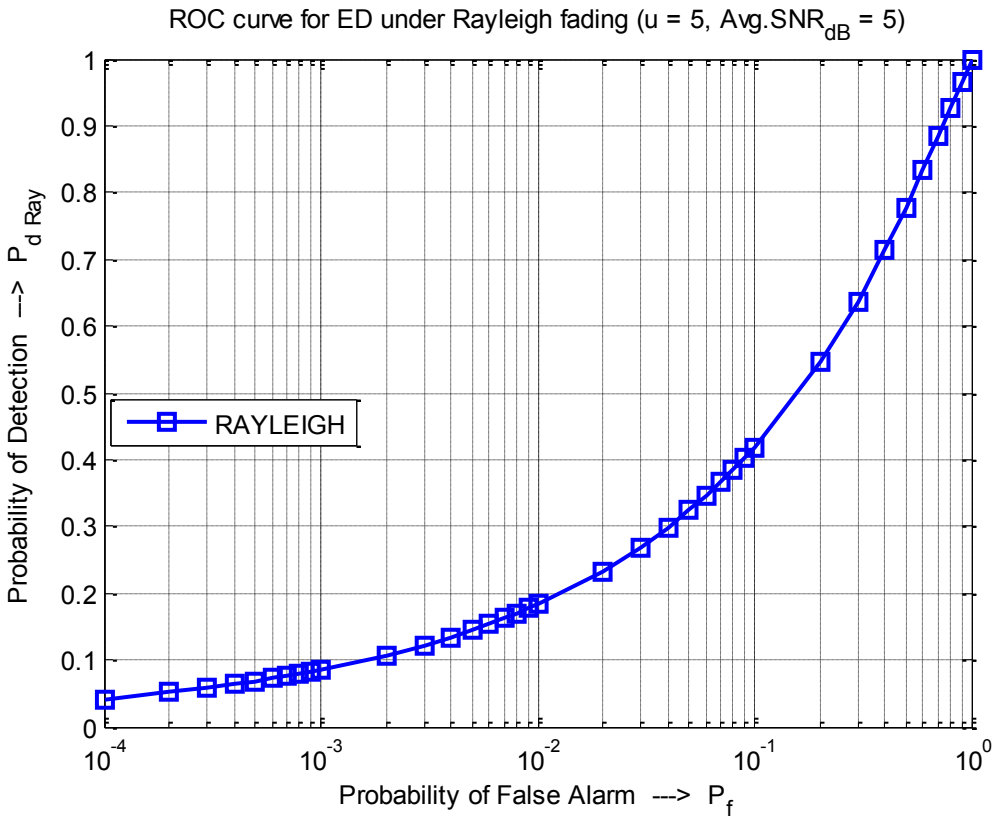

Figure 2.21: ROC for Conventional Single-threshold Energy Detector (Rayleigh fading case, SNR = 5 dB)

Here, again, if we fix probability of false alarm to 0.1, the probability of detection reduces to 40%, which will not be acceptable in practical scenarios. The C-ROC for single CR Rayleigh fading case is shown in Figure 2.22.

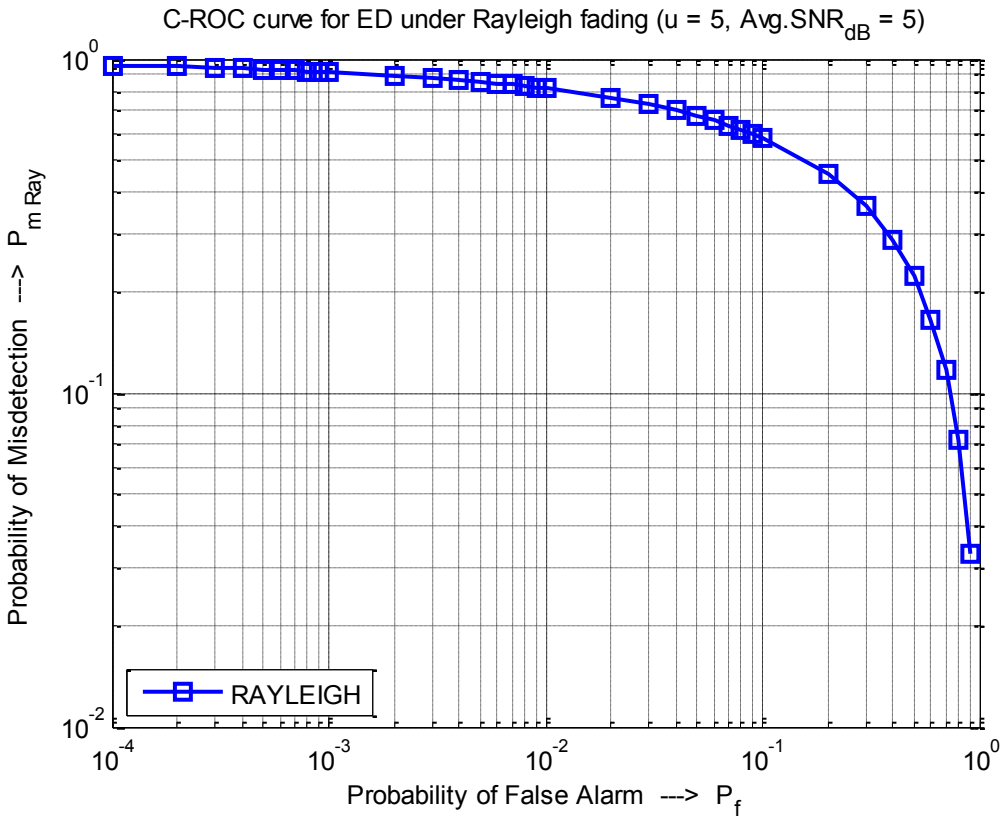

Figure 2.22: C-ROC for Conventional Single-threshold Energy Detector (Rayleigh case, SNR = 5 dB)

Now, in order to see the effect in terms of detection performance of increased SNR, we assume that the received average SNR at the single-antenna CR node has been doubled, i.e., SNR = 10 dB, as opposed to the case in Figure 2.21 and Figure 2.22, we observe a definite performance improvement in terms of the probability of detection as shown in Figure 2.23.

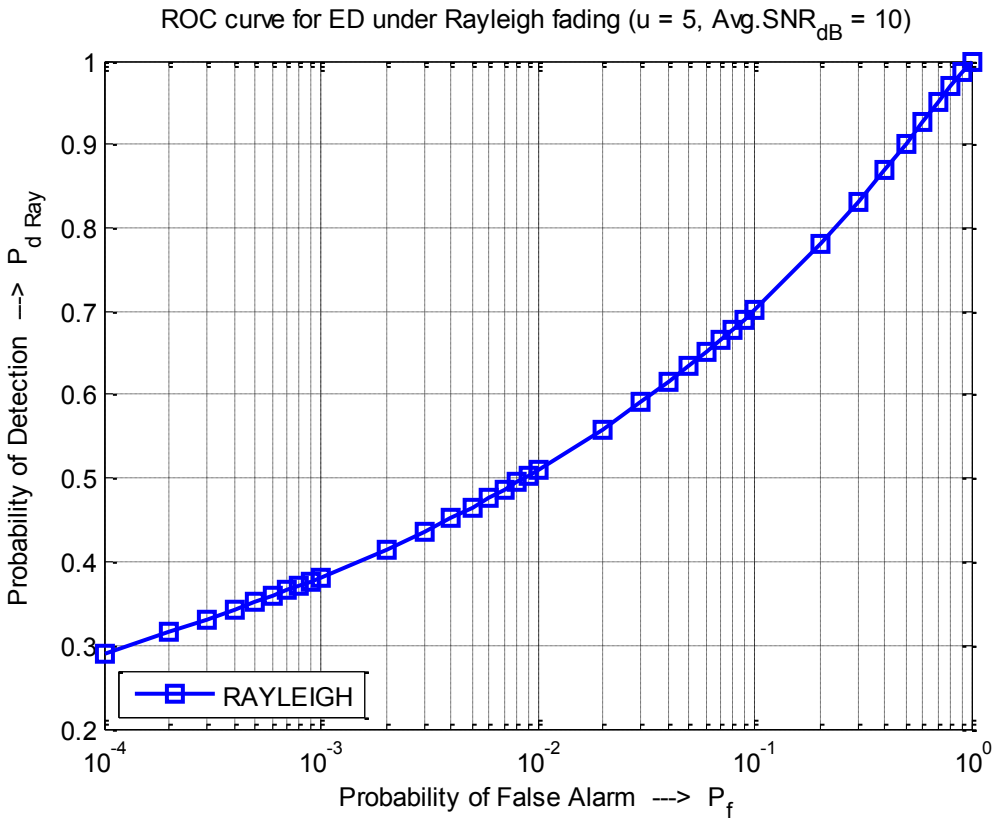

Figure 2.23: ROC for Conventional Single-threshold Energy Detector (Rayleigh fading case, SNR = 10 dB)

As compared to Figure 2.21 (where the average received SNR was assumed to be 5 dB), in Figure 2.23 shows the detection performance has been increased to 70% when the probability of false alarm is 0.1, however, 70% is still below the specified value of 90% by the IEEE 802.22 standard. The corresponding C-ROC for single CR Rayleigh fading case of Figure 2.23 is shown in Figure 2.24.

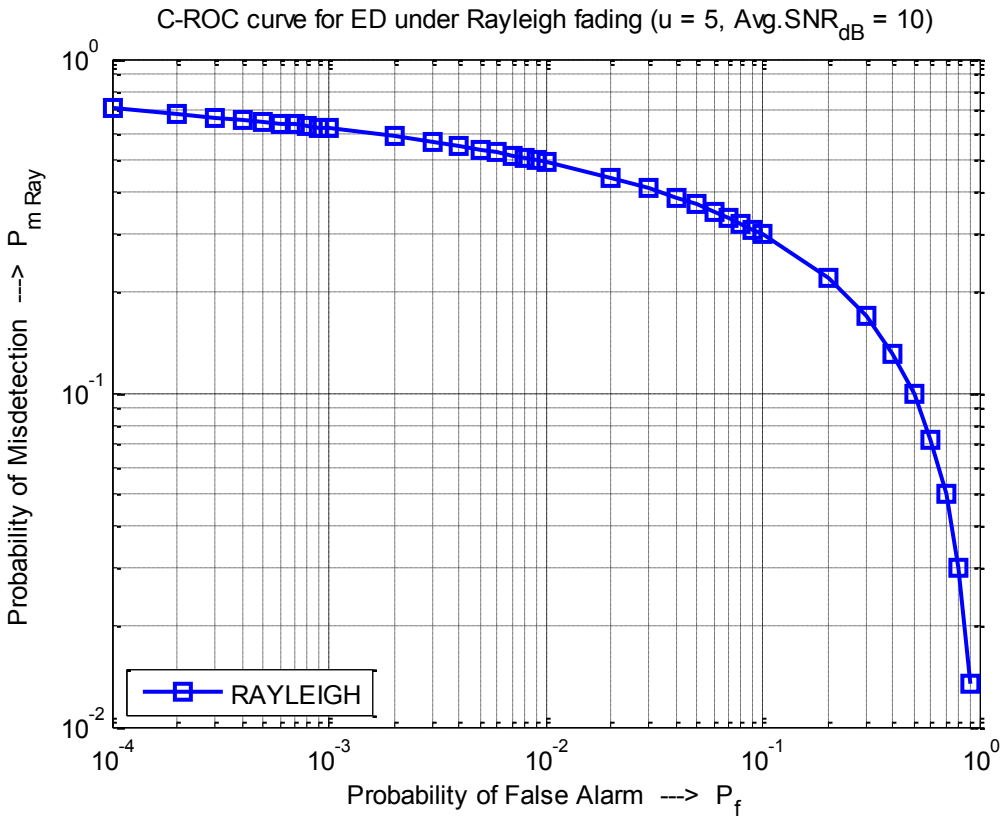

Figure 2.24: C-ROC for Conventional Single-threshold Energy Detector (Rayleigh case, SNR = 10 dB)

From the simulation results of single-antenna CR cases shown above, it is easy to conclude that the spectrum sensing performance of a single CR is not reliable enough even at a higher received SNR. The performance degrades very much under fading channels. As mentioned before, collaboration among CRs has been proposed to mitigate the effects of fading and to improve performance. In the next section, we will demonstrate the spectrum sensing performance when a number of CRs are cooperatively performing the spectrum sensing task.

2.2.4.2 Spectrum Sensing with Cooperation

As mentioned in Section 2.2.1, the performance degradation under fading environments can be mitigated by the use of multiples cooperating CR nodes. Below we will show the simulation results under AWGN and Rayleigh fading environments which shows the performance gain in combining 10 cooperating CRs and using either data- or decision-fusion techniques. In [71], it was shown that 10 cooperating users are sufficient enough to: 1) Provide high detection performance while keeping the probability of false-alarm extremely low, 2) Lower the required observation time and bandwidth, 3) Lower the required received SNR value, 4) Mitigate the fading effects.

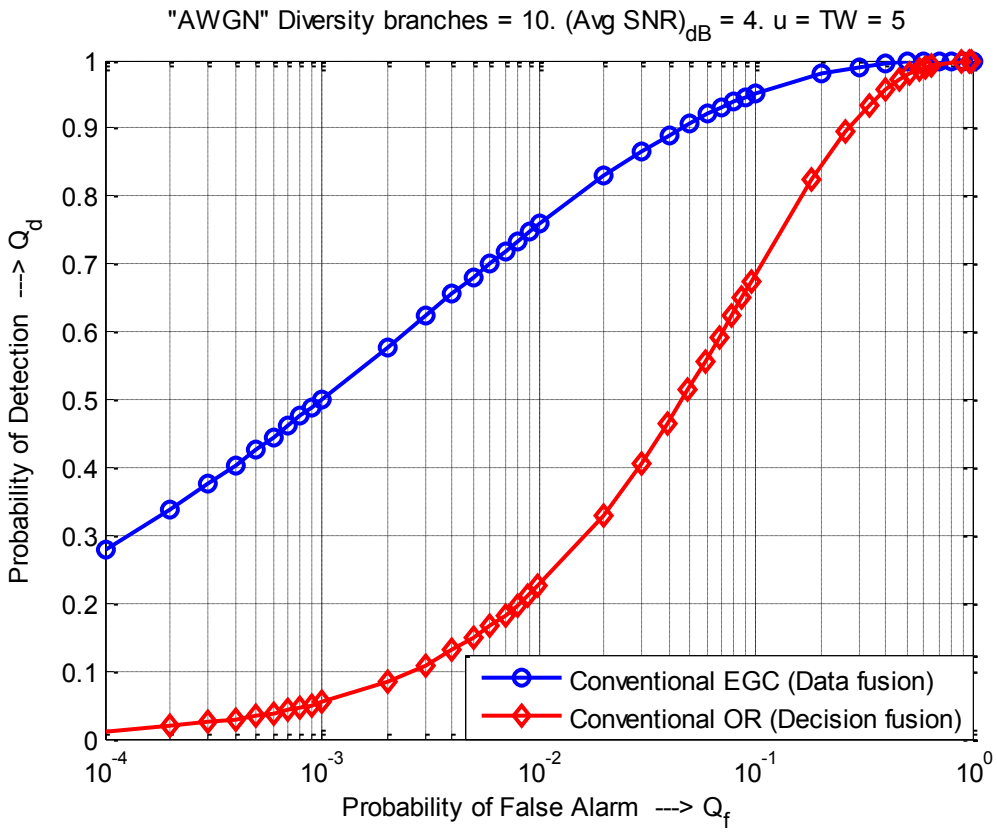

Figure 2.25: ROC - Data fusion versus Decision fusion under AWGN (SNR = 4 dB)

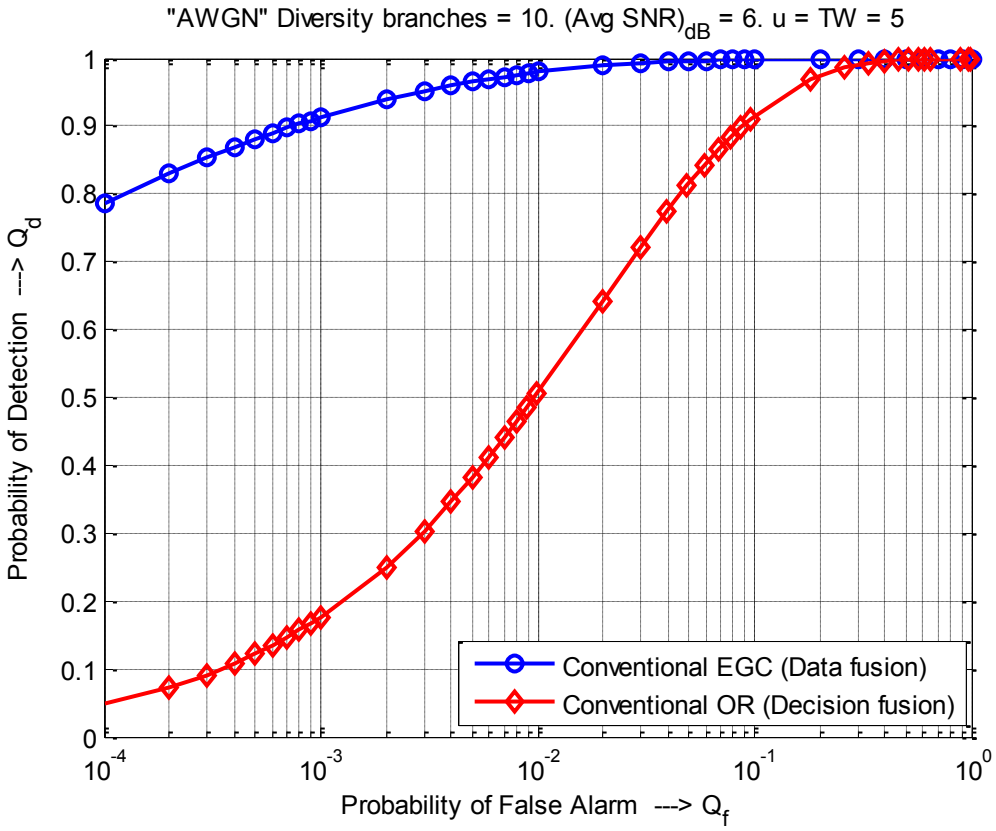

Figure 2.26: ROC - Data fusion versus Decision fusion under AWGN (SNR = 6 dB)

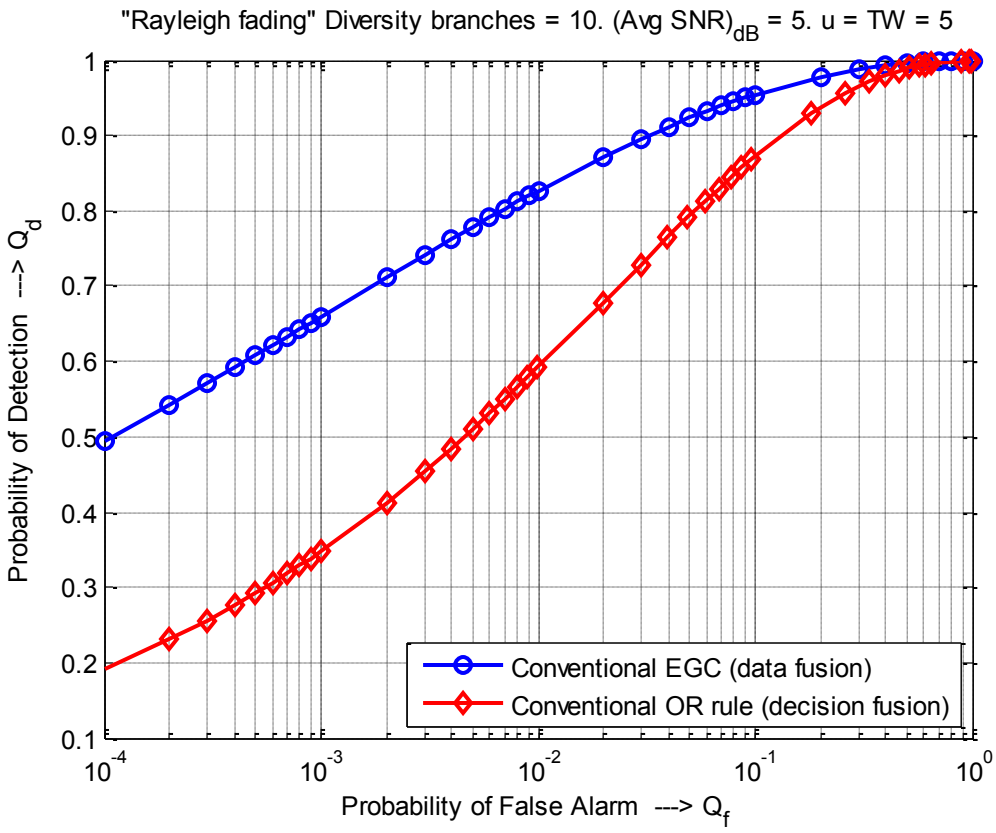

Figure 2.27: ROC - Data fusion versus Decision fusion under Rayleigh fading (SNR = 5 dB)

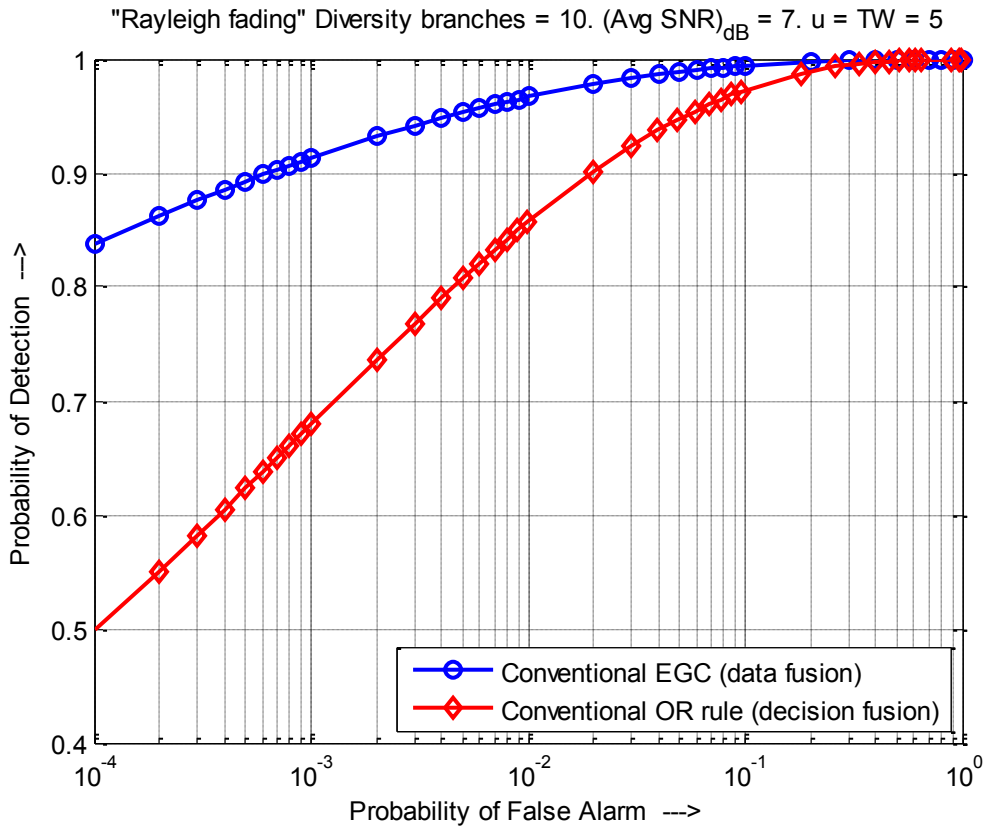

Figure 2.28: ROC - Data fusion versus Decision fusion under Rayleigh fading (SNR = 7 dB)

Obviously, the decision fusion (OR rule) approach requires fewer bits over the reporting channel (1-bit per user). On the other hand, when data fusion EGC is used, more feedback bits are required (m-bits per user, $m \geq 1\text{m} \geq 1$), which sacrifices the spectral efficiency. However, as shown in the simulation results above for cooperative spectrum sensing, data fusion outperforms decision fusion. Therefore, as can be seen from the above, we have a very clear tradeoff between performance and number of bits.

In Chapter 4, we will show that by dividing the cooperative users into a set of CRs with binary decisions and another set of CRs providing energy measures, but not decision, to the fusion center, we can substantially reduce the overall number of sensing bits over the

reporting channel at the expense of a negligible loss in performance compared to EGC. The division of CRs will be carried using a bi-threshold energy detector approach discussed earlier in [78]. The CRs with reliable local sensing results would send their decisions, while others would send their observed energy values to the fusion center. In fact, this is the difference between the work proposed in this thesis and the work in [78] in which the authors neglected the CRs with unreliable sensing results, while in this work we try to exploit the information of those CRs to improve the performance. We derive the closed form expressions for the probability of false alarm Q_f and the probability of detection Q_d at the fusion center for the proposed algorithm. Furthermore, we provide a closed form expression for the average savings in bits.

Starting with the next chapter (Chapter 3), we will revisit the wavelet-based spectrum sensing approach with the proposed improvements. In Chapter 4, we will revisit the time domain approach of spectrum sensing using a bi-threshold energy detector which will allow reducing feedback bits over the reporting channel while still harvesting the performance benefits from the proposed modified linear combining scheme (Hybrid EGC-OR).

CHAPTER 3

A NOVEL APPROACH FOR SPECTRUM SENSING USING THE WAVELET TRANSFORM

3.1 Introduction

To mitigate the issue of spectrum scarcity, Cognitive Radio (CR) technology has gained a lot of popularity among researchers in recent times. However, the accurate detection of holes in the spectrum (white spaces) is still a very challenging task. In this chapter, we discuss the power of the Wavelet Transform (WT) in sensing spectrum using an edge-detection approach. The simulation results show that the WT is robust and computationally efficient in wideband spectrum sensing. It allows the CR to quickly and accurately identify the number of subbands within the interested wideband. Finally, using a simple estimator, the PSDs of each of the subbands is easily calculated.

The original approach to wavelet-based spectrum sensing [26] has been briefly described in Chapter 2. The wavelet transform was used to detect edges in the wideband signal's PSD. However, due to the inherent frequency measurement error of the PSD measuring devices, such as spectrum analyzer, the resultant wavelet transform coefficients is a mixture of true edges and the noise induced edges. In this chapter, we propose various techniques to improve the detection of the actual frequency edges. In particular, we propose to improve edge detection using median filtering to smooth out the noise

disturbance. We also propose the use of multi-scale sum, instead of the previously studied multi-scale product. Furthermore, we develop a thresholding method to remove the noise induced wavelet coefficients. Finally, we study the effect of using different mother wavelets for edge detection.

3.2 Enhancing Edge Detection using Median Filtering

As emphasized in Section 2.1.6, there will always be some Gaussian (thermal) noise disturbance at the receiver. In order to cope with it, we propose to apply Median Filtering to the received signal's PSD $S_r(f)$ before calculating the wavelet transform coefficients. Median filter is a nonlinear digital filtering technique used to remove noise from a signal while preserving the edges of the image or signal. Median filtering technique applies sliding window to a sequence, where the sliding window runs through the entire signal entry by entry, replacing the center value in the window with the median value of all the other points in the window [79]. While performing the median filtering operation over a noisy sequence, typically, the sliding window is assumed to be of odd length, i.e., having a width of *2N+1*, where *N* is some positive integer. At a particular instant, suppose the window is centered at sample *k* in the input sequence, then the time-ordered window of *2N+1* points can be specified in the vector form as:

$$(x_{k-N}, x_{k-N+1}, \dots, x_k, \dots, x_{k+N}) \tag{3.1}$$

The output of the median filter at the time when the window is centered at sample *k* in the input sequence, denoted as y_k, can be represented as:

$$y_k = median(x_{k-N}, x_{k-N+1}, \dots, x_k, \dots, x_{k+N}) \tag{3.2}$$

The samples in the window are first reordered based on their rank (magnitude):

$$(x_{(1)}, x_{(2)}, \dots, x_{(2N+1)}) \tag{3.3}$$

where x_i denoted the sample of the i^{th} rank. For example, if *N=2*, and the time-ordered samples in the sliding window are:

$$(x_{k-N}, x_{k-N+1}, \dots, x_k, \dots, x_{k+N}) = (8,1,6,4,1), \tag{3.4}$$

then the rank ordered samples would be:

$$(x_{(1)}, x_{(2)}, x_{(3)}, x_{(4)}, x_{(5)}) = (1,1,4,6,8). \tag{3.5}$$

Thus the median filter output for this example would simple be $y_k = x_{(3)} = 4$. The same procedure would be repeated for all the input signal samples.

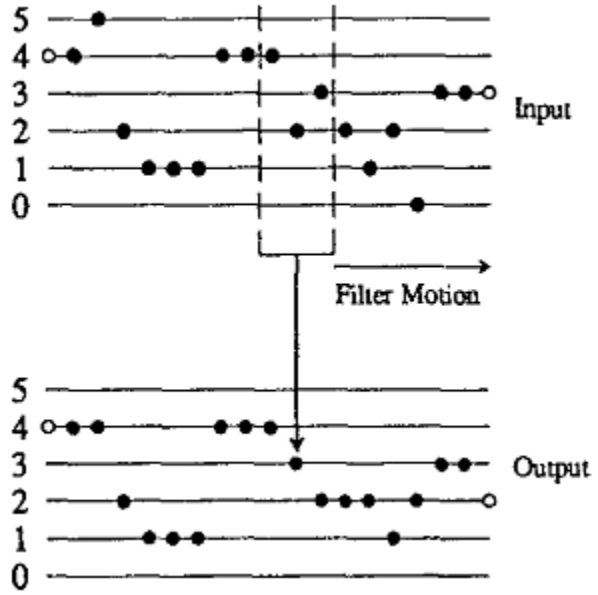

Figure 3.1: Operation of median filter of order 3.

Figure 3.1 shows the operation of a median filter of order 3. As mentioned before, one of the key properties of a median filter is that it does not smear out sharp edges in the input signal, as long as the duration of the edge exceeds some critical duration [80]. This property makes the median filter a good candidate for a signal smoother. This property can be further illustrated using a simple example shown in Figure 3.2 [80]. The input signal *x(n)* is fed into a 3rd order median filter, where *y(n)* represents the output of the filter. There exists sharp irregularities in the input signal at $n = 6$ and $n = 11$. As shown, the output *y(n)* is found to be exactly the same as input signal. The authors in [80] claim that even after increasing the order of median filter to 9, the output *y(n)* remains the same. However, increasing the filter order beyond 9 would smoothen out the discontinuity in *x(n)* and the output becomes flat. Hence, the selected order of the median filter is dependent on the required minimum duration of discontinuity that should be preserved [81].

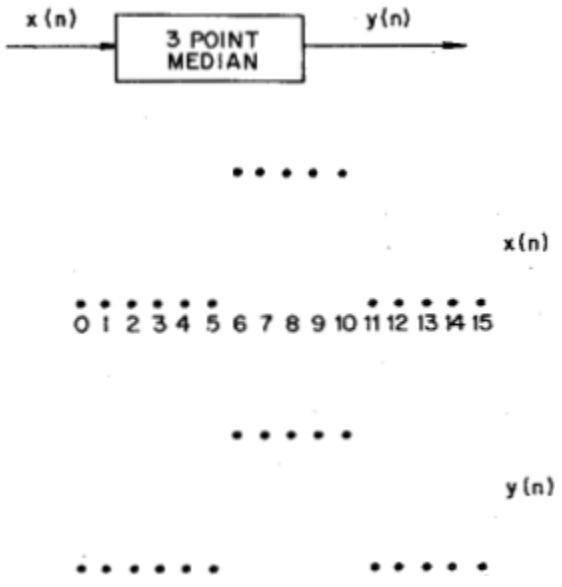

Figure 3.2: Edge preserving property of a median filter.

In Figure 3.3, the observed signal PSD $S_r(f)$ was the same as the one in Figure 2.8. We tried several lengths for the sliding window, the order 7 worked best in our case. If we increase the order of the median filter beyond 7, the median filter smears out the edges of the narrowband, B_6, and makes it flat. Consequently, we lose the edge information of band B_6. Therefore, below we apply a Median filter of order 7 to $S_r(f)$ in order to get a smoothed version of $S_r(f)$. We then calculate with the wavelet transform modulus of filtered $S_r(f)$ using the same mother wavelet and corresponding scales as in Section 2.1.6.

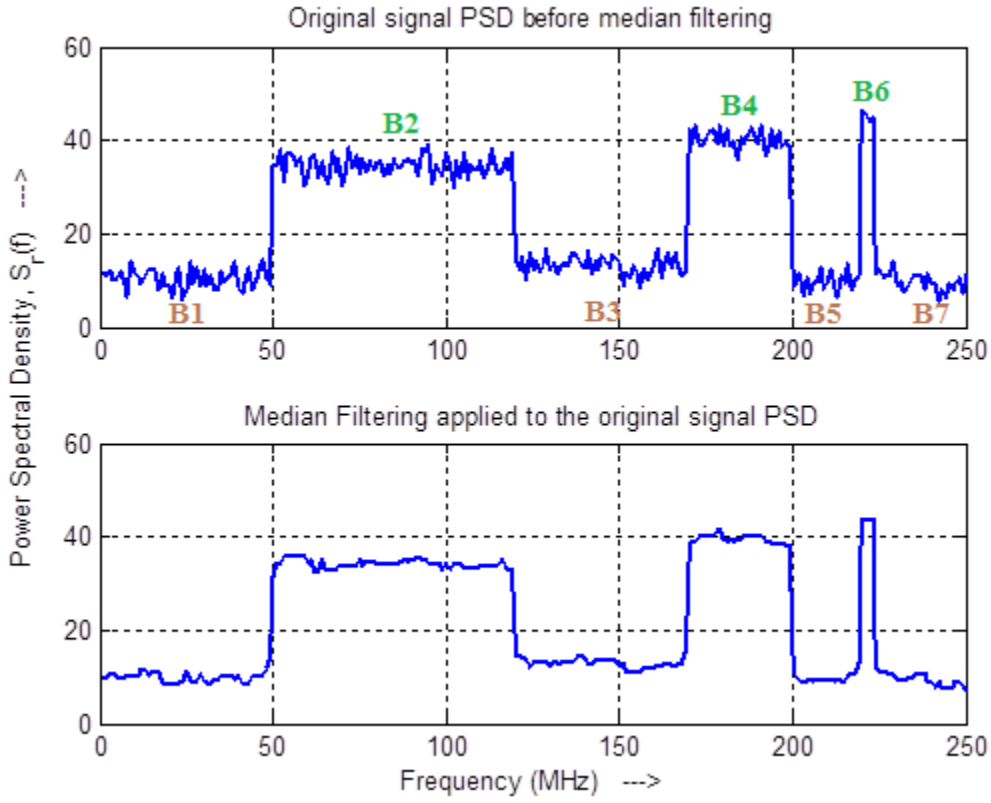

Figure 3.3: Median Filtering applied to the observed signal PSD

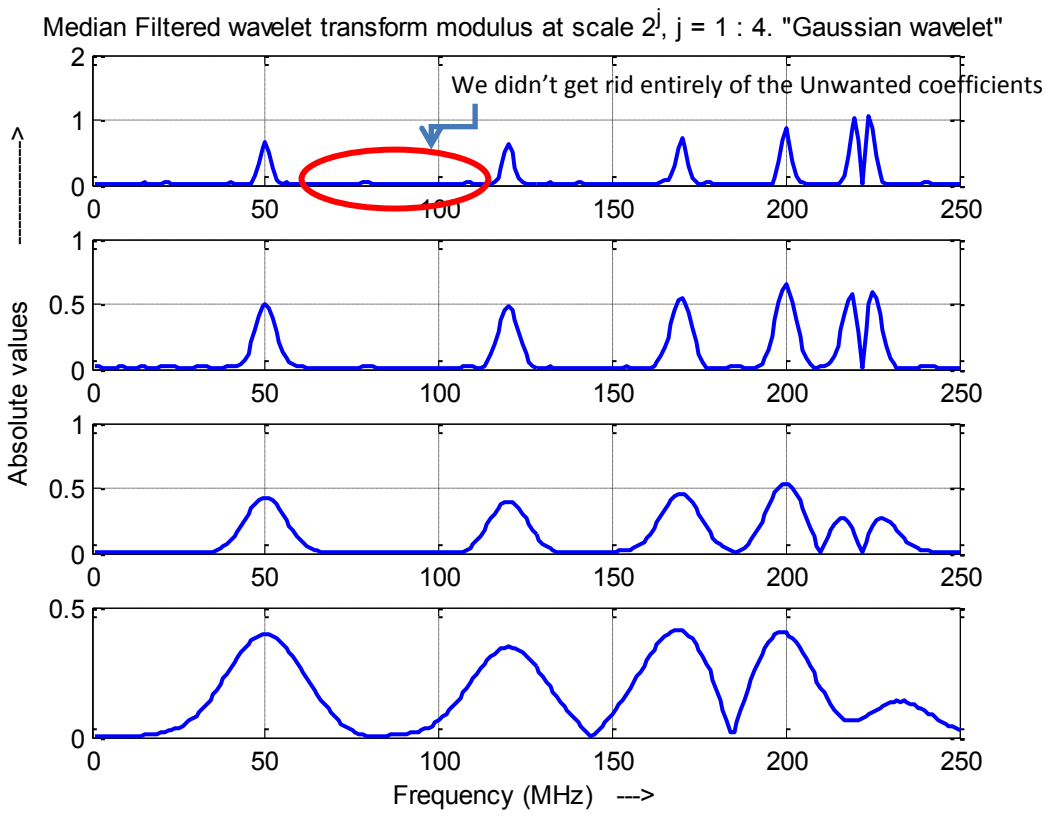

Figure 3.4: Wavelet transforms modulus, at scales *s* = 2^j, *j = 1, 2, 3, and 4*, after Median Filtering

Recall from Section 2.1.6 (Figure 2.8) that the received signal's PSD contains frequency boundaries located at $\{f_n\}_{n=1}^{N-1=6} = [50, 120, 170, 200, 220, 224\,]$. Now if we compare WT coefficients in Figure 2.10 with those in Figure 3.4, we find that the coefficients at the frequency locations which do not correspond to the actual frequency edges in the PSD have been suppressed, and hence, it is clear that the smoothing effect of Median filtering does suppress the noise-induced peaks. For example, the first graph in Figure 3.4 is WT coefficients at scale $2^j, j = 1$, and corresponds to the first graph in Figure 2.10. The value of the highest noise-wavelet-coefficient in Figure 2.10 was 0.2, while the value of the highest noise-wavelet-coefficient in Figure 3.4 is 0.070. Hence, the WT coefficients (of

the median filtered PSD) in Figure 3.4 at the frequencies which are not the true frequency edges have negligible values as compared to those WT coefficients (without using the median filter) found in Figure 2.10.

Although, simulations above showed that performing median filtering results in a smooth PSD $S_r(f)$, and consequently less spurious local extrema due to noise have been observed in the wavelet transform curves, however, we did not get rid entirely of the unwanted coefficients. Also, as we discussed earlier in this section, to set the order of the median filter, the CR should know beforehand the width of the narrowest band inside the wideband of interest. Increasing the order of the median filter unnecessarily may result in losing the edge information of a narrowband. Our next effort towards the perfect edge detection is the use of multi-scale wavelets as described below.

3.3 Multi-Scale Sum

It was mentioned previously that integration of multi-scale wavelet transform modulus could increase the detection performance, as was shown in Figure 2.11. However, a close examination of Figure 2.11 reveals that performance improvement might not be the case for all the occupied subbands. To understand this more thoroughly, let us examine Figure 2.8 again. Note that subband B_6 is quite narrow as compared to the other occupied subbands, B_2, B_4. As a result, it can be seen clearly in Figure 2.10 that in the wavelet transform modulus curve at level $s = 2^4 = 16$, the coefficients at the frequency edges of B_6 are quite low. Consequently, in the multi-scale product operation of Figure 2.11, note

that P_{1234} for B_6 is very small. This is because the low coefficients of B_6 at level $s = 2^4 = 16$ have a dominating effect in the product operation [82].

To solve this problem, we can limit ourselves to lower scales. However, we would like to use higher scales in the case of *non-ideal PSD in Real Channel Environment* [82]. At the higher scales, the smooth edges in PSD have higher correlation with the scaled wavelets and thus are more likely to be detected with the stretched wavelet. Therefore, we propose to change slightly the definition in (2.13) to get a formula for the multi-scale sum as:

$$H_J S_r(f) = \sum_{j=1}^{J} W'_{s=2^j} S_r(f) \tag{3.6}$$

Observe the comparison of multi-scale product and multi-scale sum in Figure 3.5 for scales 1, 2, 3, 4. Here, P_{1234} represents the product operation of (2.13), while H_{1234} represent the sum operation of (3.6). From the comparison of multi-scale product and multi-scale sum in Figure 3.5, it is obvious that multi-scale sum has some performance advantage over multi-scale product for edge detection purposes. For example, consider the frequency edges shown in Figure 3.5. At the boundaries of band B_2, the WT coefficients for the multi-scale product values are 0.07167 and 0.04911, respectively, while for multi-scale sum the values are 2.13 and 1.962, respectively. At the boundaries of band B_4, the multi-scale product values are 0.113 and 0.1353, respectively, while for multi-scale sum the values are 2.4 and 2.529. Finally for the boundaries of the narrow band B_6, the values of the multi-scale product are 0.004467 and 0.008125, respectively, while for the multi-scale sum the values are 1.64 and 1.783, respectively. The performance of multi-scale sum is better than multi-scale product simply because, unlike

in multi-scale product, in the multi-scale sum, small value of coefficients at higher scales do not suppress other coefficients at lower scales when we combine coefficients across higher and lower scales.

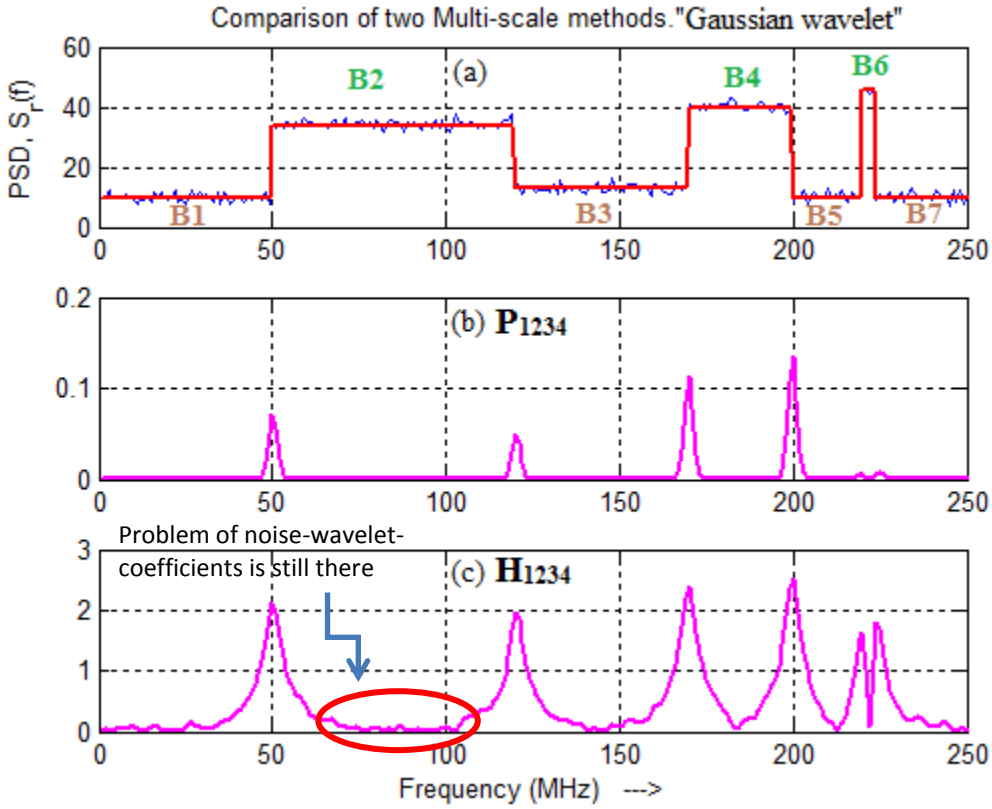

Figure 3.5: Example 1: Performance comparison of Multi-scale product and Multi-scale sum; scales $s = 2^j$, $j = 1, 2, 3,$ and 4. (a) Original signal's PSD. (b) Multi-scale product. (c) Multi-scale sum

Let's take another example, in Figure 3.6, of a wideband signal snapshot where the range of wideband spectrum is the same as before, i.e., [0, 250] MHz. Here the simulated received signal's PSD shows that only two bands (B_3 and B_5) out of the 7 bands have higher PSD values, which implies that only two bands are being utilized by the corresponding primary users. The frequency boundaries of the occupied bands are located

at, $B_3: \{f \in B_3: 120 \leq f < 170\}$ and $B_5: \{f \in B_5: 200 \leq f < 220\}$. For comparison between multi-scale product and multi-scale shown in Figure 3.6, consider the frequency boundaries of band B_3, the WT coefficients for the multi-scale product values are 0.1655 and 0.1741, respectively, while for multi-scale sum the values are 2.652 and 2.682, respectively. Also, at the boundaries of band B_5, the multi-scale product values are 0.04584 and 0.04678, respectively, while for multi-scale sum the values are 1.971 and 1.979, respectively.

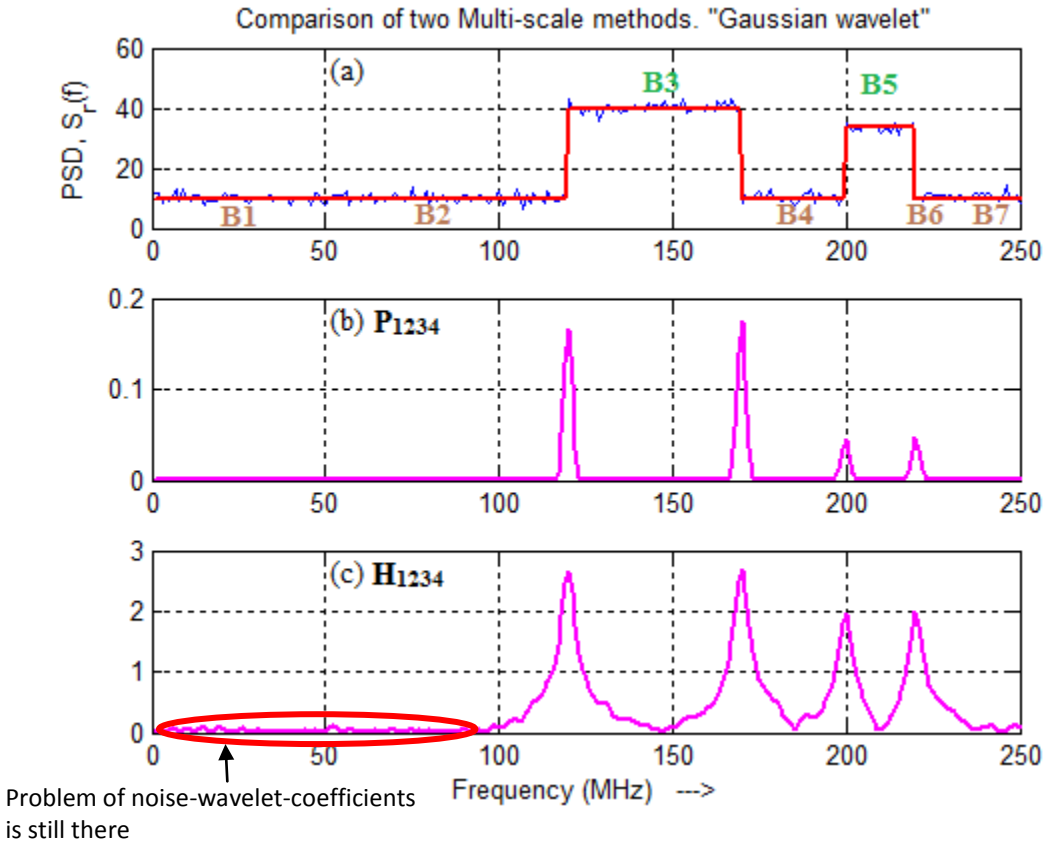

Figure 3.6: Example 2: Performance comparison of Multi-scale product and Multi-scale sum; scales $s = 2^j$, $j = 1, 2, 3,$ and 4. (a) Original signal's PSD. (b) Multi-scale product. (c) Multi-scale sum

Although, using the sum operation across the multi-scale wavelets does improve the coefficients' values corresponding to the true frequency edges in the PSD, however, the

problem of noise-wavelet-coefficients still exists. Our next effort towards the perfect edge detection is to develop a simple yet effective method to threshold the noise-wavelet-coefficients while restricting the computation of the WT for only one scale.

3.4 Thresholding of Noise-Coefficients

We explained in Section 2.1.6 that the disturbance in the received signal's PSD $S_r(f)$ due to thermal noise is a challenge in estimating the exact frequency boundaries of subbands. This is because; the wavelet transform coefficients curves contain peaks not only due to spectrum edges, but also due the Gaussian (thermal) noise. Consequently, it is not straightforward to extract frequency edges from CWT coefficients directly and use these in equations (2.7) and (2.8) to estimate the PSD levels $\{\alpha_n^2\}_{n=1}^{N-1}$. To this end, we propose the following strategy.

We checked the data sheets from a couple of famous manufacturers of Spectrum Analyzers, e.g., Agilent [33] and Anritsu [32]. Based on the reported Absolute Frequency error, our simulations first calculated separately the CWT of Gaussian noise with zero-mean and $\sigma = 2$. We stored the maximum value of Gaussian-noise-CWT coefficient. After that, in the simulations, the CWT, with scale $s = 2^l$, was performed on the received signal's PSD $S_r(f)$. We thresholded the CWT coefficients of $S_r(f)$ such that all the coefficients which were below or equal to the maximum value of Gaussian-noise-CWT coefficient were set to zero. This way, we were left only with true peaks corresponding to the frequency edges. Figure 3.7 demonstrates the results.

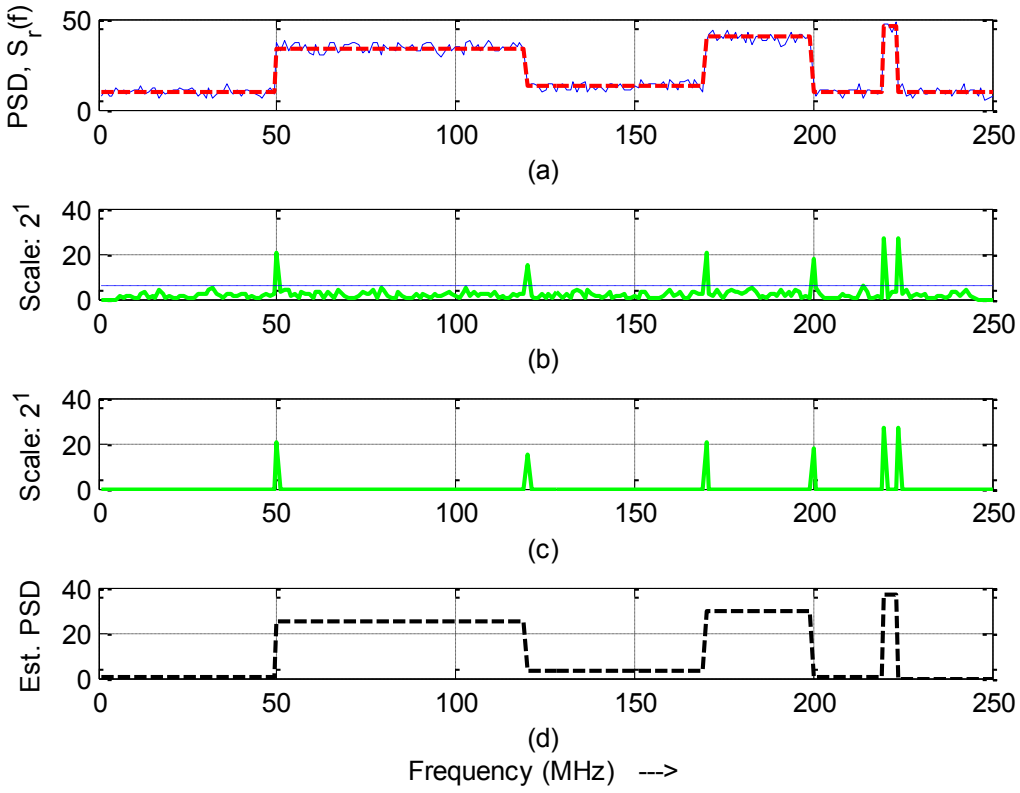

Figure 3.7: Thresholding of Noise-coefficients applied to the WT modulus of Figure 2.10, at scale s = 2^1. (a) Original signal's PSD, $S_r(f)$. (b) CWT coefficients of $S_r(f)$ without the thresholding of noise-induced coefficients (c) CWT coefficients of $S_r(f)$ after the thresholding of noise-induced coefficients. (d) The estimated PSD after thresholding noise-induced coefficients and removing the estimated noise PSD, $\widehat{S}_w(f)$.

In Figure 3.7, the first curve shows the PSD $S_r(f)$ of interest. It is the same PSD as was used in Section 2.1.6; Figure 2.8.The second curve shows CWT coefficients at scale $s = 2^1$, where noise-induced spurious local maxima are also evident. However, the third curve shows the peaks where the noise-coefficients have been filtered out, and these peaks correspond to the true edges in $S_r(f)$, $\{f_n\}_{n=1}^{N-1}$. Hence, the perfect identification of true frequency edges has been performed by our thresholding scheme.

After $\{f_n\}_{n=1}^{N-1}$ have been detected, equations (2.7) and (2.8) were used as a simple spectral density estimator to estimate the noise and signal PSD levels (Figure 3.7 (d)). The estimated values are:

$\{\hat{\alpha}_n^2\} = [0.1569 \quad 24.7008 \quad 3.3028 \quad 29.9964 \quad 0.5119 \quad 36.5986 \quad 0]$ corresponding to the true signal PSD values [0, 24, 3, 30, 0, 36, 0] respectively, and

$$\hat{S}_w(f) = 9.6049$$

corresponding to the true noise PSD value 10.

From these estimated values, it is clear that our method provides very satisfactory detection results.

3.5 Effect of Using Different Mother Wavelets in Spectrum Sensing

There has been a little discussion found in the literature on the use of the simple Haar wavelet system for the purpose of spectrum sensing [83], [84], [85]. Authors argue that when the spectrum of interest contains abrupt/sharp changes, as is the case with our simulations, the use of Haar mother-wavelet is more appropriate to capture the edges at multiple resolutions. On the other hand, Gaussian mother-wavelet was employed when the spectrum of interest exhibits smooth edges/singularities. Such smooth type of PSD is the result of either the unideality of RF filter in transmitter, or the multipath fading and/or Doppler effect in real channel environment [82].

In all the previous examples of wavelet-based sensing that are shown in this chapter, we have used Gaussian wavelet for the purpose of spectrum sensing. Now we will discuss other mother wavelets. The results shown in Figure 3.9 are obtained using the Haar wavelet (Figure 3.8). It can be seen in Figure 3.9 that there are slight differences in the curves corresponding to different scales. The wavelet transform is essentially a correlation between the wavelets and the signal that is to be analyzed, and the resultant coefficients are the measure of that correlation. Since the PSD in Figure 2.8 is piecewise flat, Haar wavelet shows more correlation when we evaluate the coefficients, even at higher scales, as compared to those evaluated by Gaussian wavelet in Figure 2.10.

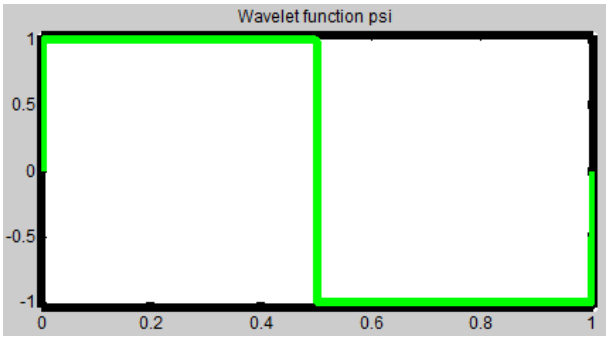

Figure 3.8: Haar wavelet

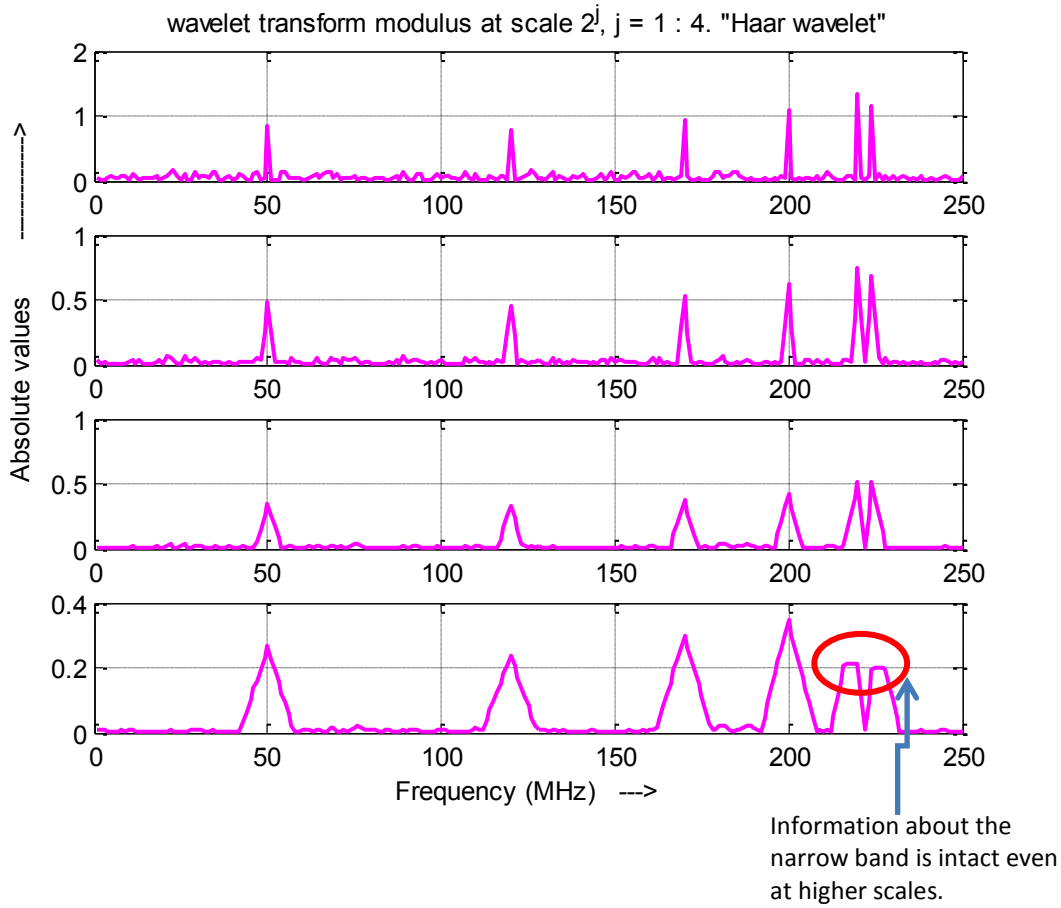

Figure 3.9: Wavelet transform modulus curves using Haar wavelet at scales $s = 2^j$, $j = 1, 2, 3,$ and 4.

Figure 3.11 is an example of using biorthogonal wavelet (Figure 3.10) for the purpose of edge detection. The PSD used here is shown in Figure 2.8. As compared to haar wavelet, although the wavelet coefficients using the biorthogonal wavelet is smoother, yet the information about the frequency edges of the PSD is intact even at higher scales.

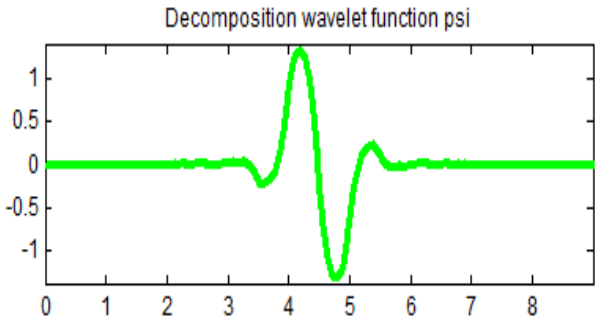

Figure 3.10: Biorthogonal wavelet

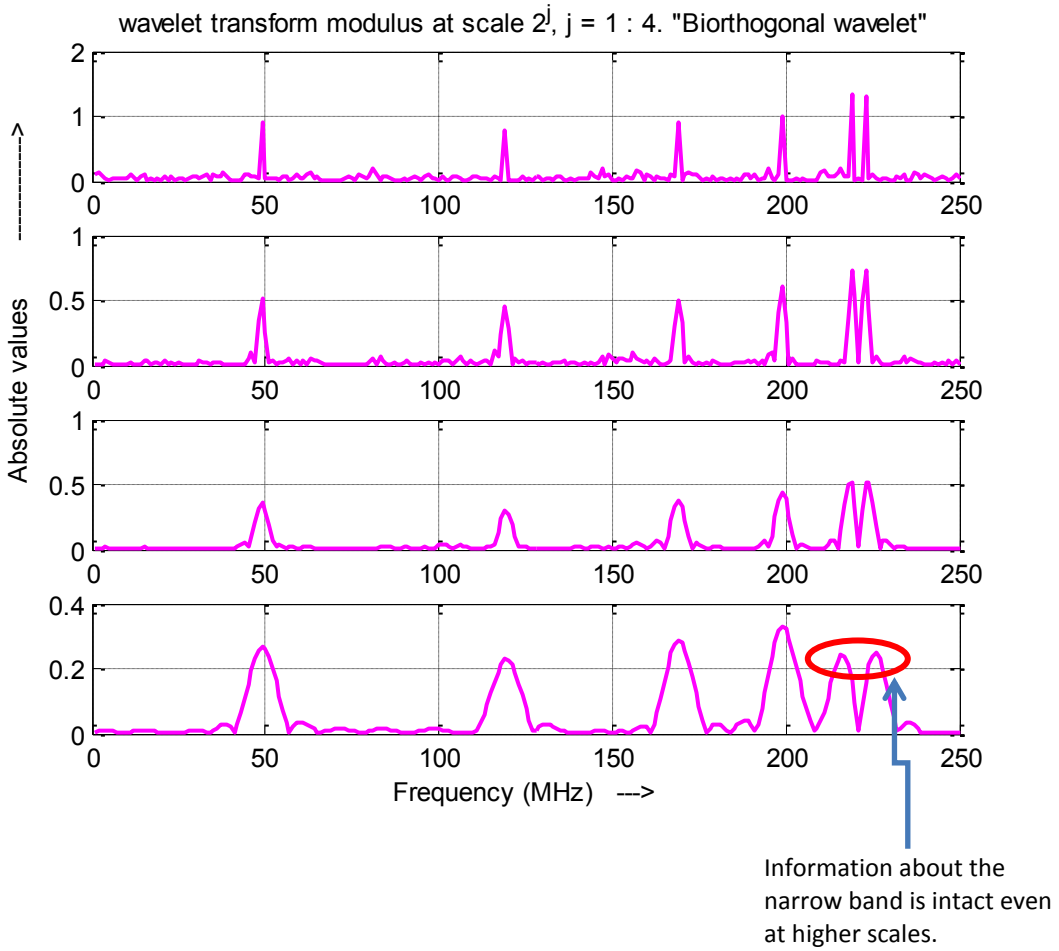

Figure 3.11: Wavelet transform modulus curves using biorthogonal wavelet at scales $s = 2^j$, $j = 1, 2, 3,$ and 4.

3.6 Summary

In this chapter, we discussed a frequency domain approach to spectrum sensing. Mainly, we showed that the WT can be effectively used to identify frequency boundaries of the sub bands within a wideband of interest. We proposed several techniques to improve the detection of frequency edges, such as the application of median filtering, the use of multiscale sum, and the development of a simple method for thresholding of noise-wavelet-coefficients. The accompanying simulations showed that our methods provide excellent performance. Last but not the least; we extended the wavelet analysis to cover other types of mother wavelets besides the Gaussian wavelet. We showed that for the case of sharp-edged PSD, the Gaussian wavelet is not the best choice to detect narrowband edges, rather, Haar and biorthogonal wavelets produce better results.

In the next chapter (Chapter 4), we will investigate the problem of spectrum sensing in time domain. Mainly, we will focus on the use of a bi-threshold energy detector and develop an algorithm to reduce the communication burden over the reporting channel at the cost of a negligible performance loss. We will show that using a combination of hard-decision and soft-decision CRs, we can achieve a performance close to EGC, yet we can save a lot of feedback bits over the feedback/reporting channel as compared to EGC. We will derive the close form expressions for the performance analysis of the proposed hybrid approach, as well as for the bits saving over the reporting channel.

CHAPTER 4

HYBRID COOPERATIVE SPECTRUM SENSING ALGORITHM USING ENERGY DETECTOR

4.1 Introduction

In this chapter, we propose a new hybrid technique for cooperative spectrum sensing (CSS) in cognitive radio oriented wireless networks (CROWN) in which we combine hard and soft decisions. A two-threshold energy detector is used at each CR to classify it as either a hard-decision CR (HDCR) or a soft-decision CR (SDCR). While the HDCRs transmit a binary decision to the fusion center, the SDCRs only transmit a quantized version of their measured energies. We show that the proposed technique can drastically reduce the number of feedback bits at the cost of a negligible loss in performance compared to equal gain combining (EGC). We derive the closed form expressions for the probability of detection (Q_d) and the probability of false alarm (Q_f). Furthermore, we derive a closed form expression for the average savings in the total number of feedback bits. We validate our derivations using simulations under AWGN and Rayleigh fading environments.

4.2 System Model

In our system model, we consider a centralized cooperative SS network with N CRs. Each of the cooperating CRs uses a bi-threshold energy detector [78] as shown in Figure 4.1. The two thresholds λ_1 and λ_2 are used to measure the reliability of the decision on the received energy, Y_i. The received energy value, Y_i, can fall in one of three regions as shown in Fig. 1. If Y_i is less than λ_1, "Decision H_0" is sent, while if Y_i exceeds λ_2, "Decision H_1" is sent. The fuzzy region models the situation where the energy value is not reliable enough for the CR to make a hard decision. The CRs whose received energy falls in the fuzzy region would directly report their received energy to the fusion center. Finally, the fusion center will combine all the soft- and hard-decisions into a single hard decision; the presence or the absence of the primary user.

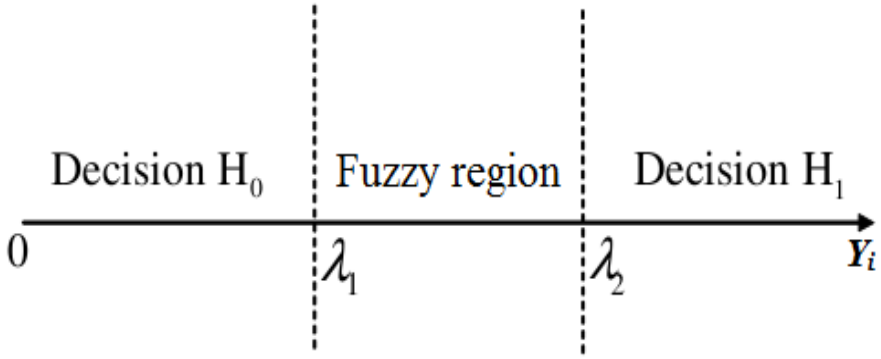

Figure 4.1: Bi-threshold energy detector with three regions.

Based on the above description of the model, we outline below the different steps of the proposed cooperative spectrum sensing algorithm:

1) Each of the N cooperating CRs performs independent spectrum sensing of the targeted frequency band and, based on the observed energy value, Y_i, sends either its hard-decision (HD_i), H_0 or H_1, or the received energy value Y_i to the fusion center. The fusion center (FC) thus receives the following types of information from each CR:

$$FC_i = \begin{cases} Y_i, & \lambda_1 \le Y_i \le \lambda_2 \\ HD_i, & otherwise \end{cases}, \quad i = 1,2,\dots N \tag{4.1}$$

where, the hard decision HD_i can be either H_0 (absent) at which case a binary 0 will be transmitted or H_1 (present) at which case a binary 1 will be transmitted.

$$HD_i = \begin{cases} 0, & 0 \le Y_i \le \lambda_1 \\ 1, & Y_i \ge \lambda_2 \end{cases}. \tag{4.2}$$

2) Suppose now that K out of N cognitive users report HDs, and N-K users report energies to the fusion center. The fusion center will first take an initial decision (soft decision) by adding all the reported raw energies from N-K users using EGC scheme [36]. The soft decision (SD) is represented as follows:

$$SD = \begin{cases} 0, & 0 \le \sum_{i=1}^{N-K} Y_i \le \lambda \\ 1, & \sum_{i=1}^{N-K} Y_i \ge \lambda \end{cases}, \tag{4.3}$$

where λ used in soft decision can be calculated using Eq. (10) from [43].

3) The fusion center will then make the final decision (FD) as follows:

$$FD = \begin{cases} 1, & SD + \sum_{i=1}^{K} HD_i \geq 1 \\ 0, & otherwise \end{cases} \quad (4.4)$$

Hence, the fusion center will assume that the targeted frequency band is available for secondary usage only if the combination of hard- and soft-decision is equal to 0.

4.3 Performance Analysis of the Proposed Cooperative Spectrum Sensing Algorithm

In this section, we derive the closed form expressions for the probability of misdetection (Q_m), the probability of detection (Q_d), and the probability of false-alarm (Q_f). Let us start by defining the probability that a given CR receives an energy value in the fuzzy region by $\Delta_0 = Pr(\lambda_1 < Y < \lambda_2 | H_0) = F_Y(\lambda_2) - F_Y(\lambda_1)$ and $\Delta_1 = Pr(\lambda_1 < Y < \lambda_2 | H_1) = G_Y(\lambda_2) - G(\lambda_1)$, under hypotheses H_0 and H_1, respectively. The functions $G_Y(.)$ and $F_Y(.)$ are defined as:

$$G_Y(\lambda) = Pr(Y < \lambda / H_1) \quad (4.5)$$

$$F_Y(\lambda) = Pr(Y < \lambda / H_0). \quad (4.6)$$

We also define the probability of misdetection P_m, the probability of detection P_d, and the probability of false-alarm P_f, for a single CR as:

$$P_d(\lambda_2) = Pr(Y > \lambda_2 | H_1) \tag{4.7}$$

$$P_m(\lambda_1) = Pr(Y < \lambda_1 | H_1) = 1 - \Delta_1 - P_d(\lambda_2) \tag{4.8}$$

$$P_f(\lambda_2) = Pr(Y > \lambda_2 | H_0). \tag{4.9}$$

Now, we define the cooperative probability of misdetection, Q_m as:

$$Q_m = Pr(FD = 0 | H_1). \tag{4.10}$$

Using the total probability theorem,

$$= Pr(FD = 0, K \neq N | H_1) + Pr(FD = 0, K = N | H_1)$$

$$= Pr\left(\sum_{i=1}^{K} HD_i = 0 \cap SD = 0, K \neq N \middle| H_1\right)$$

$$+ Pr\left(\sum_{i=1}^{K} HD_i = 0, K = N \middle| H_1\right)$$

$$= Pr\left(\sum_{i=1}^{K} HD_i = 0, K \neq N \middle| H_1\right) . Pr(SD = 0, K \neq N | H_1)$$

$$+ Pr\left(\sum_{i=1}^{K} HD_i = 0, K = N \middle| H_1\right)$$

$$= \sum_{K=0}^{N-1} \binom{N}{K} [Pr(Y_i < \lambda_1 | H_1)]^K [\Delta_1]^{N-K} . Pr\left(\sum_{i=1}^{N-K} Y_i < \lambda | H_1\right)$$

$$+ [Pr(Y_i < \lambda_1 | H_1)]^N$$

$$= \sum_{K=0}^{N-1} \binom{N}{K} [P_m(\lambda_1)]^K [\Delta_1]^{N-K} . \left\{ 1 - Pr\left(\sum_{i=1}^{N-K} Y_i > \lambda | H_1 \right) \right\}$$

$$+ [P_m(\lambda_1)]^N$$

$$= \sum_{K=0}^{N-1} \binom{N}{K} [P_m(\lambda_1)]^K [\Delta_1]^{N-K} . \{ 1 - P_{d,EGC(N-K)}(\lambda) \}$$

$$+ [P_m(\lambda_1)]^N$$

$$= \sum_{K=0}^{N} \binom{N}{K} [P_m(\lambda_1)]^K [\Delta_1]^{N-K} . 1 - P_{d,EGC(N-K)}(\lambda), \quad (4.11)$$

where $P_{d,EGC(N-n)}(\lambda)$ is the probability of detection for EGC with *N*-*K* users, and is defined as:

$$P_{d,EGC(N-K)}(\lambda) = Pr\left(\sum_{i=1}^{N-K} Y_i \geq \lambda \middle| H_1 \right). \quad (4.12)$$

The cooperative probability of detection Q_d is readily expressed as:

$$Q_d = 1 - Q_m. \quad (4.13)$$

On the other hand, we express the cooperative probability of false-alarm (Q_f) as:

$$Q_f = Pr(FD = 1 | H_0) = 1 - Pr(FD = 0 | H_0). \quad (4.14)$$

Again using the total probability theorem:

$$= 1 - [Pr(FD = 0, K \neq N | H_0) + Pr(FD = 0, K = N | H_0)]$$

$$= 1 - \left[Pr\left(\sum_{i=1}^{K} HD_i = 0 \cap SD = 0, K \neq N | H_0 \right) \right.$$

$$\left. + Pr\left(\sum_{i=1}^{K} HD_i = 0, K = N | H_0 \right) \right]$$

$$= 1 - \left[Pr\left(\sum_{i=1}^{K} HD_i = 0, K \neq N | H_0 \right) \right.$$

$$\times Pr(SD = 0, K \neq N | H_0)$$

$$\left. + Pr\left(\sum_{i=1}^{K} HD_i = 0, K = N | H_0 \right) \right]$$

$$= 1 - \left[\sum_{K=0}^{N-1} \binom{N}{K} [Pr(Y_i < \lambda_1 | H_0)]^K [\Delta_0]^{N-K} \right.$$

$$\left. \times Pr\left(\sum_{i=1}^{N-K} Y_i < \lambda | H_0 \right) + [Pr(Y_i < \lambda_1 | H_0)]^N \right]$$

$$= 1 - \left[\sum_{K=0}^{N-1} \binom{N}{K} \left[1 - \Delta_0 - P_f(\lambda_2)\right]^K [\Delta_0]^{N-K} \right.$$

$$\times \left\{ 1 - Pr\left(\sum_{i=1}^{N-K} Y_i > \lambda | H_0 \right) \right\}$$

$$\left. + \left[1 - \Delta_0 - P_f(\lambda_2)\right]^N \right]$$

$$= 1 - \left[\sum_{K=0}^{N-1} \binom{N}{K} \left[1 - \Delta_0 - P_f(\lambda_2)\right]^K [\Delta_0]^{N-K} \times \left\{1 - P_{f,EGC(N-K)}(\lambda)\right\} + \left[1 - \Delta_0 - P_f(\lambda_2)\right]^N\right]$$

$$= 1 - \left[\sum_{K=0}^{N} \binom{N}{K} \left[1 - \Delta_0 - P_f(\lambda_2)\right]^K [\Delta_0]^{N-K} \times \left\{1 - P_{f,EGC(N-K)}(\lambda)\right\}\right] \quad (4.15)$$

$$= 1 - \left\{\sum_{n=0}^{N} \binom{N}{n} [F_Y(\lambda_1)]^n [\Delta_0]^{N-n} \times \left[1 - P_{f,EGC(N-n)}(\lambda)\right]\right\}, \quad (4.16)$$

where $P_{f,EGC(N-n)}(\lambda)$ is the probability of false alarm for EGC with *N-K* users and is defined as:

$$P_{f,EGC(N-K)}(\lambda) = Pr\left(\sum_{i=1}^{N-K} Y_i \geq \lambda \middle| H_0\right). \quad (4.17)$$

In (4.12) above, the exact expression of $P_{d,EGC(N-n)}(\lambda)$ depends on the wireless environment considered. In the case of Additive White Gaussian Noise (AWGN), (2.32) can be used [36]. On the other hand, $P_{d,EGC(N-n)}(\lambda)$, for independent and identically distributed (i.i.d) Rayleigh fading diversity branches, is given as (2.33) [36].

In (4.17) above, $P_{f,EGC(N-K)}(\lambda)$ does not depend on the wireless channel statistics, and is simply given by (2.31) [43].

Note that in our proposed spectrum sensing algorithm, if we neglect the energy values from the users that fall in the fuzzy region, and base our final decision on hard decisions only, we will end up with the following expressions for and Q_f, Q_d, and Q_m, respectively, which are corrected version of the expressions derived in [78]:

$$Q_f = P(FD = 1, K \geq 1|H_0) = 1 - [F_Y(\lambda_2)]^N \tag{4.18}$$

$$Q_d = P(FD = 1, K \geq 1|H_1) = 1 - [G_Y(\lambda_2)]^N \tag{4.19}$$

$$\begin{aligned} Q_m = P(FD = 0, K \geq 1|H_1) &= 1 - \Delta_1{}^N - Q_d \\ &= [G_Y(\lambda_2)]^N - \Delta_1{}^N = [G_Y(\lambda_1)]^N \end{aligned} \tag{4.20}$$

4.4 Bit Savings in the Reporting Channel

In order to determine the average communication load over the feedback (reporting) channel, we need first to note that, in any spectrum sensing cycle, the fusion center receives $B = [K + m(N - K)]$ bits in total (assuming *K* HDCRs), where *m* is the number of bits used to send the quantized energy values to the fusion center.

Let us start by defining T_K as the event of having "*K* cognitive users report hard decisions to the fusion center". The probability of event T_K is just: $Pr(T_K) = (1 - P\{\lambda_1 < Y < \lambda_2\})^K$. Also define $U_{(N-K)}$ as the event of having "*(N-K)* users report their energies to the fusion center". The probability of the event $U_{(N-K)}$ can be written as: $Pr\left(U_{(N-K)}\right) = P\{\lambda_1 < Y < \lambda_2\}^{(N-K)}$. For simplicity let us use P_0 and P_1 for $Pr(H_0)$ and $Pr(H_1)$

respectively which represent the probabilities of the primary user being absent and present, respectively. Using the above assumptions, the average number of users reporting their energies can be expressed as:

$$\psi_{avg} = \sum_{K=0}^{N} (N-K)[\binom{N}{K} Pr(U_{(N-K)}|H_0) Pr(T_K|H_0).Pr(H_0) + \binom{N}{K} Pr(U_{(N-K)}|H_1) Pr(T_K|H_1).Pr(H_1)] \tag{4.21}$$

$$= \sum_{K=0}^{N} N\left[\binom{N}{K} Pr(U_{(N-K)}|H_0) Pr(T_K|H_0).Pr(H_0) + \binom{N}{K} Pr(U_{(N-K)}|H_1) Pr(T_K|H_1).Pr(H_1)\right] - \sum_{K=0}^{N} K\left[\binom{N}{K} Pr(U_{(N-K)}|H_0) Pr(T_K|H_0).Pr(H_0) + \binom{N}{K} Pr(U_{(N-K)}|H_1) Pr(T_K|H_1).Pr(H_1)\right] \tag{4.22}$$

$$\psi_{avg} = N - \{P_0 \sum_{K=1}^{N} K \binom{N}{K} Pr(U_{(N-K)}|H_0) Pr(T_K|H_0) + P_1 \sum_{K=1}^{N} K \binom{N}{K} Pr(U_{(N-K)}|H_1) Pr(T_K|H_1)\} \tag{4.23}$$

$$\psi_{avg} = N - K_{avg}, \tag{4.24}$$

where K_{avg} is the average number of CRs with hard decisions [78], which can be also expressed as $K_{avg} = P_0 N(1-\Delta_0) + P_1 N(1-\Delta_1) = N[P_0(1-\Delta_0) + P_1(1-\Delta_1)]$.

Once the average number of users with soft decisions, ψ_{avg}, is known, the total average number of bits B_{avg} can be expressed as:

$$B_{avg} = K_{avg} + m\psi_{avg} \tag{4.25}$$

$$= K_{avg} + m\left(N - K_{avg}\right) \tag{4.26}$$

$$= K_{avg} + mN - mK_{avg} \tag{4.27}$$

$$= mN - (m-1)K_{avg}. \tag{4.28}$$

Finally, the normalized total average number of feedback bits becomes:

$$\bar{B} = \frac{B_{avg}}{N} = m - (m-1)\bar{K}, \tag{4.29}$$

where $\bar{K} = \frac{K_{avg}}{N}$ [78].

From expression (4.29), we note that the total normalized average number of feedback bits is always less than *m*. Therefore, in our proposed cooperative spectrum sensing algorithm, the average number of sensing bits is always smaller than that of conventional single-threshold EGC scheme in which every cooperative cognitive user send *m* bits to the fusion center. Note that, as $\Delta_0 \to 0$ (λ_1 and λ_2 coincides), the normalized average number of reporting bits $\bar{B}$ converges to *1*, while as $\Delta_0 \to 1$ (distance between λ_1 and λ_2 approaches infinity), the normalized average number of reporting bits $\bar{B}$ becomes *m*, which corresponds to the case of single-threshold EGC.

4.5 Numerical Examples

In this section, we present a sample of simulation results to demonstrate the performance of the cooperative spectrum sensing algorithm proposed in this chapter. In our simulation results, we assume that the system has time-bandwidth product, u = 5, N = 10 CRs and each CR is subjected to: 1) AWGN, 2) Rayleigh fading, respectively.

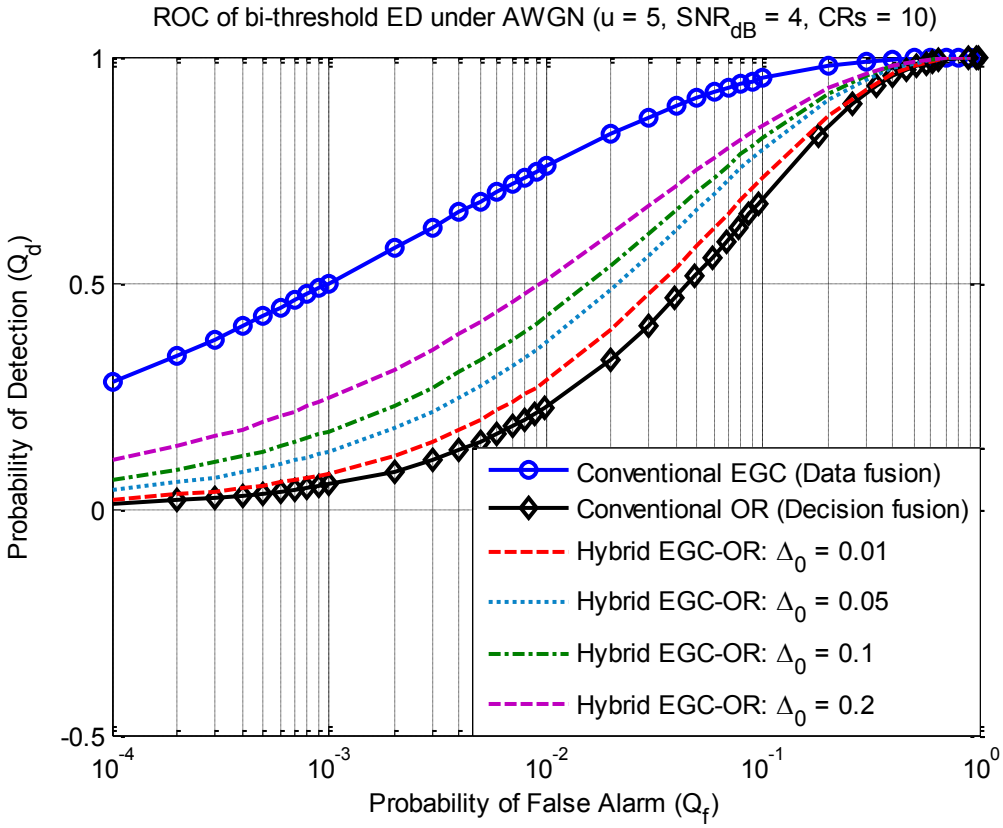

Figure 4.2: ROCs for the proposed algorithm, conventional EGC, and conventional OR under AWGN (SNR 4 dB).

Figure 4.2 and Figure 4.3 examine the AWGN case with SNR = 4 dB and SNR = 6 dB, respectively. The ROC performance of three schemes is compared; namely, the

conventional EGC (data fusion), the conventional OR-rule (decision fusion), and the proposed hybrid EGC-OR scheme. The hybrid EGC-OR scheme is examined for different values of Δ_0, which is proportional to the width of the fuzzy region. The performance of our proposed hybrid EGC-OR scheme lies between the two conventional schemes.

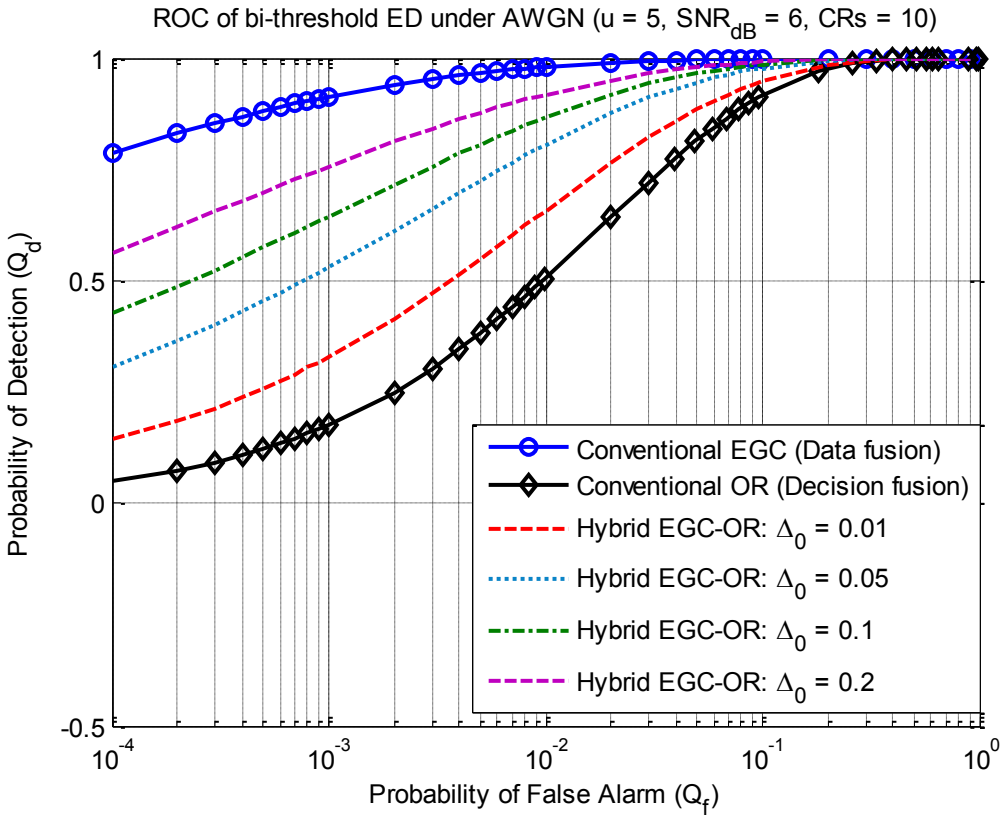

Figure 4.3: ROCs for the proposed algorithm, conventional EGC, and conventional OR under AWGN (SNR 6 dB).

Figure 4.4 and Figure 4.5, repeat the same experiment in the case of Rayleigh channel with SNR = 6 dB and SNR = 8 dB, respectively. We note that, under both of the wireless environments, the performance of our proposed Hybrid EGC-OR lies in between the two conventional single-threshold schemes. For small Δ_0, the performance of Hybrid ECG-

OR is close to decision-fusion scheme (OR rule). However, as Δ_0 increases, the performance of Hybrid EGC-OR approaches that of data-fusion scheme (EGC) but with a much smaller number of feedback bits as shown in Figure 4.6 - Figure 4.9. The two thresholds, i.e., λ_1 and λ_2, for the proposed approach was found numerically from (4.16) using the grid search method for a given Δ_0 and a given Q_f.

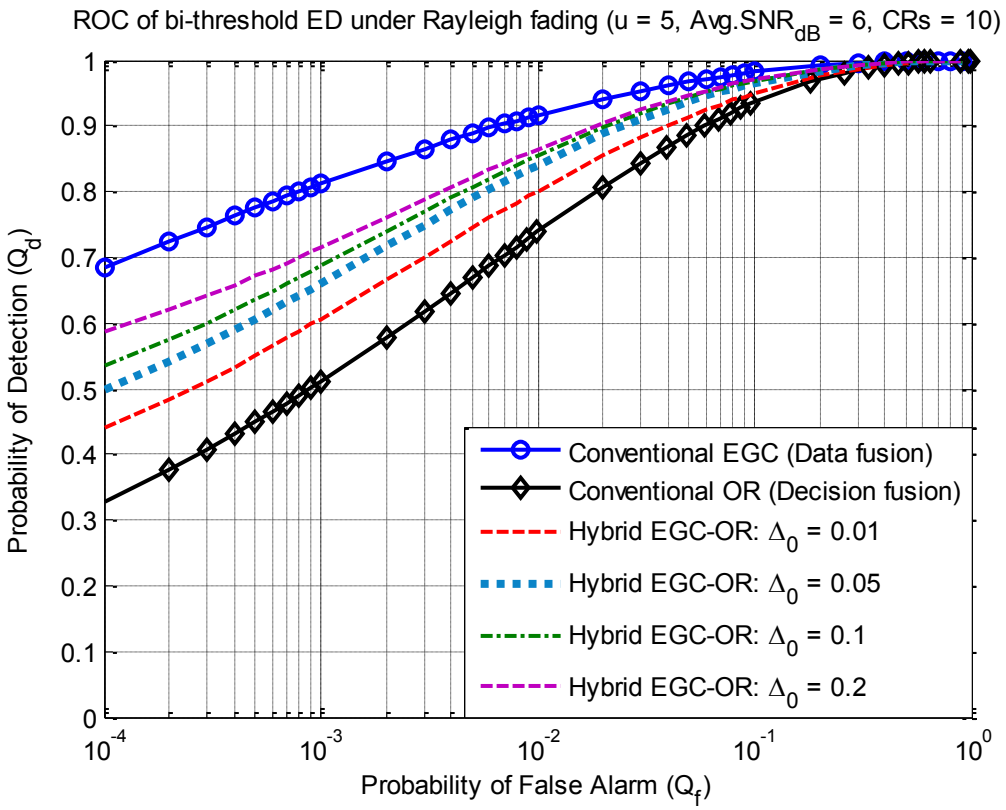

Figure 4.4: ROCs for the proposed algorithm, conventional EGC, and conventional OR under Rayleigh fading (SNR = 6 dB).

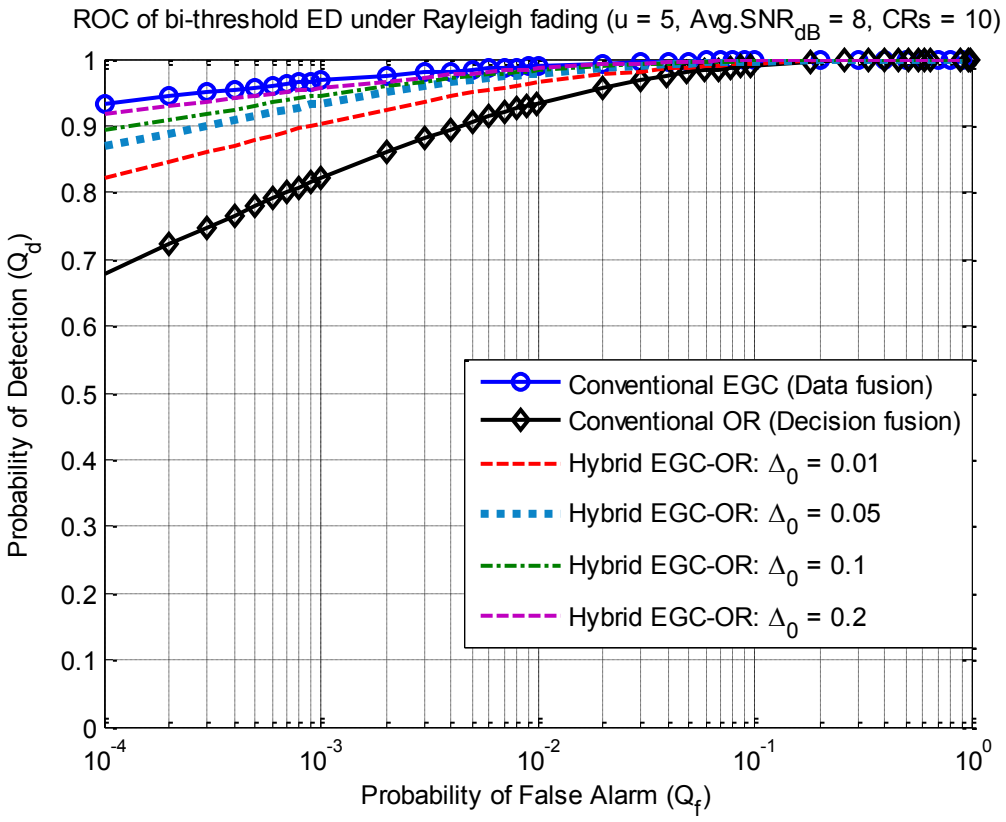

Figure 4.5: ROCs for the proposed algorithm, conventional EGC, and conventional OR under Rayleigh fading (SNR = 8 dB).

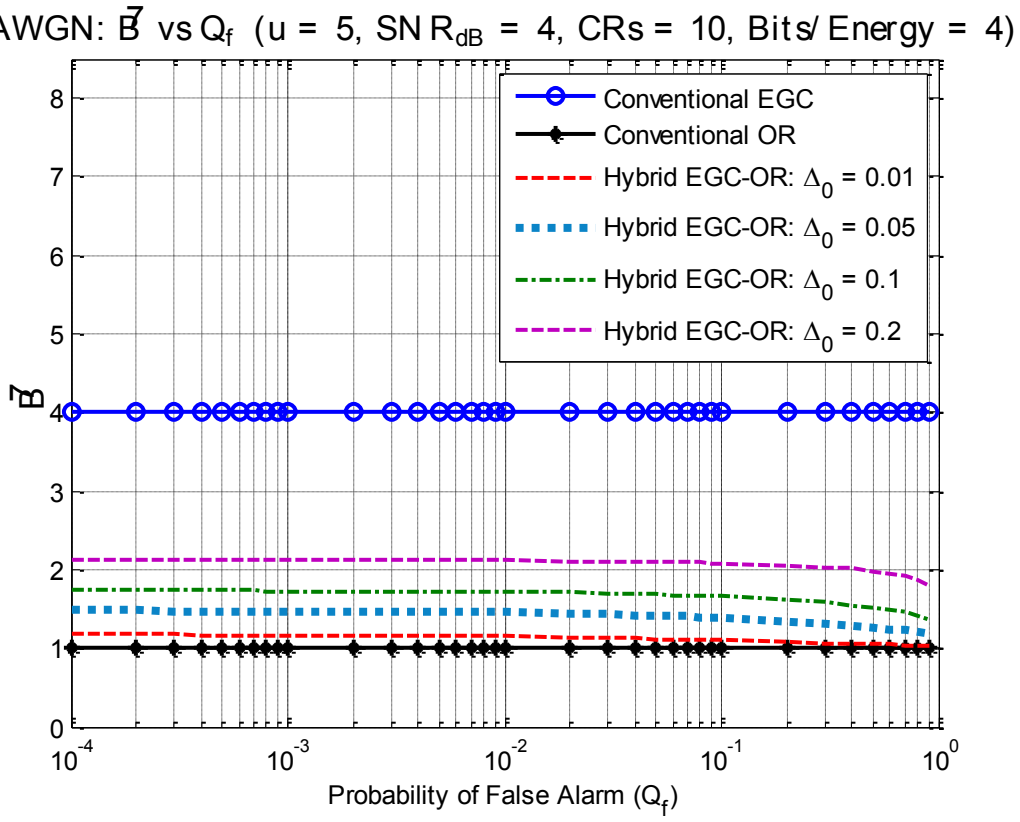

Figure 4.6: AWGN case (SNR = 4 dB): Normalized average number of bits per user $\bar{B}$ Vs. Q_f.

Figure 4.6 and Figure 4.7 compare the average required feedback bits of the three schemes under the same scenarios considered in Figure 4.2 and Figure 4.3, respectively. As can be seen in these figures, for $\Delta_0 = 0.2$ the average required number of feedback bits decreases from 4-bits/CR to 2.36-bits/CR for each sensing cycle in the case of AWGN (for most of the Q_f range) while the ROC performance stays well above the OR-rule and close to that of the conventional EGC.

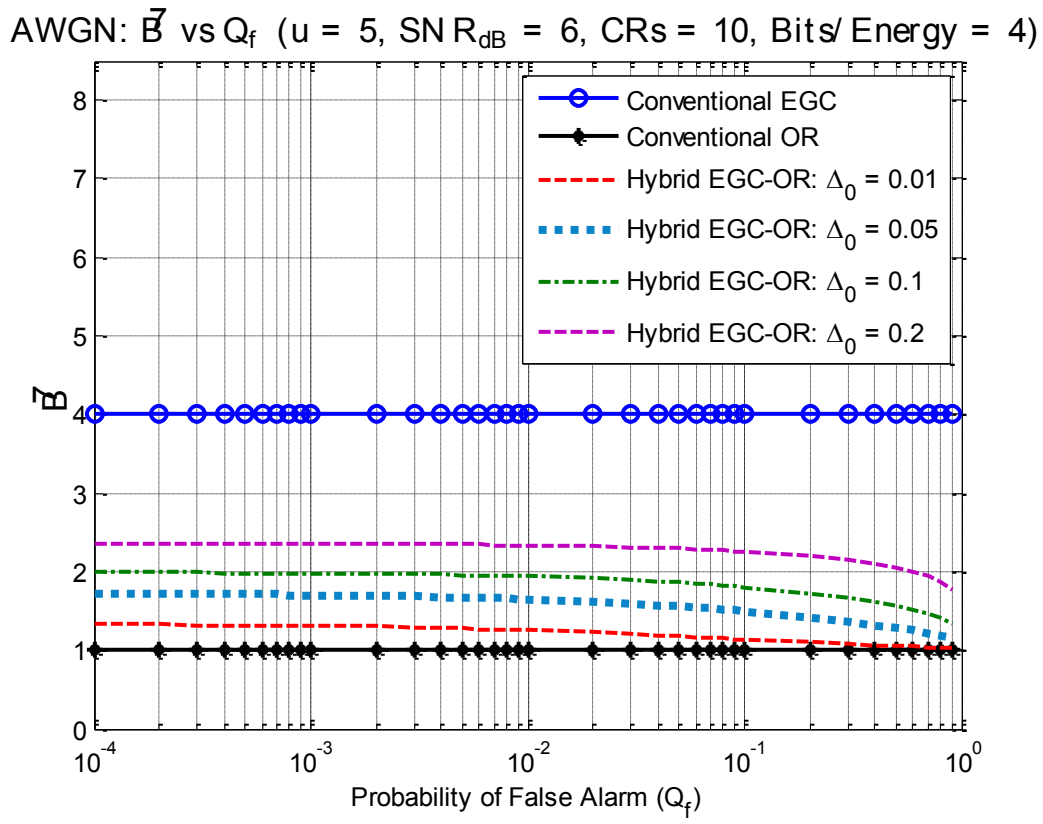

Figure 4.7: AWGN case (SNR = 6 dB): Normalized average number of bits per user $\bar{B}$ Vs. Q_f.

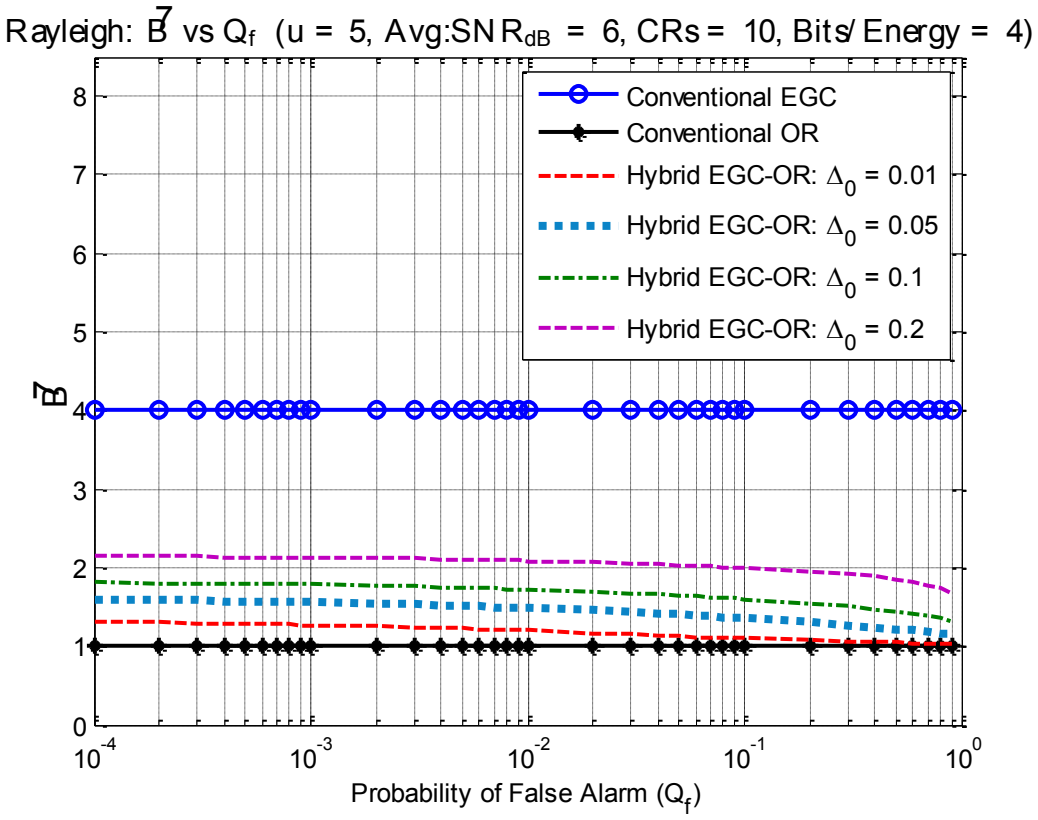

Figure 4.8: Rayleigh fading case (SNR = 6 dB): Normalized average number of bits per user $\bar{B}$ Vs. Q_f.

Similarly, Figure 4.8 and Figure 4.9 (Rayleigh fading cases) compare the average required feedback bits of the three schemes under the same scenarios considered in Figure 4.4 and Figure 4.5, respectively. It can be seen from these figures that under Rayleigh fading, the average required number of feedback bits decreases from 4-bits/CR (conventional EGC) to an average of 2-bits/CR (averaged over the Q_f range) for each sensing cycle when $\Delta_0 = 0.2$. At the same time, the ROC performance is very close to that of the conventional EGC, especially for high SNR and high values of Q_f. For example, under Rayleigh fading, SNR = 8 dB, $Q_f = 10^{-2}$, the average number of required

bits decreases by almost 50% or more from the EGC (from 4-bits/CR to 2-bits/CR) as shown in Figure 4.9, while Q_d decreases by only 0.003 as shown in Figure 4.5.

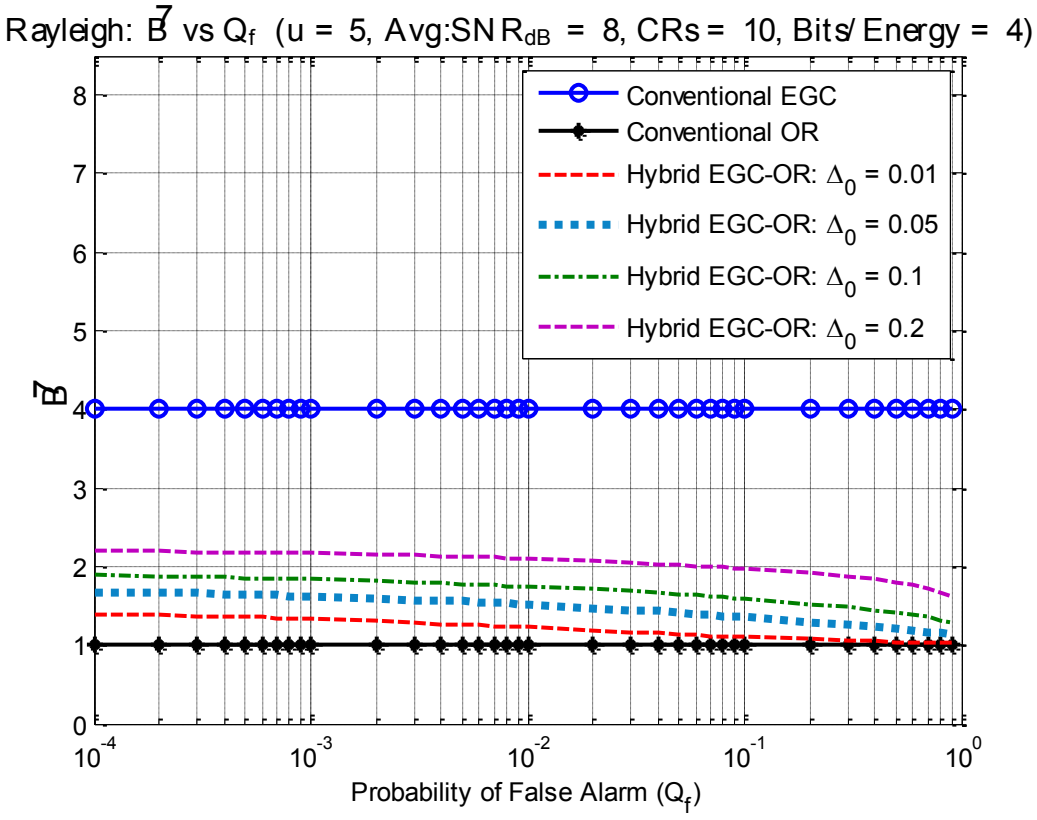

Figure 4.9: Rayleigh fading case (SNR = 8 dB): Normalized average number of bits per user $\bar{B}$ Vs. Q_f.

This shows that the proposed scheme can substantially reduce the average required number of feedback bits while keeping the performance very close to that of the EGC.

4.6 Summary

In this chapter, using a bi-threshold energy detector, we developed a hybrid linear combing scheme, Hybrid EGC-OR. We derived the corresponding closed form expression for the performance of our proposed Hybrid EGC-OR scheme. Through simulations it was shown that our proposed algorithm sufficiently reduces the feedback bits over the reporting channel while achieving performance close to that of EGC.

In the next chapter (Chapter 5), we present the conclusion for the thesis and future directions of our work.

CHAPTER 5

CONCLUSION AND FUTURE WORK

5.1 Summary of Results

Cognitive Radio has gained a lot of popularity among researchers in the last few years. However, the accurate detection of holes in the spectrum is still a very challenging task. In this thesis we proposed various techniques to perform robust spectrum sensing. In the first part, we addressed the spectrum sensing problem in the frequency domain, while in the second part we deal with the time domain view of the problem.

In the frequency domain, we discussed the power of the Wavelet Transform in sensing spectrum using an edge-detection approach [26]. Several extensions for improvement in wavelet-based spectrum sensing have been addressed and corresponding simulations have been shown. The simulations showed that performing median filtering results in a smooth PSD $S_r(f)$, and consequently less spurious local extrema due to noise have been observed in the wavelet transform curves. Furthermore, a simple yet effective method for thresholding the noise-wavelet-coefficients was presented. The targeted spectrum was a wide band spectrum which would require high sampling rates in order to properly characterize the wide band spectrum. However, we could reduce this complexity by inserting guard bands during CR transmission or when the primary goal of the wavelet approach is a rough estimation of spectrum holes [26]. During off-load hours, there will

be spectrum-holes even within a specific band $\{B_n\}$. In such a case, the overall operation of the wavelet approach will not be affected negatively, since the wavelet technique will still be able to identify those holes.

For the time domain approach, we proposed a hybrid cooperative spectrum sensing algorithm which combines decision fusion and data fusion techniques using bi-threshold energy detector at the distributed CRs. Closed form expressions for the ROC performance and the average number of reporting bits of the proposed algorithm were obtained and simulated. It was shown that at the cost of a negligible performance loss from the EGC, the average number of reporting bits dramatically decreases from that of the EGC. Therefore, the proposed algorithm reduces the communication burden over the reporting channels as compared to EGC.

5.2 Future directions: Wavelet Detection

As a continuation of our work for the improvement of Wavelet based sensing, we would like to propose some extensions of the work into the following directions:

5.2.1 Extension of the work over the Frequency-Selective Fading

Such a case will be a more realistic in practical applications. This case is more challenging since the PSD levels within the occupied frequency sub-bands will no longer

be flat and hence it will affect the sensing results. One can investigate the different types of wavelet decompositions including wavelet packets which are optimal in the sense of entropy.

5.2.2 Performance analysis with non-Gaussian noise

So far, the noise in the received wideband signal (Equation (2.6)) was assumed to be white, and hence the frequency components of this noise was flat. An interesting direction for future research is to see the effect of other types of noises whose power spectral density is no longer flat.

5.3 Future directions: Energy Detection

As a continuation of our work on energy detection based sensing, the bi-threshold energy detector can further be explored. Specifically, one can investigate to utilize more effectively the observations of the CRs whose energies fall in the "Fuzzy region". The proposed approaches are:

5.3.1 Apply Particle Swarm Optimization to fuzzy CRs

One direction for future research is to apply particle swarm optimization (PSO) for the CRs that fall into the "Fuzzy region". Instead of blindly combining the received energies from the fuzzy CRs, the fusion center may combine the energies in an optimal fashion using the popular particle swarm optimization technique [86]. PSO is a population based, stochastic optimization approach designed to mimic the social behavior of flock of birds, where each particle in a population is a candidate solution to the optimization problem. The fusion center would use the PSO algorithm to obtain the optimal weights for the received energies from the fuzzy CRs. The calculation of these weights depends on a fitness function which takes into consideration the noise variances of the fuzzy CRs. Energy combining using optimal weights is expected to improve performance over the EGC technique when each fuzzy CR has a different local SNR.

5.3.2 A New Estimate of the Energy Statistic

The energy detector model described in Section 2.2 provides the decision statistic by first passing the observed signal through a band-pass filter, followed by the squaring device and then the sum operation is performed over the squared samples. The statistical distribution of the decision statistic, Y, obtained in this manner is represented as in Equation (2.16). As a future work, we can modify the model of the energy detector in such a way that the sum operation precedes the squaring device. Doing so, the resultant

decision statistic, Y, would be different as compared to that of Equation (2.16), and further mathematical analysis would be needed to investigate the performance of the modified energy detector.

5.3.3 Effect of different types of noise

As a more challenging task, one would also like to investigate the case where a non-Gaussian noise in the received signal (see Equation (2.15)) is considered, such as impulsive noise. In this case, the decision statistic Y (Equation (2.16)) will no longer be a chi-square distributed random variable. With the change in the distribution statistics, Y, probably the performance of the energy detector will also be changed. This problem would need further mathematical analysis in order to derive new equations for the performance of the energy detector.

Publications

The publications out of the thesis work are as follows:

- H. K. Kathuria and M. A. Deriche, "A Novel Approach for Spectrum Sensing using the Wavelet Transform," in *The 3rd Student Scientific Conference*, 2012.
- H. K. Kathuria and M. A. Deriche, "A Survey of Wavelet-based Spectrum Sensing Techniques," in *The 15th Saudi Technical Exchange Meeting*, 2012.
- H. K. Kathuria, M. A. Deriche, and W. Mesbah, "A Hybrid EGC-OR Detection Algorithm for Cooperative Spectrum Sensing," in (submitted to) *The 38th International Conference on Acoustics, Speech, and Signal Processing (ICASSP)*, 2013.
- H. K. Kathuria, M. A. Deriche, and W. Mesbah, "Hybrid Cooperative Spectrum Sensing Algorithm using Bi-threshold Energy Detector," (submitted to) *IEEE Transactions on Communications*, 2013.

References

[1] FCC, “Spectrum Policy Task Force Report,” *ET Docket*, 2002.

[2] J. Mitola and G. Q. Maguire, “Cognitive radio: making software radios more personal,” *IEEE Personal Communications*, vol. 6, no. 4, pp. 13–18, 1999.

[3] C. Stevenson, G. Chouinard, S. Shellhammer, and W. Caldwell, “IEEE 802.22: The first cognitive radio wireless regional area network standard,” *IEEE Communications Magazine*, vol. 47, no. 1, pp. 130–138, Jan. 2009.

[4] S. Haykin, “Cognitive radio: brain-empowered wireless communications,” *IEEE Journal on Selected Areas in Communications*, vol. 23, no. 2, pp. 201–220, Feb. 2005.

[5] I. F. Akyildiz, W.-Y. Lee, M. C. Vuran, and S. Mohanty, “NeXt generation/dynamic spectrum access/cognitive radio wireless networks: A survey,” *Computer Networks*, vol. 50, no. 13, pp. 2127–2159, Sep. 2006.

[6] R. Umar and A. U. H. Sheikh, “A comparative study of spectrum awareness techniques for cognitive radio oriented wireless networks,” *Physical Communication*, Aug. 2012.

[7] T. Yucek and H. Arslan, “A survey of spectrum sensing algorithms for cognitive radio applications,” *IEEE Communications Surveys & Tutorials*, vol. 11, no. 1, pp. 116–130, 2009.

[8] FCC, “ET Docket No 03-237 Notice of inquiry and notice of proposed Rulemaking,” 2003.

[9] T. X. Brown, “An analysis of unlicensed device operation in licensed broadcast service bands,” in *First IEEE International Symposium on New Frontiers in Dynamic Spectrum Access Networks, 2005. DySPAN 2005.*, pp. 11–29.

[10] A. Ghasemi and E. S. Sousa, “Collaborative spectrum sensing for opportunistic access in fading environments,” in *First IEEE International Symposium on New Frontiers in Dynamic Spectrum Access Networks, 2005. DySPAN 2005.*, pp. 131–136.

[11] A. Sahai and N. Hoven, “Some fundamental limits on cognitive radio,” *Allerton Conference on Comm., Control and Computing.*, 2004.

[12] H. Urkowitz, “Energy detection of unknown deterministic signals,” *Proceedings of the IEEE*, vol. 55, no. 4, pp. 523–531, 1967.

[13] Y. Zeng, C. L. Koh, and Y.-C. Liang, “Maximum Eigenvalue Detection: Theory and Application,” in *2008 IEEE International Conference on Communications*, 2008, pp. 4160–4164.

[14] P. Cheraghi, Y. Ma, and R. Tafazolli, “A Novel Blind Spectrum Sensing Approach for Cognitive Radios,” in *The 11th Annual PostGraduate Symposium on The Convergence of Telecommunications, Networking and Broadcasting*, 2010, pp. 1–5.

[15] L. Shen, H. Wang, W. Zhang, and Z. Zhao, “Blind Spectrum Sensing for Cognitive Radio Channels with Noise Uncertainty,” *IEEE Transactions on Wireless Communications*, vol. 10, no. 6, pp. 1721–1724, Jun. 2011.

[16] R. Wang and M. Tao, “Blind Spectrum Sensing by Information Theoretic Criteria for Cognitive Radios,” *IEEE Transactions on Vehicular Technology*, vol. 59, no. 8, pp. 3806–3817, Oct. 2010.

[17] A. Ghasemi and E. S. Sousa, “Spectrum sensing in cognitive radio networks: requirements, challenges and design trade-offs,” *IEEE Communications Magazine*, vol. 46, no. 4, pp. 32–39, Apr. 2008.

[18] J. G. Proakis, *Digital Communications*, 4th ed. McGraw-Hill, 2001.

[19] R. Tandra and A. Sahai, “Fundamental limits on detection in low SNR under noise uncertainty,” in *2005 International Conference on Wireless Networks, Communications and Mobile Computing*, vol. 1, pp. 464–469.

[20] D. Cabric, S. M. Mishra, and R. W. Brodersen, “Implementation issues in spectrum sensing for cognitive radios,” in *Conference Record of the Thirty-Eighth Asilomar Conference on Signals, Systems and Computers, 2004.*, vol. 1, pp. 772–776.

[21] J. Lunden, V. Koivunen, A. Huttunen, and H. V. Poor, “Spectrum Sensing in Cognitive Radios Based on Multiple Cyclic Frequencies,” in *2007 2nd International Conference on Cognitive Radio Oriented Wireless Networks and Communications*, 2007, pp. 37–43.

[22] A. Fehske, J. Gaeddert, and J. H. Reed, “A new approach to signal classification using spectral correlation and neural networks,” in *First IEEE International Symposium on New Frontiers in Dynamic Spectrum Access Networks, 2005. DySPAN 2005.*, pp. 144–150.

[23] H. Tang, “Some physical layer issues of wide-band cognitive radio systems,” in *First IEEE International Symposium on New Frontiers in Dynamic Spectrum Access Networks, 2005. DySPAN 2005.*, pp. 151–159.

[24] K. Ben Letaief, “Cooperative Communications for Cognitive Radio Networks,” *Proceedings of the IEEE*, vol. 97, no. 5, pp. 878–893, May 2009.

[25] S. Mallat and W. L. Hwang, “Singularity detection and processing with wavelets,” *IEEE Transactions on Information Theory*, vol. 38, no. 2, pp. 617–643, Mar. 1992.

[26] Z. Tian and G. B. Giannakis, “A Wavelet Approach to Wideband Spectrum Sensing for Cognitive Radios,” in *2006 1st International Conference on Cognitive Radio Oriented Wireless Networks and Communications*, 2006, pp. 1–5.

[27] I. Daubechies, *Ten Lectures on Wavelets*, 1st ed. SIAM, 1992.

[28] S. G. Mallat, “A theory for multiresolution signal decomposition: the wavelet representation,” *IEEE Transactions on Pattern Analysis and Machine Intelligence*, vol. 11, no. 7, pp. 674–693, Jul. 1989.

[29] G. Strang and T. Nguyen, *Wavelets and Filter Banks*, 2nd ed. Wellesley College, 1996, p. 520.

[30] S. Mallat and S. Zhong, “Characterization of signals from multiscale edges,” *IEEE Transactions on Pattern Analysis and Machine Intelligence*, vol. 14, no. 7, pp. 710–732, Jul. 1992.

[31] B. Peterson, “Agilent Spectrum Analysis Basics,” *Agilent Technologies, Inc.* [Online]. Available: http://cp.literature.agilent.com/litweb/pdf/5952-0292.pdf.

[32] Anritsu, “Product Brochure; Signal Analyzer MS2830A,” *Data Sheet*, 2011. [Online]. Available: http://www.metrictest.com/catalog/pdfs/product_pdfs/MS2830A_E1300.pdf.

[33] A. Technologies, “Agilent ESA Series Spectrum Analyzers Data Sheet,” *Data S*, 2005. [Online]. Available: http://cp.literature.agilent.com/litweb/pdf/5968-3386E.pdf.

[34] R. Umar and A. Sheikh, “Cognitive Radio oriented wireless networks: Challenges and solutions,” in *Multimedia Computing and Systems (...*, 2012, pp. 992–997.

[35] S. M. Kay, *Fundamental of Statistical Signal Processing: Detection Theory*. Englewood Cliffs, NJ: Prentice-Hall, 1998.

[36] F. F. Digham, M. S. Alouini, and M. K. Simon, “On the energy detection of unknown signals over fading channels,” in *IEEE International Conference on Communications, 2003. ICC ’03.*, 2003, vol. 5, pp. 3575–3579.

[37] A. Nuttall, “Some integrals involving the<tex>Q_M</tex>function (Corresp.),” *IEEE Transactions on Information Theory*, vol. 21, no. 1, pp. 95–96, Jan. 1975.

[38] S. M. Alamouti, “A simple transmit diversity technique for wireless communications,” *IEEE Journal on Selected Areas in Communications*, vol. 16, no. 8, pp. 1451–1458, 1998.

[39] A. Ghasemi and E. S. Sousa, “Spectrum sensing in cognitive radio networks: the cooperation-processing tradeoff,” *Wireless Communications and Mobile Computing*, vol. 7, no. 9, pp. 1049–1060, Nov. 2007.

[40] W. A. Gardner, “Signal interception: a unifying theoretical framework for feature detection,” *IEEE Transactions on Communications*, vol. 36, no. 8, pp. 897–906, 1988.

[41] G. Ganesan, Y. Li, and S. Li, “Spatiotemporal Sensing in Cognitive Radio Networks,” in *2007 IEEE 18th International Symposium on Personal, Indoor and Mobile Radio Communications*, 2007, pp. 1–5.

[42] J. Ma, G. Y. Li, and B. H. Juang, “Signal processing in cognitive radio,” *Proceedings of the IEEE*, vol. 97, no. 5, pp. 805–823, 2009.

[43] F. F. Digham, M.-S. Alouini, and M. K. Simon, “On the Energy Detection of Unknown Signals Over Fading Channels,” *IEEE Transactions on Communications*, vol. 55, no. 1, pp. 21–24, Jan. 2007.

[44] I. F. Akyildiz, B. F. Lo, and R. Balakrishnan, “Cooperative spectrum sensing in cognitive radio networks: A survey,” *Physical Communication*, vol. 4, no. 1, pp. 40–62, Mar. 2011.

[45] X. Zheng, J. Wang, L. Cui, J. Chen, and Q. Wu, “A Novel Cooperative Spectrum Sensing Algorithm in Cognitive Radio Systems,” in *2008 4th International Conference on Wireless Communications, Networking and Mobile Computing*, 2008, pp. 1–4.

[46] D. Duan, L. Yang, and J. C. Principe, “Cooperative Diversity of Spectrum Sensing in Cognitive Radio Networks,” in *2009 IEEE Wireless Communications and Networking Conference*, 2009, pp. 1–6.

[47] S. Mishra, A. Sahai, and R. Brodersen, “Cooperative Sensing among Cognitive Radios,” in *2006 IEEE International Conference on Communications*, 2006, pp. 1658–1663.

[48] G. Ganesan and Y. Li, “Cooperative Spectrum Sensing in Cognitive Radio, Part I: Two User Networks,” *IEEE Transactions on Wireless Communications*, vol. 6, no. 6, pp. 2204–2213, Jun. 2007.

[49] G. Ganesan and Y. Li, “Cooperative Spectrum Sensing in Cognitive Radio, Part II: Multiuser Networks,” *IEEE Transactions on Wireless Communications*, vol. 6, no. 6, pp. 2214–2222, Jun. 2007.

[50] G. Ganesan, “Agility improvement through cooperative diversity in cognitive radio,” in *GLOBECOM ’05. IEEE Global Telecommunications Conference, 2005.*, 2005, p. 5 pp.–2509.

[51] F. Visser, G. J. M. Janssen, and P. Pawelczak, “Multinode Spectrum Sensing Based on Energy Detection for Dynamic Spectrum Access,” in *VTC Spring 2008 - IEEE Vehicular Technology Conference*, 2008, pp. 1394–1398.

[52] Z. Quan, S. Cui, H. Poor, and A. Sayed, “Collaborative wideband sensing for cognitive radios,” *IEEE Signal Processing Magazine*, vol. 25, no. 6, pp. 60–73, Nov. 2008.

[53] C. Sun, W. Zhang, and K. Ben Letaief, “Cluster-Based Cooperative Spectrum Sensing in Cognitive Radio Systems,” in *2007 IEEE International Conference on Communications*, 2007, pp. 2511–2515.

[54] E. Visotsky, S. Kuffner, and R. Peterson, “On collaborative detection of TV transmissions in support of dynamic spectrum sharing,” in *First IEEE International Symposium on New Frontiers in Dynamic Spectrum Access Networks, 2005. DySPAN 2005.*, pp. 338–345.

[55] Y. Selen, H. Tullberg, and J. Kronander, “Sensor Selection for Cooperative Spectrum Sensing,” in *2008 3rd IEEE Symposium on New Frontiers in Dynamic Spectrum Access Networks*, 2008, pp. 1–11.

[56] L. De Nardis, M.-G. Di Benedetto, D. Tassetto, S. Bovelli, A. Akhtar, O. Holland, and R. Thobaben, “Impact of mobility in cooperative spectrum sensing: Theory vs. simulation,” in *2012 International Symposium on Wireless Communication Systems (ISWCS)*, 2012, pp. 416–420.

[57] X. Zhou, G. Y. Li, D. Li, D. Wang, and A. C. K. Soong, “Bandwidth efficient combination for cooperative spectrum sensing in cognitive radio networks,” in *2010 IEEE International Conference on Acoustics, Speech and Signal Processing*, 2010, pp. 3126–3129.

[58] X. Zhou, J. Ma, G. Li, Y. Kwon, and A. K. Soong, “Probability-based combination for cooperative spectrum sensing,” *IEEE Transactions on Communications*, vol. 58, no. 2, pp. 463–466, Feb. 2010.

[59] C. Guo, T. Zhang, Z. Zeng, and C. Feng, “Investigation on Spectrum Sharing Technology Based On Cognitive Radio,” in *2006 First International Conference on Communications and Networking in China*, 2006, pp. 1–5.

[60] J. Perez-Romero, O. Sallent, R. Agusti, and L. Giupponi, “A Novel On-Demand Cognitive Pilot Channel Enabling Dynamic Spectrum Allocation,” in *2007 2nd IEEE International Symposium on New Frontiers in Dynamic Spectrum Access Networks*, 2007, pp. 46–54.

[61] P. Pawełczak, C. Guo, R. V. Prasad, and R. Hekmat, “Clusterbased spectrum sensing architecture for opportunistic spectrum access networks,” in *IEEE Vehicular Technology Conference VTC2007*, 2007.

[62] L. Musavian and T. Le-Ngoc, “Cross-layer design for cognitive radios with joint AMC and ARQ under delay QoS constraint,” in *2012 8th International Wireless Communications and Mobile Computing Conference (IWCMC)*, 2012, pp. 419–424.

[63] P. K. Varshney, *Distributed Detection and Data Fusion*. New York: Springer-Verlag, 1997, p. 299.

[64] D. J. Thomson, “Spectrum estimation and harmonic analysis,” *Proceedings of the IEEE*, vol. 70, no. 9, pp. 1055–1096, 1982.

[65] D. Slepian, “Prolate spheroidal wave functions, Fourier analysis and uncertainty,” *Bell Syst. Tech. J.*, vol. 57, pp. 1371–1430, 1978.

[66] S. Xu, Y. Shang, and H. Wang, “Eigenvalues based spectrum sensing against untrusted users in cognitive radio networks,” in *2009 4th International Conference on Cognitive Radio Oriented Wireless Networks and Communications*, 2009, pp. 1–6.

[67] J. Ma, G. Zhao, and Y. Li, “Soft Combination and Detection for Cooperative Spectrum Sensing in Cognitive Radio Networks,” *IEEE Transactions on Wireless Communications*, vol. 7, no. 11, pp. 4502–4507, Nov. 2008.

[68] A. Pandharipande and J.-P. M. G. Linnartz, “Performance Analysis of Primary User Detection in a Multiple Antenna Cognitive Radio,” in *2007 IEEE International Conference on Communications*, 2007, pp. 6482–6486.

[69] D. Brennan, “Linear Diversity Combining Techniques,” *Proceedings of the IRE*, vol. 47, no. 6, pp. 1075–1102, Jun. 1959.

[70] S. P. Herath, N. Rajatheva, and C. Tellambura, “Energy Detection of Unknown Signals in Fading and Diversity Reception,” *IEEE Transactions on Communications*, vol. 59, no. 9, pp. 2443–2453, Sep. 2011.

[71] A. Ghasemi and E. S. Sousa, “Opportunistic Spectrum Access in Fading Channels Through Collaborative Sensing,” *Journal of Communications*, vol. 2, no. 2, pp. 71–82, Mar. 2007.

[72] S. P. Herath and N. Rajatheva, “Analysis of Equal Gain Combining in Energy Detection for Cognitive Radio over Nakagami Channels,” in *IEEE GLOBECOM 2008 - 2008 IEEE Global Telecommunications Conference*, 2008, pp. 1–5.

[73] Q. Wang, D.-W. Yue, and Y. Wang, “Performance Analysis of Spectrum Sensing Using Diversity Technique,” in *2009 5th International Conference on Wireless Communications, Networking and Mobile Computing*, 2009, no. 2008, pp. 1–5.

[74] K. T. Hemachandra and N. C. Beaulieu, “Novel Analysis for Performance Evaluation of Energy Detection of Unknown Deterministic Signals Using Dual Diversity,” in *2011 IEEE Vehicular Technology Conference (VTC Fall)*, 2011, pp. 1–5.

[75] S. Haghani and N. C. Beaulieu, “On decorrelation in dual-branch diversity systems,” *IEEE Transactions on Communications*, vol. 57, no. 7, pp. 2138–2147, Jul. 2009.

[76] S. Rodriguez-Parera, V. Ramon, A. Bourdoux, F. Horlin, and R. Lauwereins, “Spectrum Sensing over SIMO Multi-Path Fading Channels Based on Energy Detection,” in *IEEE GLOBECOM 2008 - 2008 IEEE Global Telecommunications Conference*, 2008, pp. 1–6.

[77] R. Tandra and A. Sahai, “SNR Walls for Signal Detection,” *IEEE Journal of Selected Topics in Signal Processing*, vol. 2, no. 1, pp. 4–17, Feb. 2008.

[78] C. Sun, W. Zhang, and K. Ben Letaief, “Cooperative Spectrum Sensing for Cognitive Radios under Bandwidth Constraints,” in *2007 IEEE Wireless Communications and Networking Conference*, 2007, pp. 1–5.

[79] M. Gabbouj, E. J. Coyle, and N. C. Gallagher, “An overview of median and stack filtering,” *Circuits Systems and Signal Processing*, vol. 11, no. 1, pp. 7–45, Mar. 1992.

[80] L. Rabiner, M. Sambur, and C. Schmidt, “Applications of a nonlinear smoothing algorithm to speech processing,” *IEEE Transactions on Acoustics, Speech, and Signal Processing*, vol. 23, no. 6, pp. 552–557, Dec. 1975.

[81] A. C. Bovik, T. S. Huang, and D. C. Munson, “The Effect of Median Filtering on Edge Estimation and Detection,” *IEEE Transactions on Pattern Analysis and Machine Intelligence*, vol. PAMI-9, no. 2, pp. 181–194, Mar. 1987.

[82] Y.-L. Xu, H.-S. Zhang, and Z.-H. Han, “The Performance Analysis of Spectrum Sensing Algorithms Based on Wavelet Edge Detection,” in *2009 5th International Conference on Wireless Communications, Networking and Mobile Computing*, 2009, pp. 1–4.

[83] K. Divakaran, N. M. P, and S. H. R R, “Wavelet Based Spectrum Sensing Techniques for Cognitive Radio - A Survey,” *International Journal of Computer Science and Information Technology*, vol. 3, no. 2, pp. 123–137, Apr. 2011.

[84] D. Karthik, P. N. Manikandan, R. R. S. Hari, and A. R. Srinivas, “A novel algorithm for spectrum sensing using adaptive Wavelet Edge Detection scheme,” in *2011 3rd International Conference on Electronics Computer Technology*, 2011, vol. 3, no. 1, pp. 118–122.

[85] E. P. L. de Almeida, P. H. P. de Carvalho, P. A. B. Cordeiro, and R. D. Vieira, “Experimental study of a Wavelet-based spectrum sensing technique,” in *2008 42nd Asilomar Conference on Signals, Systems and Computers*, 2008, pp. 1552–1556.

[86] S. Zheng, C. Lou, and X. Yang, “Cooperative spectrum sensing using particle swarm optimisation,” *Electronics Letters*, vol. 46, no. 22, p. 1525, 2010.

Vitae

Name	: Humayun Khalid Yusuf Kathuria
Nationality	: Pakistani
Date of Birth	:3/23/1984
Email	: engr.humayun@gmail.com
Present Address	: KFUPM, P.O.Box 8639, Dhahran 31261, KSA
Permanent Address	: 177 – Garden Block, New Garden Town, Lahore, Pakistan
Contact numbers	: +966-557409063, +966-2-6739884
Academic Background	: BS Computer Engineering